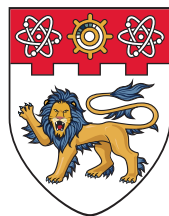




## AIAA 2021-2022 DESIGN COMPETITION

UNDERGRADUATE TEAM AIRCRAFT DESIGN

FINAL DESIGN REPORT | FIREFLIGHTER



**NANYANG  
TECHNOLOGICAL  
UNIVERSITY**  
**SINGAPORE**

School of Mechanical and Aerospace Engineering








*Nanyang Technological University, Singapore, 639798*

Date of Submission: May 14, 2022

## Team Firefly

 <b>Puay Him <u>Ler</u></b> Propulsion, Landing Gear	 <b>Wenhui <u>Tock</u></b> Wing Design, Aerodynamics	 <b>Szecsenyi <u>Tamas</u></b> Weight, Avionics
 <b>Kenneth <u>Neoh</u></b> Market Analysis, Structures	 <b>Cherng En <u>Lee</u></b> Retardant Tank, Aircraft Systems	 <b>Wen Yue <u>Tang</u></b> Empennage, Stability

**Table 1: Member Affiliations**

Name	AIAA #	Signature
Puay Him <u>Ler</u>	1344009	
Wenhui <u>Tock</u>	1342844	
Szecsenyi <u>Tamas</u>	1344003	
Kenneth <u>Neoh</u>	1342855	
Cherng En <u>Lee</u>	1342852	
Wen Yue <u>Tang</u>	1241181	
Wai Tuck <u>Chow</u> (Faculty Advisor)	-	

## I.Executive Summary

Climate change is a global phenomenon that cannot be ignored. With an increasing number and intensity of wildfires across the world, the annual expenditure on wildfire suppression is forecasted to increase up to \$30 billion annually in 2050. Many countries are thus looking to build up their fleets of firefighting aircraft – but aging airframes and demanding missions means that not many aircraft are available, especially large air tankers with capacities over 4,000 gallons.

The Firefighter is a next generation purpose-built firefighting aircraft with a retardant capacity of 8,000 gallons. With two loading ports and electronically controlled drop doors, flexible and precise drop patterns can be achieved, along with fast reloading times. Four PW150A turboprop engines coupled with R408 propellers propel the aircraft to a dash speed of at least 400 knots between drops, with a large fuel tank capacity enabling the operational range and ferry range to exceed RFP requirements by 38% and 33% respectively while being economical to operate at \$1.46 per gallon dropped. The aircraft is also equipped with the latest technologies for safe low-level flying, including a terrain-following radar, Synthetic Vision Systems and Enhanced Flight Vision Systems. As a purpose-built firefighting aircraft, Firefighter offers a versatile, capable, and cost-effective platform to tackle the increasing numbers and intensities of forest fires worldwide.

**Table 2: Aircraft specifications.**

<b>Aircraft Specifications</b>	
Crew	<ul style="list-style-type: none"> <li>• 2</li> </ul>
Dimensions	<ul style="list-style-type: none"> <li>• Height: 32.16 ft</li> <li>• Width: 149.96 ft</li> <li>• Length: 93.18 ft</li> </ul>
Speed	<ul style="list-style-type: none"> <li>• 102 knots @ ≤300ft AGL (Payload Drop)</li> <li>• 254 knots (Optimum Speed @ 20,000 ft, Design Mission)</li> <li>• 410 knots (Dash Speed @20,000 ft, Design Mission)</li> </ul>
Range	<ul style="list-style-type: none"> <li>• 553 nm Operational Range (Full Payload)</li> <li>• 4015 nm Ferry Range (No Payload)</li> </ul>
Payload	<ul style="list-style-type: none"> <li>• 8,000 gallons of fire retardant (72,000 lbs at density 9lbs/gallon)</li> <li>• Multi-drop capable, variable gallons per drop with constant-flow delivery system</li> <li>• Fire retardant reload ≥ 500 gallons/min</li> </ul>
Engines	<ul style="list-style-type: none"> <li>• 4x PW150 A driving Dowty Rotol R408 propellers</li> </ul>
Weight	<ul style="list-style-type: none"> <li>• Empty Weight 68,711 lbs</li> <li>• MTOW=MLW=191,212 lbs (Max Payload with 50,000lbs fuel)</li> </ul>

Fuel	<ul style="list-style-type: none"> <li>Maximum Capacity 8385 gallons</li> </ul>
Ceiling	<ul style="list-style-type: none"> <li>33,200 ft Service Ceiling</li> </ul>
Takeoff Distance	<ul style="list-style-type: none"> <li>4,533 ft Balanced Field Length @ 5000 ft MSL elevation (Design Mission)</li> </ul>
Landing Distance	<ul style="list-style-type: none"> <li>4,101 ft @ 5000 ft MSL elevation (Design Mission, no payload drop)</li> </ul>
Certifications	<ul style="list-style-type: none"> <li>VFR and IFR flight with autopilot (Able to operate in controlled and uncontrolled airspace)</li> <li>Capable of flight in known icing conditions</li> <li>FAA 14 CFR Part 25</li> </ul>
Production	<ul style="list-style-type: none"> <li>\$75 million targeted unit price</li> <li>15 aircraft per year over 20 years</li> </ul>

A CAD model of Firefly is also viewable online at: <https://a360.co/3vmjkv1>

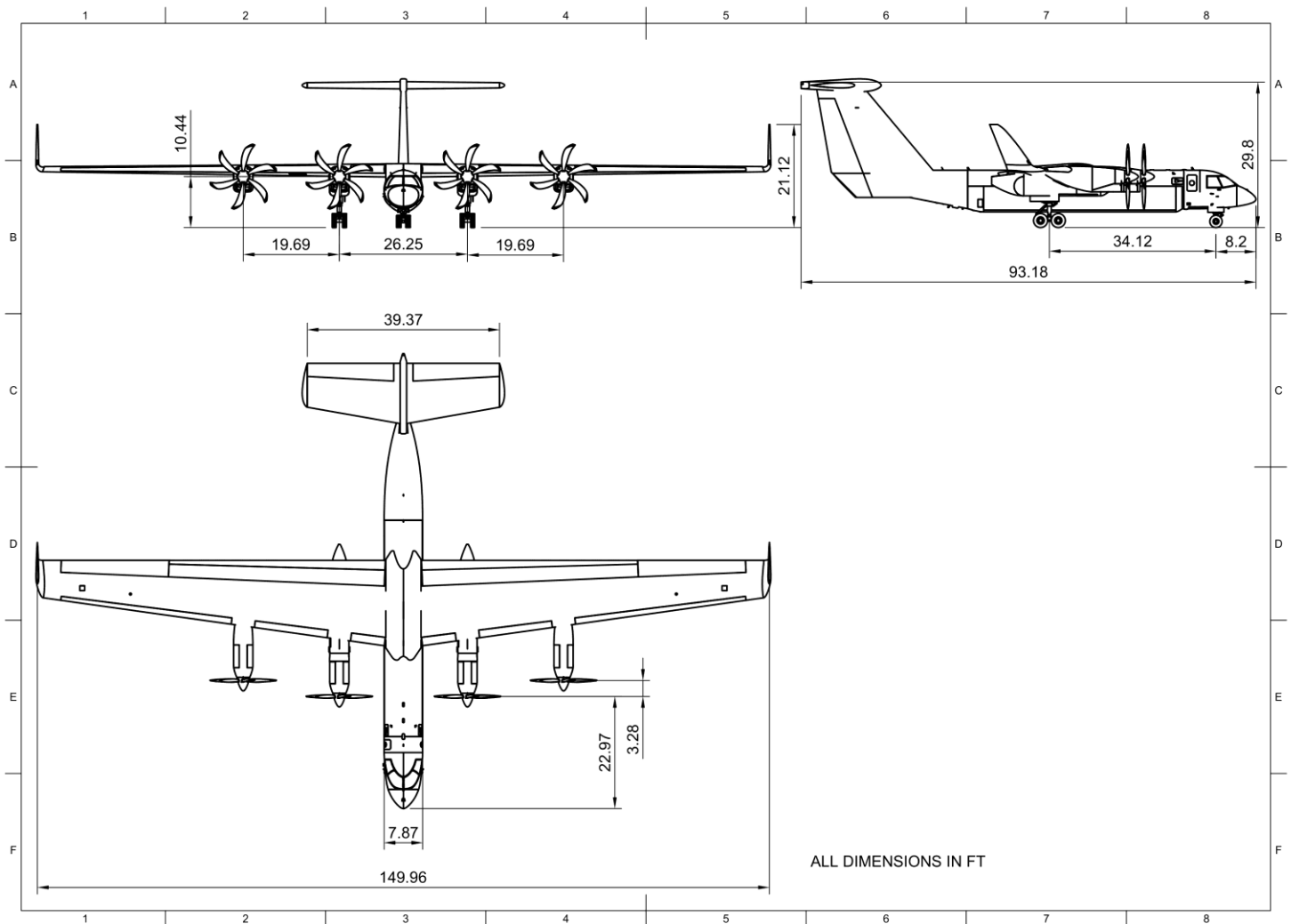


**Figure 1: 3-view drawing of aircraft.**



## Contents

I.	Executive Summary .....	i	7.3	Full Authority Digital Engine Control (FADEC) .....	27
II.	List of Figures .....	iv	7.4	Maintenance Access .....	27
III.	List of Tables .....	vi	7.5	Fuel System .....	28
IV.	Nomenclature .....	vii	8	Retardant Tank .....	30
1	Introduction.....	1	8.1	Selection of Retardant Delivery System	31
1.1	Wildfire Firefighting .....	1	8.2	Tank Structure .....	34
1.2	Market Analysis .....	2	8.3	Drop System .....	35
1.2.1	Gap in Firefighting Capabilities.....	2	8.4	Loading System .....	37
1.2.2	Purpose-Built Firefighting Aircraft..	4	8.5	Vent System .....	38
1.2.3	Projected Increase in Demand .....	4	9	Weight and Balance .....	39
2	Conceptual Design.....	5	9.1	Weight Estimation .....	39
2.1	Concept Generation.....	5	9.2	CG Location .....	40
2.1.1	Concept 1 .....	5	10	Structural Layout.....	41
2.1.2	Concept 2 .....	6	10.1	Materials.....	41
2.1.3	Concept 3 .....	6	10.2	Wing Structural Design .....	42
2.1.4	Concept 4.....	7	11	Empennage.....	45
2.2	Stakeholder Weightings .....	7	11.1	Empennage Design.....	46
3	Initial Sizing.....	9	11.2	Horizontal Stabiliser Sizing.....	46
3.1	Initial Sizing Procedure.....	9	11.3	Vertical Stabiliser Sizing .....	48
3.2	Design Mission Profile.....	10	11.4	Moment Coefficient Slope .....	48
3.3	Ferry Mission Profile .....	11	11.5	Deep Stall .....	50
3.4	Initial Weight Estimation .....	12	11.6	Stability Derivatives .....	50
4	Constraint Analysis.....	13	12	Landing Gear.....	51
5	Wing Design .....	15	12.1	Tire and Wheel Sizing .....	53
5.1	Airfoil Selection .....	15	12.2	Oleo Sizing .....	54
5.2	Winglet Trade Study .....	17	12.3	Gear Retraction and Storage.....	54
5.3	Wing Geometry.....	17	12.4	Turnover Angle .....	56
5.4	Wing Lift Characteristics .....	19	12.5	Aircraft Classification Number (ACN)	57
5.5	High-Lift Devices .....	20	12.6	Turning Radius .....	58
6	Drag Estimation .....	22	13	Flight Performance.....	59
6.1	Parasite Drag .....	22	13.1	Methodology .....	59
6.2	Leakage and Protuberance Drag .....	23	13.2	Design Mission.....	59
6.3	Induced Drag .....	23	13.3	Ferry Mission .....	60
6.4	Trim Drag.....	24	13.4	Performance Summary .....	61
6.5	Drag Polar .....	24	13.5	V-n Diagram.....	62
7	Propulsion .....	26	13.6	Payload Range Diagram .....	64
7.1	Engine and Propeller .....	26	13.7	Fuel Range Diagram.....	65
7.2	Bypass Doors .....	26			

14	Aircraft Systems .....	65	16.1	Avionics Systems .....	75
14.1	De-icing System .....	65	16.2	Autonomous Operations .....	77
14.2	Crew Oxygen Supply System .....	66	16.3	Aircraft Vision Systems .....	78
14.3	Weather and Terrain-Following Radar	66	17	Cost Estimation .....	79
14.4	Electrical System.....	68	17.1	Research Development Test and Evaluation (RDT&E) and Flyaway Costs .....	79
14.5	Hydraulic System.....	70	17.2	Operating Cost Estimation .....	80
14.6	Fire Protection System .....	71	17.2.1	Fuel and Oil Costs .....	80
15	Crew Compartment.....	72	17.2.2	Crew Costs.....	81
15.1	Flight Deck.....	72	17.2.3	Maintenance Costs.....	81
15.2	Cockpit Visibility .....	73	17.2.4	Material Costs.....	81
15.3	Main Entrance Hatch and Emergency Exit	74	17.3	Total Operating Cost and Comparison	81
15.4	Air Conditioning .....	75	18	Conclusion .....	83
16	Avionics.....	75	19	References.....	83

## II. List of Figures

Figure 1: 3-view drawing of aircraft.....	ii	Figure 18: Rear view with flaps extended to 40 degrees (full extension).....	21
Figure 2: Scatter plot of retardant capacity against aircraft range.....	3	Figure 19: Side view of flaps extended to 40 degrees (full extension). Note inboard nacelle deflects together with flaps. ....	21
Figure 3: Wireframe and shaded model of Concept 1.....	5	Figure 20: Extension of ground spoilers together with full flaps and slats deflection. Ground spoilers aid in dumping lift after landing and shortens landing distance. ....	22
Figure 4: Wireframe and shaded model of Concept 2.....	6	Figure 21: Graph of Tail, Wing and Total Lift Coefficients Against Alpha.....	24
Figure 5: Wireframe and shaded model of Concept 3.....	6	Figure 22: Drag Polar Curve at Cruise Conditions .....	25
Figure 6: Wireframe and shaded model of Concept 4.....	7	Figure 23: Bypass door of a DHC-8 in the open position, labelled 'A' [56].....	27
Figure 7: Propulsive efficiency of turbine engines. Chart from ref [38]. ....	9	Figure 24: Open maintenance panels on both sides and lower part of the nacelle. Engine truss structure can also be seen.....	27
Figure 8: Mission profile of design mission. ....	10	Figure 25: Front view of open maintenance panels. .....	28
Figure 9: Mission profile of ferry mission. ....	12	Figure 26: Rear view of open maintenance panels. .....	28
Figure 10: Constraint diagram. ....	14		
Figure 11: Airfoil Profile of NACA 64-2-415.....	16		
Figure 12: Cruise Lift Coefficients Traced onto NACA 64-2-415 Airfoil Graphs.....	17		
Figure 13: Geometry of wing (left side) with flaps, slats, aileron and winglet. ....	18		
Figure 14: Slats extended to 30 degrees. ....	21		

Figure 27: Layout of fuel tanks. ....	28	Figure 52: Dimensioned drawing of main landing gear .....	51
Figure 28: Pressure refueling port on the underside of the right wing. ....	30	Figure 53: Labelled diagram of nose landing gear .....	52
Figure 29: Retardant tank overall dimensions. ....	30	Figure 54: Dimensioned drawing of nose landing gear .....	52
Figure 30: Retardant tank with labelled subcomponents. ....	31	Figure 55: Wheel load geometry.....	53
Figure 31: Types of retardant delivery systems. From top left, clockwise: Internal Discrete Tank in a C-130 [60], External Discrete Tank on a DC-10 [61], Integral Tank on a CL-415 [62], Internal Pressurised Tank in the 747 SuperTanker [63]....	32	Figure 56: Nose landing gear in extended and retracted positions .....	55
Figure 32: Retardant tank design. ....	34	Figure 57: Storage volume estimation (left) 4-wheel bogey, (right) twin .....	56
Figure 33: Exploded view of drop system. ....	35	Figure 58: Main landing gear in extended and retracted positions .....	56
Figure 34: Dimensioned drawing of drop doors, torque tubes and control links.....	35	Figure 59: Turnover angle calculation .....	57
Figure 35: Retardant tank doors in the closed, one-third open, and fully open positions.....	36	Figure 60: Graph of main gear location against turnover angle .....	57
Figure 36: Exploded view of loading system. ....	37	Figure 61: Turning radius diagram .....	58
Figure 37: Loading port showing Camlock coupling and control panel.....	38	Figure 62: Best cruise velocity at different altitudes .....	62
Figure 38: Retardant tank vent system. ....	38	Figure 63: V-n diagram of design mission at sea level.....	63
Figure 39: Aircraft datum and centre of gravity limits. ....	39	Figure 64: V-n diagram of ferry mission at sea level.....	63
Figure 40: Weight and balance diagram. ....	41	Figure 65: Payload Range Diagram for Design Mission without Payload Drop .....	64
Figure 41: Wing structure showing spars and stringers for left wing .....	42	Figure 66: Fuel Range Diagram for ferry mission	65
Figure 42: Stringer sections .....	42	Figure 67: Oxygen supply system.....	66
Figure 43: Spanwise lift distribution at different load factors .....	43	Figure 68: Weather and terrain radar in the nose of the aircraft .....	67
Figure 44: Stress distribution at 1G loading .....	44	Figure 69: Physical layout of electrical system....	68
Figure 45: Stress distribution at 3.25G loading ...	44	Figure 70: Electrical System Schematic Diagram	68
Figure 47: Dimensioned drawing of empennage.	45	Figure 71: External power door.....	70
Figure 48: Scissor plot for horizontal stabiliser sizing. ....	47	Figure 72: Hydraulic System Schematic Diagram	70
Figure 49: VSPAERO simulation using vortex lattice method with elevator deflection $\delta e = -10^\circ$ .....	49	Figure 73: Fire protection system .....	71
Figure 50: Moment Coefficient Chart. ....	49	Figure 75: Dimensioned drawings of flight deck.	72
Figure 51: Labelled diagram of main landing gear .....	51	Figure 76: Cockpit view angles (elevation) .....	73
		Figure 77: Cockpit view angles (side, vertical)....	73
		Figure 78: Cockpit view angles (side, horizontal)	74
		Figure 79: Main Entrance Hatch and Emergency Exit.....	75

Figure 80: Glass cockpit and head-up display unit.  
..... 76

Figure 81: Locations of antennas and probes. .... 77

Figure 82: Enhanced Vision System located on the  
nose of the aircraft. .... 78

Figure 83: Production break-even point..... 80

### III. List of Tables

Table 1: Member Affiliations .....	1	Table 22: CG Position for each loading condition. .....	40
Table 2: Aircraft specifications. ....	i	Table 23: Material properties of Al-7075-T651 [68].....	41
Table 3: Specifications of comparable aircraft. ....	2	Table 24: Dimensions of T-section .....	42
Table 4: Score of each concept with reference to stakeholder weightings. ....	8	Table 25: Dimensions of Z-section .....	42
Table 5: Fuel fractions of design mission. ....	10	Table 26: Parameters of horizontal and vertical stabilisers. ....	45
Table 6: Fuel fractions of ferry mission.....	12	Table 27: CG Limits. ....	48
Table 7: Weight estimation of first sizing. ....	13	Table 28: Parameters of moment coefficient chart. .....	49
Table 8: Flow Characteristics at Cruise Conditions .....	15	Table 29: Stability derivatives. ....	50
Table 9: Performance Specifications of Shortlisted Airfoils.....	15	Table 30: Values for wheel load geometry .....	53
Table 10: Wing parameters.....	19	Table 31: Selected tires for landing gear.....	54
Table 11: Wing Lift Characteristics.....	19	Table 32: Oleo outer diameter .....	54
Table 12: Wing Maximum Lift Coefficient for each Flap and Slat Combination. ....	20	Table 33: Expanded dimensions .....	55
Table 13: Breakdown of Parasite Drag (Excluding Propellers).....	22	Table 34: ACN comparison .....	58
Table 14: Increase in Parasite Drag Coefficient due to Flaps .....	23	Table 35: Fuel Fraction and Fuel Consumed for Mission Segments (Design Mission) .....	59
Table 15: Increase in Lift and Induced Drag Coefficients due to Flaps .....	23	Table 36: Fuel Fraction and Fuel Consumed for Mission Segments (Ferry Mission). ....	60
Table 16: Angle of Attack and Wing and Tail Lift Coefficients at Cruise Lift Coefficient.....	24	Table 37: Summary of aircraft performance. ....	61
Table 17: Total Drag Coefficient for Different Configurations .....	25	Table 38: Maximum Velocity, Absolute and Service Ceilings .....	61
Table 18: Shortlisted Engines and Propellers. ....	26	Table 39: Payload and Range Calculated for Design Mission without Payload Drop .....	64
Table 19: Capacities of each fuel tank.....	29	Table 40: Onboard sensors and their purpose .....	76
Table 20: Pugh matrix showing the score of each tank system with reference to the factor weightings. .....	33	Table 41: DAPCA IV Model Parameters.....	79
Table 21: Component weights and positions. ....	39	Table 42: Results for RDT&E Costs.....	79
		Table 43: Results for flyaway costs per aircraft... 80	
		Table 44: Operating Cost Breakdown.....	82

Table 45: Operating Cost Comparison with  
Commercially Available Firefighting Aircraft [87].

..... 82

#### IV. Nomenclature

AR	= Aspect Ratio	$C_{l_p}$	= Derivative of rolling moment w.r.t roll rate coefficient
$A_p$	= Tire Contact Area	$C_{l_{\delta a}}$	= Derivative of rolling moment w.r.t $\delta_a$ coefficient
b	= Wingspan	$C_m$	= Coefficient of moments
B	= Distance between front and aft wheel	$C_{m_{L=0}}$	= Coefficient of moment at zero lift
BFL	= Balanced Field Length	$C_{m_Q}$	= Derivative of pitching moment w.r.t pitch rate
bhp	= Brake horsepower	$C_{n_\beta}$	= Derivative of yawing moment w.r.t sideslip coefficient
c	= Chord length	$C_{n_R}$	= Derivative of yawing moment w.r.t roll rate coefficient
C	= Specific Fuel Consumption	$C_T$	= Coefficient of Thrust
$C_t$	= Coverages	$C_P$	= Coefficient of Power
CBR	= California Bearing Ratio	$C_{VT}$	= Coefficient of vertical tail
$CBR_1$	= CBR for 1 coverage	$\bar{C}_w$	= Non-dimensional weight
CG	= Centre of gravity	d	= Fuselage diameter
$C_{m,ac}$	= Coefficient of moments about aerodynamic center	$d_t$	= Tire diameter
$C_d$	= Coefficient of Drag for individual components	D	= Drag
$C_D$	= Coefficient of Drag	$D_p$	= Diameter of propeller
$C_{D,min}$	= Minimum Coefficient of Drag	e	= Oswald Efficiency Factor
$C_{D,0}$	= Zero lift drag coefficient	E	= Endurance
$C_{D0_{flap}}$	= Zero lift drag coefficient for flaps	F	= Fuselage lift factor
$C_L$	= Coefficient of lift	$F_{flap}$	= Flap factor
$C_{L,min drag}$	= Coefficient of lift during minimum drag flight	g	= Gravitational Acceleration
$C_{L,climb}$	= Coefficient of lift during climb	G	= Climb Gradient
$C_{l,max}$	= Maximum coefficient of lift for airfoil	hp	= horsepower
$C_{L,max}$	= Maximum coefficient of lift	$h_{obs}$	= Obstacle height
$C_{L_{TO}}$	= Coefficient of lift during take-off	H	= Distance from ground to forward CG
$C_{L,\alpha}$	= Lift slope	$i_t$	= Tail incidence angle
$C_{L,\alpha 0}$	= Coefficient of lift at zero angle of attack	$I_{xx}$	= Moment of inertia about x axis
$C_{l_\beta}$	= Derivative of rolling moment w.r.t sideslip coefficient	$I_{yy}$	= Moment of inertia about y axis



$I_{zz}$	=	Moment of inertia about z axis	$V_{cruise}$	=	Speed during cruise
$J$	=	Advance Ratio	$V_{loiter}$	=	Speed during loiter
$K$	=	Drag polar constant	$V_{stall}$	=	Stall Speed
$K_f$	=	Correction factor	$V_{tip}$	=	Tip Speed of propeller
$K_0, K_{100}$	=	Drag polar constant at 0 and 100 percent suction	$W_f$	=	Weight of Fuel Consumed
$KE_{braking}$	=	Kinetic energy lost due to braking	$w_r$	=	Tire width
$L$	=	Lift	$W_0$	=	Take-off Weight
$L/D$	=	Lift-to-drag ratio	$W_i$	=	Weight of Aircraft during phase $i$
$L_{ht}$	=	Moment arm of horizontal tail	$W_{i-1}$	=	Weight of Aircraft during phase $i - 1$
$L_{vt}$	=	Moment arm of vertical tail	$W/S$	=	Wing loading
$M$	=	Mach number	$X_{ac}$	=	Location of aerodynamic center, expressed with respect to chord length
$M_a$	=	Distance from aft CG to aft wheel	$\bar{X}_{cg}$	=	Location of center of gravity, as a ratio of mean aerodynamic chord
$M_{crit}$	=	Critical Mach Number	$\bar{X}_{np}$	=	Location of neutral point, as a ratio of mean aerodynamic chord
$M_f$	=	Distance from forward CG to aft wheel	$\alpha$	=	Angle of attack
$n$	=	Load factor	$\alpha_{C_{L,max}}$	=	Angle of attack for the maximum lift coefficient
$N_a$	=	Length from front wheel to Aft CG	$\alpha_{L=0}$	=	Angle of attack at zero lift
$P$	=	Roll rate	$\alpha_{stall}$	=	Stall angle of attack
$q$	=	Dynamic pressure	$\gamma$	=	Climb/Descent Angle
$Q$	=	Pitch Rate	$\Gamma$	=	Dihedral angle
$\dot{Q}$	=	Nondimensional pitch rate	$\delta_{emin}$	=	Minimum elevator deflection
$R$	=	Range	$\delta_{flap}$	=	Flap deflection
$R_r$	=	Equivalent radius	$\Delta$	=	Change in
$S$	=	Wing Area	$\theta_{MLG,CG}$	=	Angle of main landing gear with CG
$S_{exposed}$	=	Exposed surface area	$\theta_{Overturn}$	=	Overturn Angle
$S_{flapped}$	=	Area of flaps	$\lambda$	=	Taper Ratio
$S_{ht}$	=	Area of horizontal tail	$\Lambda$	=	Sweep Angle
$S_{land}$	=	Landing distance required to clear obstacle	$\Lambda_{HL}$	=	Hinge Line Angle
$S_{ref}$	=	Reference Area	$\eta$	=	Airfoil efficiency
$S_{vt}$	=	Area of vertical tail	$\eta_p$	=	Propeller efficiency
$S_w$	=	Wetted Area	$\rho, \rho_{SL}$	=	Density at an altitude/ sea level
$t/c$	=	Thickness to chord ratio	$\sigma$	=	Density ratio
$T_{av}$	=	Average Thrust	$\dot{\psi}$	=	Turn rate
$TOP$	=	Take-off Parameter			
$V$	=	Speed			
$V_v$	=	Vertical Speed			

## 1 Introduction

### 1.1 Wildfire Firefighting

The climate changes experienced in the recent decade have resulted in warmer and drier weather conditions, resulting in more drought occurrences and longer fire seasons throughout the year. Research has projected that an average increase of 1°C in annual temperature would trigger a 600 percent increase in the median burnt area every year in some forests. This increased wildfire risks will spark at least a 30 percent increase in burnt areas by 2060, with warmer and drier conditions causing wildfires to spread faster and add to the difficulty in putting them out [1]. With these alarming statistics, many governments worldwide are seeking for better wildfire suppression methods, one key part of which is aerial firefighting. Wildfire aerial firefighting may be costly, but it is a crucial component in ensuring effective firefighting resource planning [2]. Fixed-wing aerial firefighting aircraft are mainly categorised into Type I, Type II and Type III airtankers. Type I airtankers consist of the largest and fastest flying types while Type III airtankers are the smallest in size.

Large Air Tankers typically drop fire retardant, which adheres better to the vegetation compared to water. Thus, these drops are performed to lay retardant lines ahead of a fire to prevent further spread [3], as opposed to dropping directly on the flame front [4]. To maximise the effectiveness of the release of retardants or water, these aircraft need to fly no higher than 200 feet above the trees. For low-flying aircraft, the safe-drop altitude is between 100 feet to 120 feet above the wildfire. This height will minimise the chances of any liquid retardant turning into aerosol [5]. During the drop, aircraft fly at an altitude of 150 ft AGL following the terrain, at approximately 110-140 knots equivalent airspeed in order to provide the ideal conditions for the propellant to effectively coat the surface of the ground and vegetation. This usually results in the aircraft flying at half to full flaps and at high thrust settings, which also has the benefit of providing timely access to power on flap retraction after a drop and to execute terrain avoidance manoeuvres [6].

A seminal study performed by NASA on the operating experiences of two DC-6B aircraft (4-piston engines) in the role of retardant bombers highlights the variation in speeds, durations, and load factors that can be experienced by firefighting aircraft. Higher dash speeds were used in longer-duration flights beyond 20 minutes. Descent rates also varied depending on the terrain, with steep approaches of up to a 9,000 ft/min descent rate recorded for fires along ridge walls or bottom of canyons, and 30% of missions exceeding 3,000 ft/min. Load factors between -0.5 and 3.9 were also recorded, with the highest load factor experienced during a manoeuvre executed to avoid colliding with a canyon wall after a drop [7].

## 1.2 Market Analysis

### 1.2.1 Gap in Firefighting Capabilities

Market research was conducted on current firefighting aircraft, as shown Table 3 below.

**Table 3: Specifications of comparable aircraft.**

Aircraft	CL-415/515 <sup>1</sup>	McDonnell Douglas DC-10 <sup>2</sup>	Ilyushin Il-76 <sup>3</sup>	McDonnell Douglas MD-87 <sup>4</sup>	Martin Mars <sup>5</sup>
Type	Purpose-built amphibious aircraft	Converted Airliner	Long range heavy cargo transport (military)	Converted Airliner	Large cargo transport flying boat
Length (ft)	66.93	182.09	152.85	130.41	117.26
Height (ft)	29.46	58.07	48.43	30.35	49.21
Wingspan (ft)	92.72	155.48	165.68	107.68	200
Empty Weight (lbs)	30,000	267,200	202,825	73,193	75,572
Max Takeoff Weight (lbs)	43,850	430,000	418,878	139,994–149,473	165,000
Fire Retardant Capacity (Gallons)	1,621	12,000	11,419	4,000	7,200
Wing Area (ft <sup>2</sup> )	1076.39	3957.89	3229.17	1208.79	3685.56
Wing Loading (lbs/ft <sup>2</sup> )	40.74	108.65	129.73	123.67	44.78
Powerplant	2x PW123AF Turboprops	3x GE CF6-6D Turbofan	4x Soloviev D-30KP Turbofan	2x P & W JT8D-200 series Turbofan	4x Wright R-3350 Duplex-Cyclone
Maximum Speed (kts)	194	491	486	448	192
Stall Speed (kts)	68	115	-	-	<80
Range (Ferry) (nmi)	1310	3510	2160	2376	4300
Takeoff Distance (ft)	2570	11,670	-	6069	-
Landing Distance (ft)	2210	5,960	1,476	4691	-
Crew	2, seating available for 9 additional passengers	3, pilot, co-pilot, flight engineer	5	2	-
Unit Cost (million USD)	35 (2013) 43.4 (inflation-adjusted, 2022)	20 (1972) 138.3 (inflation-adjusted, 2022)	50 (2008) 67.1 (inflation-adjusted, 2022)	41.5 (1990) 91.8 (inflation-adjusted, 2022)	-

<sup>1</sup>[8] <sup>2</sup>[9] <sup>3</sup>[10] <sup>4</sup>[11] <sup>5</sup>[12] [13] [14] [15] [16] [17] [18] [19] [20] [21] [22] [23]



A scatter plot was also created to summarize the firefighting performance of current aircraft, as shown in Figure 2. The vertical axis denotes the retardant tank capacity of the aircraft in US gallons, while the horizontal axis denotes the range of the aircraft in nautical miles. Since the range of aircraft during a firefighting mission, or “combat radius”, is seldom available, the cross-country range of the aircraft was used as a proxy. This information is used to visualise the capabilities of current firefighting aircraft.

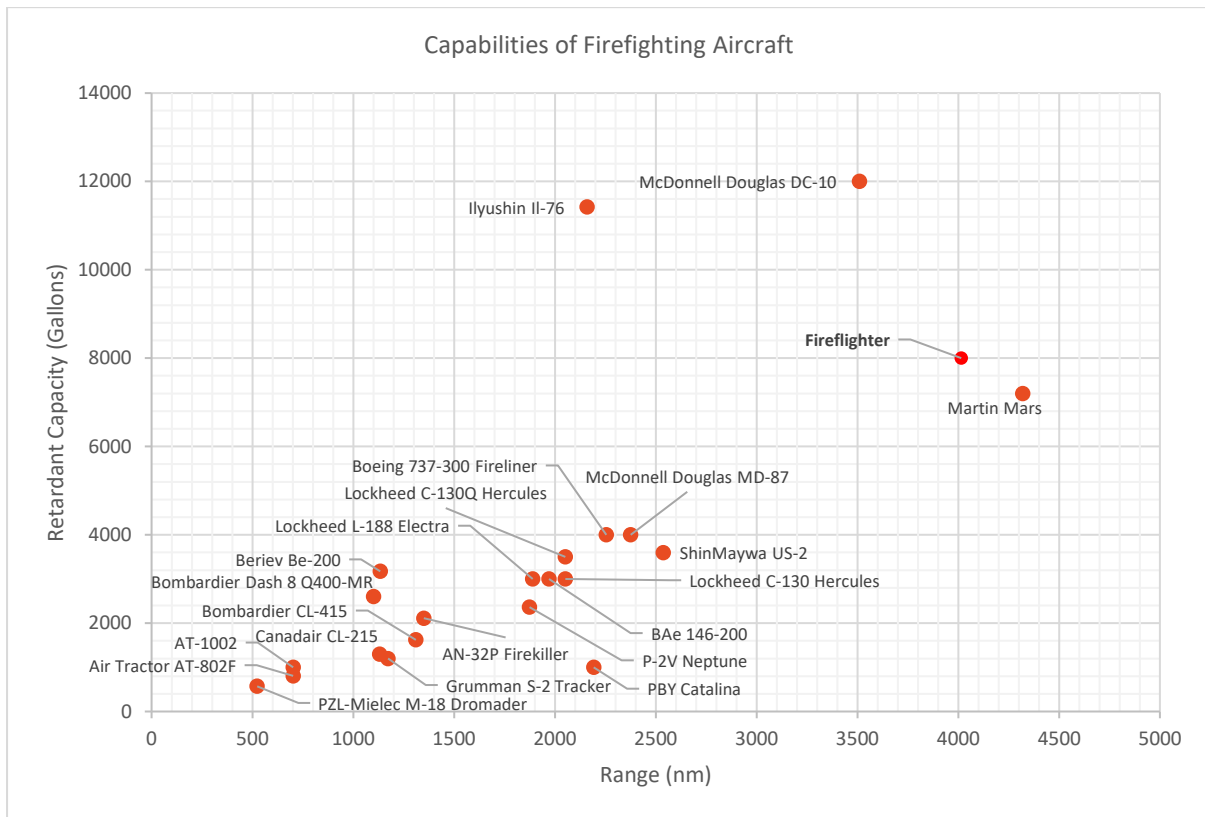


**Figure 2: Scatter plot of retardant capacity against aircraft range.**

From the plot, a market gap is apparent in the 4,000 to 10,000-gallon capacity and 2,500 to 4,000 nautical miles range capability. This corresponds closely to the specifications set out in the RFP and highlights the tremendous opportunity in the firefighting aircraft market for a design within these performance specifications. The closest comparable aircraft within this capability gap is the Martin Mars, which unfortunately has been decommissioned in 2015 after operating for 50 years [24]. Aircraft at the higher end of the capability gap such as the 747 Supertanker and the DC-10 are also expected to be phased out in the coming 10-20 years, as many are now around 20-30 years old. In fact, the Supertanker has already been forced into retirement once in 2021 when investors decided to cease operations in April [25]. Firefighter was thus designed for a retardant capacity of 8,000 gallons.

### 1.2.2 Purpose-Built Firefighting Aircraft

Firefighting aircraft also face a multitude of problems and challenges when performing their mission, such as turbulence at lower altitudes. From the statistics obtained between the years 2000 and 2013, more than half of the accidents involving firefighting aircraft occur on fixed-wing aircraft (55%). About 24% of the total accidents were caused by structural or component failure [26]. In 2002, two fatal crashes of firefighting aircraft occurred within a month in the United States. Both crashes occurred after the wings separated from the aircraft (a PB4Y-2 and C-130A) while in flight due to fatigue cracks. As a result, a review was undertaken on the safety of these firefighting aircraft, which were mostly converted from old military and civilian aircraft [27].

With the aging of airtanker fleets exacerbated by repeated excess structural loads, there is a need to evaluate the kinds of aircraft which are fit to serve in the aerial firefighting role in the future. One proposal floated in 2014 discussed converting the A-10 close air support aircraft into a 2,000-gallon air tanker, since the aircraft was originally designed for a low-altitude mission profile and high structural loads, similar to aerial firefighting. [28]. Purpose-built aircraft specially designed for the aerial firefighting role are thus a safer and more effective platform to perform the firefighting mission, as they can be designed to withstand the structural loads while meeting performance requirements, unlike converted aircraft where compromises must be made.

### 1.2.3 Projected Increase in Demand

Wildfire suppression costs are increasing rapidly worldwide. In just the United States, federal wildfire suppression costs have increased by over the past 40 years, with an annual average expenditure of \$1.6 billion from 2000 to 2019. When these estimates are applied in the context of global climate-change induced wildfires, there is a forecasted expenditure of \$5 to \$30 billion annually in 2050. This rapid increase in expenditure can be attributed to the increase in size and number of forest fires due to changes in forest fire patterns, which are expected to happen across the globe [29].

Fire seasons around the world are also getting longer each year, causing seasons from different regions to overlap with one another. As a result, countries no longer have the leeway to share their resources or render assistance to other countries experiencing wildfires. In reaction to this, countries around the world are beginning to build their own firefighting forces or expand their existing fleet [30] [31] [32]. Some notable examples include Greece, who is investing \$1.76 billion to establish their own firefighting taskforce and China, who has already made a purchase for seventeen AG600 aircraft to be delivered in 2022 [33] [34].

If these trends are to continue through the next two decades, it is likely that the demand for large firefighting tankers will increase more and more rapidly. Countries who were unable to react to the extended fire seasons are already starting to experience a huge shortage in firefighting resources. In the US, a report released by the United States Forest Service (USFS) in 2020 indicated that the resources available to firefighters were not able to keep up with the huge demand [35]. Hundreds of requests for large air tanker support have been indicated as “UTF”, or unable to be filled, meaning that there were no tankers of that size available to fill the request. This shortage is also evident in the number of aircraft which are currently available for firefighting. As of 2021, there are currently only 18 air tankers under exclusive use contracts. This is in stark contrast to 2002, where there used to be a fleet of 44 airtankers [36].

The current firefighting aircraft market is valued at \$2.21 billion, with the market expected to grow at a Compound Annual Growth Rate (CAGR) of 2.98% from 2021 to 2026 to a value of \$2.64 billion. As a result, there are ample opportunities for newer purpose-built aircraft to meet the projected demand and fill the gap left by the retirement of the current airtankers. Viking Air, the manufacturer of the popular CL-415 series of amphibious firefighting aircraft, estimates an optimistic production volume of approximately 100 aircraft, minimum, of their new CL-515 aircraft across 20-25 years [37].

## 2 Conceptual Design

### 2.1 Concept Generation

After reviewing the features of current firefighting aircraft, 4 different concepts were generated as part of the ideation process.

#### 2.1.1 Concept 1

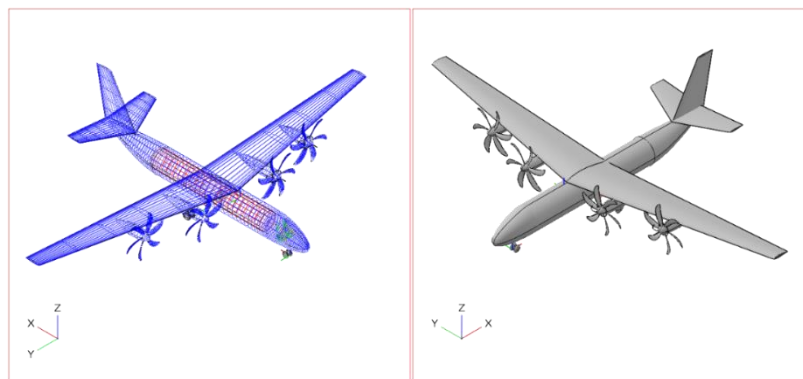


**Figure 3: Wireframe and shaded model of Concept 1.**

Concept 1 is a 4-engined turboprop design with a high wing and conventional empennage. As the wing carry-through structure passes over the fuselage, the mechanisms for releasing fire retardant can be easily installed into the bottom of the fuselage. A high-wing configuration also allows for the installation of large flaps important for low-speed flying during a payload drop, and it also contributes to additional clearance between the large propellers and the ground. The high density of the payload also means that large internal volume is unnecessary, permitting a narrow and slender fuselage that reduces frontal and wetted area, contributing to better aerodynamic performance.

### 2.1.2 Concept 2

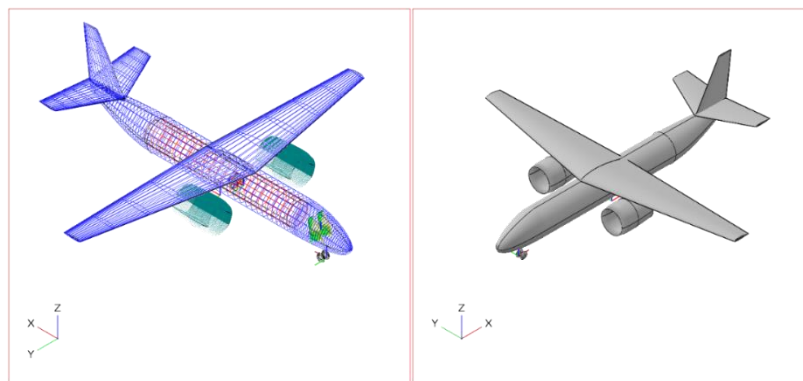


**Figure 4: Wireframe and shaded model of Concept 2.**

Concept 2 is a high-wing aircraft with wing-mounted podded engines. Similar to Concept 1, this design takes reference from the current purpose-built firefighting aircraft such as the CL-415/515 and the Be-200, which also have high-wing designs. However, the engines in Concept 2 are mounted under the wings for ease of maintenance. Due to the higher thrust available from turbofan engines, only two engines are needed in order to meet takeoff length requirements.

### 2.1.3 Concept 3

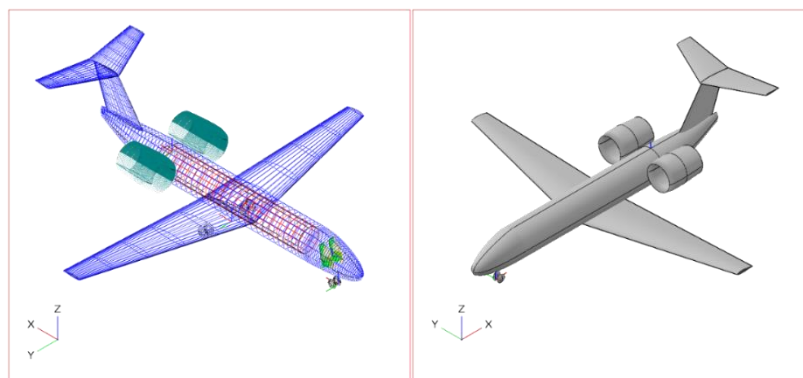


**Figure 5: Wireframe and shaded model of Concept 3.**

Concept 3 uses the same fuselage design as Concept 2. However, a low wing is used together with fuselage-mounted engines in order to provide a clean wing as well as to simplify the retraction and stowage of the landing gear. The wings also shield the engines from debris on the runway if operating on unprepared airfields. However, the engine arrangement means that there is a risk of ice ingestion into the engines if ice built-up on the wings is not properly managed. In addition, additional structures may be required under the keel beam to release the fire retardant, similar to most converted low-wing civil aircraft.

#### 2.1.4 Concept 4

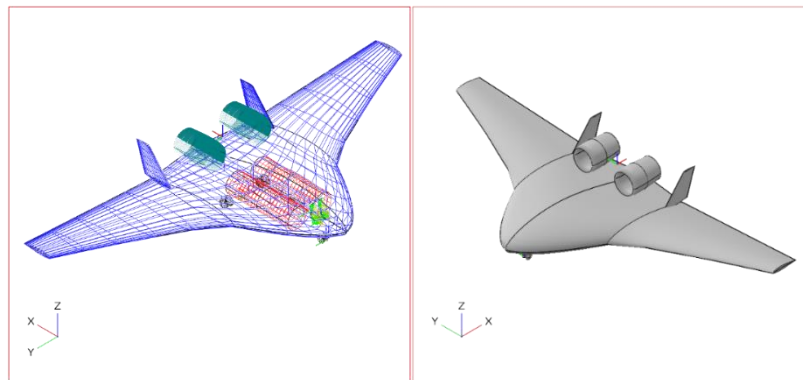


**Figure 6: Wireframe and shaded model of Concept 4.**

Concept 4 is a blended wing body design that is designed to maximise aerodynamic efficiency. Due to the shorter length of the fuselage, the payload is housed in two tanks side-by-side within the main body. Vertical surfaces are added to aid in directional stability, which would be important in the heavy manoeuvring that takes place during a payload drop. As the engines are mounted over the fuselage however, maintenance access would be difficult. In addition, large flaps may not be practical due to the large aerodynamic moments produced, although careful airfoil selection may mitigate the effects.

## 2.2 Stakeholder Weightings

To select between the concepts, stakeholder weightings were applied to quantify the features and characteristics that are the most critical for an aerial firefighting aircraft. These are cost, maintainability, manoeuvrability, aerodynamic efficiency, and takeoff performance. Of these parameters, cost is the most important and thus has the highest weighting. This is because users of aerial firefighting aircraft are mostly public agencies with a tight budget and a purpose-built aircraft has to be economical enough to justify its narrow specialisation. Maintainability has the same weighting as cost due to the heavy and repeated loads experienced during an aerial firefighting mission. Hence, provisions for structural health monitoring as well as easy repair and replacement of damaged components must be considered in the design. Manoeuvrability of the aircraft is next in importance

due to the descent, turns and pull-up manoeuvres required during a mission. Aerodynamic efficiency is less important due to the short times and distances involved transiting between the base airfield and drop point, and thus has the lowest weightage. Takeoff performance enables the aircraft to operate from smaller airfields closer to the drop point, reducing transit distances and times.

Concepts 1, 2, and 3 have the lowest cost due to being conventional configurations, with Concept 3 scoring slightly lower due to additional structures required in installing the retardant drop mechanisms. As Concept 1 is a turboprop-driven aircraft, it is the most economical both in terms of unit and operating costs despite having more engines. Concept 4, being a blended wing body, has the highest cost due to the significant investments into research and development required to overcome the stability and control issues of such a design. Concept 4 also scores slightly lower in maintainability due to the difficulty in accessing the engines. Both Concepts 2 and 3 have the same score in manoeuvrability, with Concept 1 scoring lower due to the additional mass of the outboard engines which increases the rolling moment of inertia and thus reduces roll rate. Concept 4 scores the lowest in this category due to the small tail moment arm which affects pitch control, which affects its ability to perform pull-up manoeuvres when flying near the ground. Concept 4 scores the highest in aerodynamic efficiency, followed by Concept 3 with its clean wing. Concept 1 is less aerodynamically efficient due to its wing-mounted engines, which interferes with the airflow over the wing. Concepts 2, 3, and 4 have better takeoff performance compared to Concept 1 as the turbofan engines are able to provide greater thrust compared to turboprops. The Pugh matrix below summarises the ability of each concept to meet the stakeholder weightings.

**Table 4: Score of each concept with reference to stakeholder weightings.**

Characteristic	Weighting	Concept 1	Concept 2	Concept 3	Concept 4
Cost	5	5	4	3	2
Maintainability	5	5	5	5	4
Manoeuvrability	4	4	5	5	3
Aerodynamic Efficiency	3	4	3	4	5
Takeoff Performance	4	4	5	5	5
Total Score:	-	94	94	92	77

Concepts 1 and 2 have the highest score, and thus further analysis was performed to down-select the optimal concept for further development, taking into account cost and takeoff performance. After comparing different engines currently in service (PW150, TP400, LEAP-1A, Passport 20), the cost of a turbofan engine was found to

be between 5 to 10 times higher compared to a turboprop engine, while producing only 2 to 3 times the thrust. Thus, from a unit cost perspective, it is preferable to use two turboprops instead of a single turbofan if there are no other design requirements to be met. As the aircraft will also spend most of its time between 125 knots (payload drop) and 400 knots (dash speed), a turboprop engine is ideal as it has the highest propulsive efficiency within that speed range as shown in Figure 7 below. From an operating cost perspective, turboprops are thus preferred.

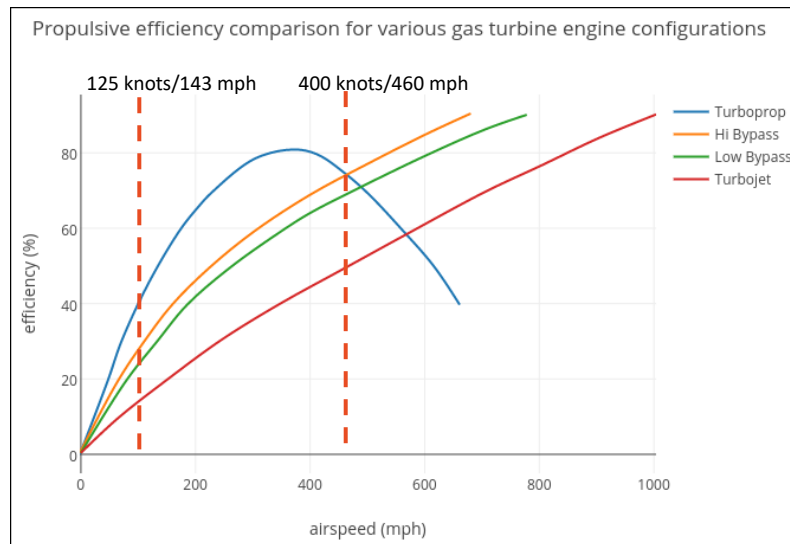


**Figure 7: Propulsive efficiency of turbine engines. Chart from ref [38].**

However, a turbofan engine may still be necessary in order to meet the Balanced Field Length (BFL) requirement of  $\leq 5000$ -8000 ft at 5000 ft MSL elevation. To estimate the BFL, an empirical formula from Raymer was used, assuming a takeoff lift coefficient of 2.5 (fowler flap and low sweep), 70 lbs/ft<sup>2</sup> wing loading (similar to the Be-200), and a take-off weight of 180,000lbs (slightly higher than the Martin Mars). From the calculations, it was shown that although turbofan engines are able to provide superior takeoff performance, turboprops are also capable of meeting the minimum requirements. Thus, the configuration in Concept 1 with turboprop engines was selected due to the lower unit and operating costs.

## 3 Initial Sizing

### 3.1 Initial Sizing Procedure

The first sizing is performed based on the process described in Raymer Chapter 3, where the weight of the aircraft is broken down into a crew weight of 500 lbs and payload weight of 72,000 lbs (8000 gallons of retardant at 9lbs/gallon), and the empty weight fraction  $W_e/W_0$  estimated using the statistical weight equations. The takeoff weight can then be estimated based on an iterative process. Based on the wetted aspect ratio of 2.20

from the conceptual design, an  $\left(\frac{L}{D}\right)_{max}$  of 17 was estimated. As the Firefly is comparable to a Large Air Tanker, the aircraft was designed to comply with FAR 25 Transport Category Airplanes as well as Part 91 General Operating and Flight Rules. This is similar to converted civil passenger or cargo aircraft such as the DC-6 which operate under their original FAR 23 or FAR 25 certifications even after being converted into airtankers [39]. This defines the fuel reserves required in the mission profile, where Part 91.151 requires 30 minutes (day) and 45 minutes (night) reserve fuel at normal cruising speed under VFR conditions [40]. Under IFR conditions, Part 91.167 applies, mandating sufficient fuel to complete the flight to the first intended airport and fly from that airport to the alternate airport with 45 minutes of reserve fuel at normal cruising speed [41].

### 3.2 Design Mission Profile

The design mission of the aircraft involves taking off from the base airfield, flying 400 nm to the area of operations, descending to less than 300 ft AGL and manoeuvring at less than 125 knots for 4 payload drops. Thereafter, the aircraft will climb back to 20,000 ft, dash at 400 knots for 400 nm before descending and landing back at the base airfield. To meet IFR requirements, however, additional reserve fuel is required for the aircraft to climb, cruise, and descend to an alternate airfield which could be 100 nm away, with an additional 45 minutes of fuel remaining.

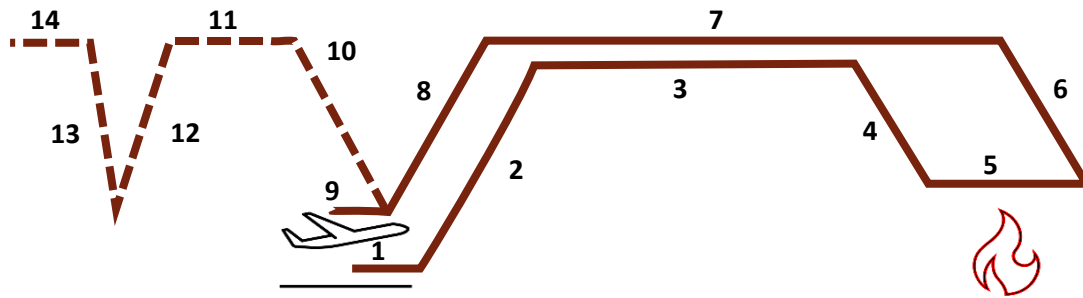


**Figure 8: Mission profile of design mission.**

**Table 5: Fuel fractions of design mission.**

Mission Segment		Fuel Fraction	
1	Warmup, taxi and takeoff	$W_1/W_0$	0.97
2	Climb to 20,000 ft	$W_2/W_1$	0.985
3	Cruise for 400 nm	$W_3/W_2$	0.962877



4	Descent	$W_4/W_3$	1
5	Manoeuvring for payload drop (Sea level conditions)	$W_5/W_4$	0.996729
6	Climb to 20,000ft	$W_6/W_5$	0.985
7	Dash at 400 knots for 400 nm	$W_7/W_6$	0.96574
8	Descent	$W_8/W_7$	1
9	Landing and Taxi	$W_9/W_8$	0.995
10	[Reserve] Climb to 20,000ft	$W_{10}/W_9$	0.985
11	[Reserve] Cruise 100 nm to divert field	$W_{11}/W_{10}$	0.990587
12	[Reserve] Descent	$W_{12}/W_{11}$	1
13	[Reserve] Climb to 5,000 ft	$W_{13}/W_{12}$	0.985
14	[Reserve] 45 minutes at cruising speed	$W_{14}/W_{13}$	0.972716
Total Mission Weight Fraction		$W_{14}/W_0$	0.7938
Mission Fuel Fraction (Including 6% allowance)		$W_f/W_0$	0.2184

### 3.3 Ferry Mission Profile

The ferry mission of the aircraft involves taking off from one airfield without payload, flying 3000 nm then descending and landing at another airfield. To meet IFR requirements, however, additional reserve fuel is required for the aircraft to climb, cruise, and descend to an alternate airfield which could be 100 nm away, with an additional 45 minutes of fuel remaining.

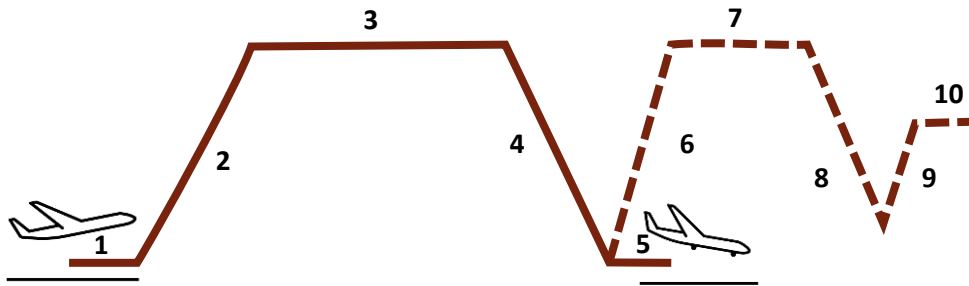


**Figure 9: Mission profile of ferry mission.**

**Table 6: Fuel fractions of ferry mission.**

Mission Segment		Fuel Fraction	
1	Warmup, taxi and takeoff	$W_1/W_0$	0.97
2	Climb to 20,000 ft	$W_2/W_1$	0.985
3	Cruise for 3000 nm	$W_3/W_2$	0.752975
4	Descent	$W_4/W_3$	1
5	Landing and Taxi	$W_5/W_4$	0.995
6	[Reserve] Climb to 20,000ft	$W_6/W_5$	0.985
7	[Reserve] Cruise 100 nm to divert field	$W_7/W_6$	0.990587
8	[Reserve] Descent	$W_8/W_7$	1
9	[Reserve] Climb to 5,000 ft	$W_9/W_8$	0.985
10	[Reserve] 45 minutes at cruising speed	$W_{10}/W_9$	0.972716
Total Mission Weight Fraction		$W_{10}/W_0$	0.6290
Mission Fuel Fraction (Including 6% allowance)		$W_f/W_0$	0.3932

### 3.4 Initial Weight Estimation

From the initial weight estimation, the takeoff weight for the design mission was calculated to be 188,422 lbs, while the takeoff weight for the ferry mission was calculated to be 2,044 lbs. The takeoff weight for the design

mission is in the same order of magnitude as current aircraft performing the same mission with similar payloads, validating the result of the first sizing. However, the sizing of the ferry mission specifies a much smaller aircraft.

This is because the ferry mission has no payload component, and thus this iterative method sizes the aircraft to only carry two crewmembers across the ferry mission profile. As a result, there is no need for a large aircraft and the weight estimation is actually close to real-life two-seater turboprop aircraft, such as the Pilatus PC-9 (3,803 lbs empty weight, 5,181lbs gross weight [42]). As the design mission results in a higher empty weight, the estimate from the design mission is used as the aircraft empty weight estimate. In addition, the fuel fraction from the ferry mission is used to calculate the amount of fuel as well as the takeoff weight of the aircraft during the ferry mission. Thus, the result of the first sizing is given in the Table 7 below.

**Table 7: Weight estimation of first sizing.**

Weight (lbs)	Design Mission	Ferry Mission
$W_e$	74,711	
$W_{crew} + W_{payload}$	72,500	500
$W_f$	41,151	48,735
$W_0$	188,422	123,946

## 4 Constraint Analysis

After completing the initial weight estimation, the other critical parameters that remain to be estimated are the wing size  $S$  as well as the required power  $P$ . These parameters are sized based on the required aircraft flight performance through constraint analysis, based on Raymer Chapters 5 and 17. The dash speed (400 knots at 20,000 ft), stall speed (100 knots based on 125 knot retardant drop speed), take-off distance (5,000 ft) and landing distance (5,000ft) requirements based on the RFP were plotted for each combination of power to weight ratio ( $P/W$ ) and wing loading ( $W/S$ ), representing the boundaries of the possible design space for which the aircraft will meet those requirements. The constraint diagram is shown in Figure 10 below.

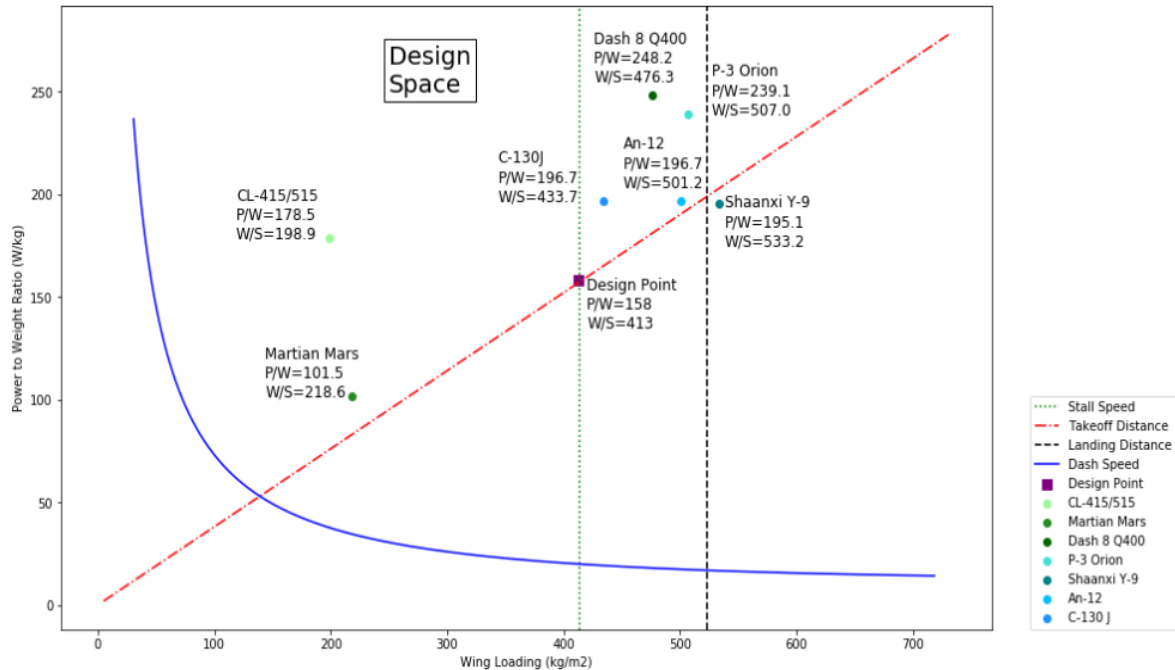


**Figure 10: Constraint diagram.**

The design point was targeted to lie in the rightmost and bottommost location of the design space, as seen in Figure 10 above. The rightmost location is desired because a higher wing loading would lead to a smaller wing area, which minimizes weight and cost. The bottommost location is desired because a lower power to weight ratio would mean that a less powerful engine can be used, which generally reduces cost. The design point, as indicated by a purple square, specifies a power to weight ratio of 0.096 hp/lb and a wing loading of 84.60 lbs/ft<sup>2</sup>. Similar aircraft were also plotted. Aircraft designed for firefighting roles such as the Martin Mars and CL-415/515 have lower wing loadings. However, it should be noted that these aircraft are amphibians and are thus designed for a much lower stall speed for water landings. Among 4-engined turboprop aircraft, the design point specifies a slightly lower wing loading as well as power-to-weight ratio, although the difference is not as significant as compared to the amphibious aircraft. Thus, this shows that the design point is achievable with current technology and would produce an aircraft with a lower stall speed and slightly longer takeoff distance compared to similar 4-engined turboprops. With a takeoff weight of 188,422 lbs estimated in the initial sizing, this means that the aircraft will require a minimum wing size of 2227.05 ft<sup>2</sup> and minimum total power of 18,108 hp, or 4527 hp per engine.

## 5 Wing Design

### 5.1 Airfoil Selection

The selection of the airfoil is crucial as it has a significant impact on the aircraft performance throughout its flight regime. In this case, flight time divided between cruising to and from the drop site and low speed and altitude manoeuvring during the drop itself, which results in opposing requirements. At low speeds, an airfoil with high maximum lift coefficient and good stalling characteristics is preferred, which can be achieved using an airfoil with high camber and large leading edge radius. However, such an airfoil is not efficient during the cruise segments of the mission. The airfoil selection thus becomes a compromise between different airfoil characteristics. Since the aircraft will spend a considerable amount of time in cruise during the ferry mission, an airfoil which was ideal for cruise conditions was selected, with the desired low-speed characteristics achieved through the use of high-lift devices. Table 8 shows the flow characteristics at cruise conditions.

**Table 8: Flow Characteristics at Cruise Conditions**

Velocity (ft/s)	Kinematic Viscosity (ft <sup>2</sup> /s)	Reynold's Number
672.57 (M0.65)	2.6203 X 10 <sup>-4</sup>	2.8129 X 10 <sup>7</sup>

Table 9 shows the five shortlisted airfoils and their performance specifications at a Reynold's number of 1,000,000 [43].

**Table 9: Performance Specifications of Shortlisted Airfoils**

Airfoil	C <sub>Lmax</sub>	C <sub>Dmin</sub>	C <sub>m</sub> range	(C <sub>L</sub> /C <sub>D</sub> ) <sub>max</sub>
NACA 4412	1.57	0.007	-0.108 to -0.045	129
NACA 23012	1.55	0.007	-0.045 to 0.02	97
NACA 64 <sub>2</sub> -415	1.40	0.006	-0.081 to -0.03	120
CLARK V	1.50	0.005	-0.09 to -0.025	129
Wortmann FX 60-126/1	1.62	0.006	-0.13 to -0.05	113

As seen from Table 9, the Wortmann FX 60-126/1 airfoil has the highest C<sub>Lmax</sub>, followed by the NACA 4412 airfoil and the NACA 23012 airfoil. The C<sub>Dmin</sub> for the airfoils do not vary significantly. The NACA 23012 airfoil has the smallest absolute C<sub>m</sub>, followed by the NACA 64<sub>2</sub>-415 airfoil and the CLARK V airfoil. The NACA 4412 airfoil and CLARK V airfoil have the highest (C<sub>L</sub>/C<sub>D</sub>)<sub>max</sub>, followed by the NACA 64<sub>2</sub>-415 airfoil.

As the aircraft will be in cruise for a long period of time, good aerodynamic efficiency is an important factor in choosing the airfoil. While the Wortmann FC 60-126/1 airfoil has the highest  $C_{L_{max}}$  and one of the highest  $(C_L/C_D)_{max}$ , making it an ideal airfoil for low speed applications, the pitching moment  $C_m$  is considerably higher than the other airfoils. This would result in a large tail moment required to trim the aircraft, resulting in high trim drag, and would also make the use of high-lift devices problematic as they would result in additional pitching moment. Thus, this airfoil is mostly used on sailplanes which have a large tail moment arm and do not have high lift devices and is seldom used elsewhere [44]. With the exception of  $C_{L_{max}}$ , the NACA 64<sub>2</sub>-415 airfoil has decent performance specifications. Thus, considering all the performance specifications of the airfoils above, the NACA 64<sub>2</sub>-415 airfoil was selected, as the laminar drag bucket also results in a small drag coefficient across a range of angles of attack, allowing the aircraft to fly efficiently across different weights. Figure 11 shows the profile of the NACA 64<sub>2</sub>-415 airfoil. Figure 12 shows cruise lift coefficients calculated using different speeds and weights traced onto the airfoil  $C_L$  vs  $C_D$ ,  $C_L$  vs  $\alpha$  and  $C_D$  vs  $\alpha$  graphs. As seen from Figure 12, all cruise lift coefficients lie within the laminar drag bucket, allowing the aircraft to experience minimal drag during cruise and thus improve aerodynamic efficiency.

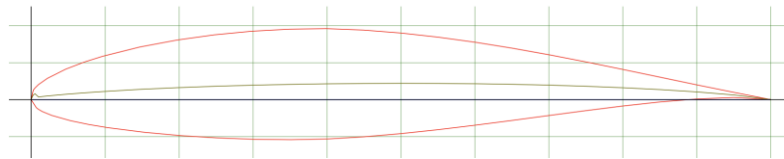


**Figure 11: Airfoil Profile of NACA 64-2-415**

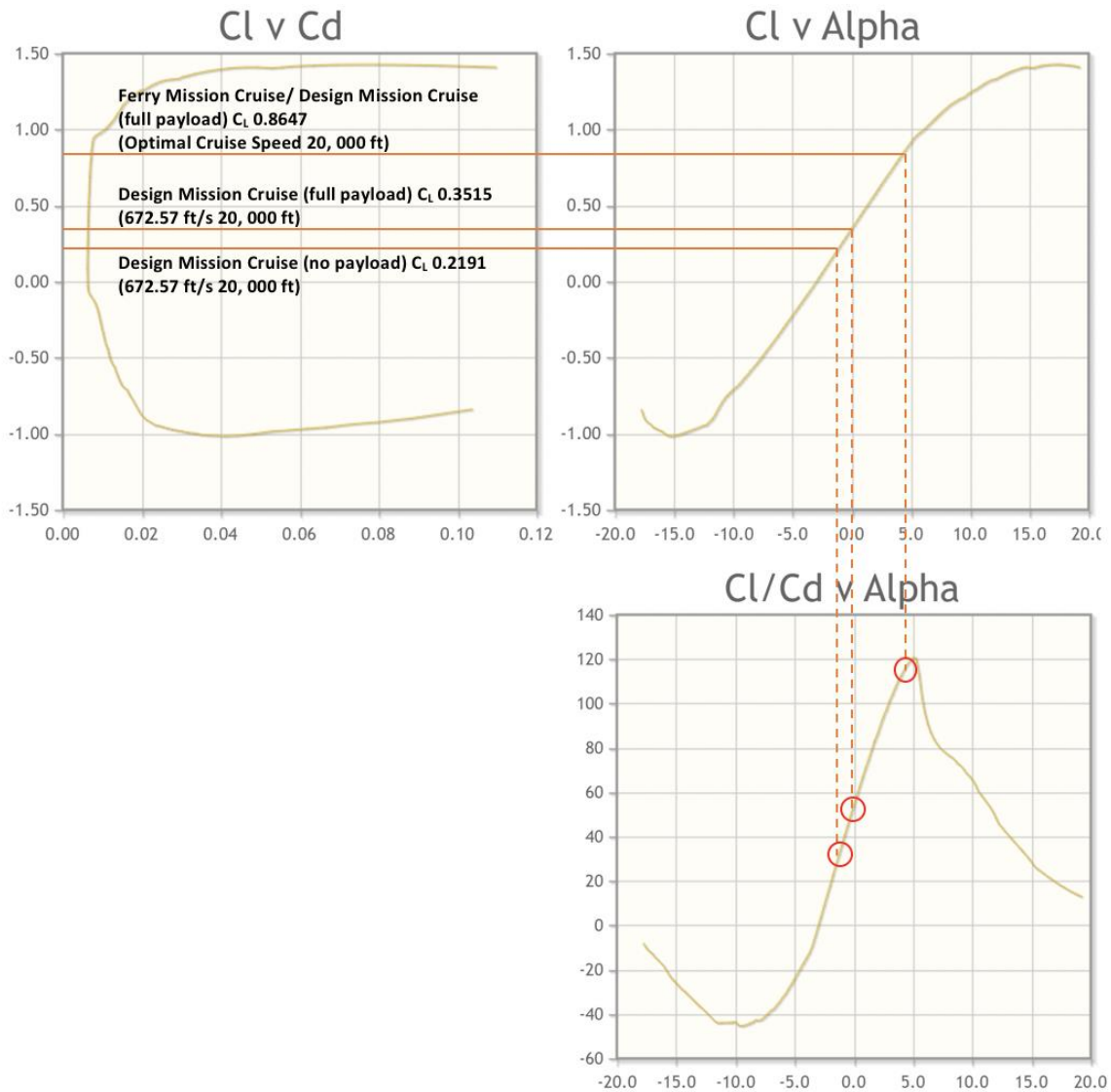


**Figure 12: Cruise Lift Coefficients Traced onto NACA 64-2-415 Airfoil Graphs**

## 5.2 Winglet Trade Study

Winglets are used in many modern commercial aircraft to help to reduce induced drag. However, they add additional weight of the aircraft. Thus, a trade study was performed in order to decide if it is feasible to add them to the aircraft. The winglet design of the A320neo (Sharklets), which reduces total drag by 4% was considered in this trade study. Using equations from Scholz [45], it was estimated that the addition of winglets and the associated strengthening of the wing structure added approximately 2.3% to the aircraft's empty weight. Thus, the addition of winglets is a justified design choice.

## 5.3 Wing Geometry

The geometry of the designed wing from Iteration 2 is shown in Figure 13 and Table 10. Although the constraint diagram specifies a minimum wing area of 2227.05 ft<sup>2</sup> in order to meet stall requirements, this value is for a

wing with fully deflection of flaps and slats. As the design of the slats and Fowler flaps increase the wing area by approximately 18% when fully deployed, the required wing area can be lower and was thus designed to be 1898.22 ft<sup>2</sup>.

A 3° twist as recommended by Raymer was used, producing a wing that stalls at the root before stalling at the tip, allowing the ailerons to maintain control at the onset of a stall. Then, the wing angle of incidence relative to the fuselage was calculated to be approximately 1°, which minimises fuselage angle of attack, and thus drag, during cruise conditions. This is consistent with the typical 1° angle of incidence for transport category aircraft.

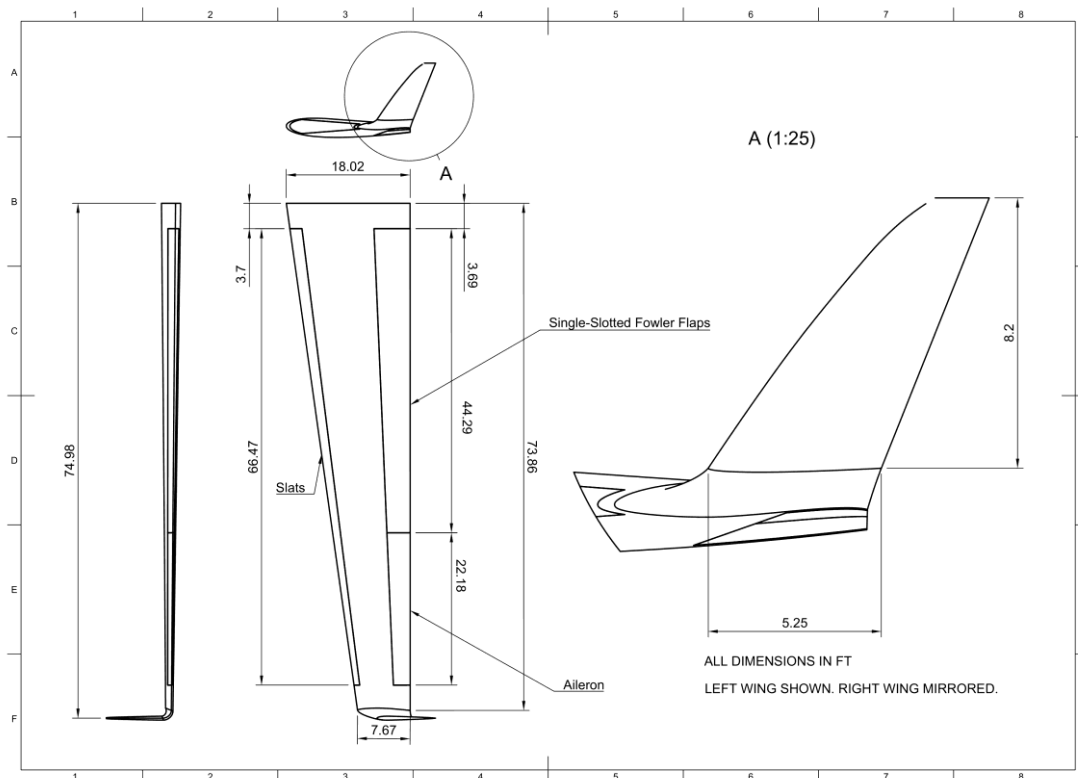


**Figure 13: Geometry of wing (left side) with flaps, slats, aileron and winglet.**



**Table 10: Wing parameters.**

<b>Wing</b>	Wingspan $b$	147.64 ft
	Wing Area $S$	1898.22 ft <sup>2</sup>
	Aspect Ratio $AR$	11.48
	Root Chord	18.04 ft
	Average Chord	12.83 ft
	Mean Aerodynamic Chord	13.55 ft
	Taper Ratio $\lambda$	0.425
	Sweep $\Lambda$	8°
	Dihedral $\Gamma$	0°
	Twist	3°
	Incidence Angle $i_w$	1°
<b>Ailerons</b>	Chord Ratio	0.3
	Span Ratio	0.3
	Maximum Deflection	25° Upwards, 20° Downwards
<b>Flaps</b>	Chord Ratio	0.3
	Span Ratio	0.6
	Maximum Deflection	40°
<b>Slats</b>	Chord Ratio	0.1
	Span Ratio	0.9
	Maximum Deflection	30°
<b>Winglet</b>	Span	8.20 ft
	Root Chord	5.25 ft
	Taper Ratio	0.312
	Sweep	40°

#### 5.4 Wing Lift Characteristics

The wing lift characteristics were calculated from the airfoil characteristics and wing geometry using equations from Raymer [46]. Table 11 shows the wing lift characteristics that were calculated.

**Table 11: Wing Lift Characteristics.**

$C_{L\alpha}$	$C_{Lmax}$	$\alpha_{C_{Lmax}}$
0.134	1.247	8.31°

## 5.5 High-Lift Devices

In order to increase the lift of the wing during critical flight regimes such as takeoff, landing, and payload drop, high-lift devices in the form of single-slotted Fowler flaps and slats were used. The slats take up 90% of the wingspan and 10% of the chord at the leading edge. Both Fowler flaps and ailerons take up 30% of the chord at the trailing edge, with Fowler flaps taking up 60% of the wingspan and ailerons taking up 30% of the wingspan. The changes in maximum lift coefficient  $\Delta C_{L_{max}}$  brought about by flaps and slats were calculated using several equations from Raymer [46] and reference [47].  $10^\circ$ ,  $20^\circ$  and  $30^\circ$  were used as the angle of deflection of the slat. A value of 1.1 is used for the ratio of chord with and without deflection of the slats.

To find the increase in maximum lift coefficient of the airfoil with the use of Fowler flaps, equations from reference [47] were used, for flap deflections of  $10^\circ$ ,  $20^\circ$ ,  $30^\circ$  and  $40^\circ$ . The effect of wing sweep was also accounted for using an empirical correction factor.

As the flaps and slats are used in combination with each other, Table 12 shows the  $C_{L_{max}}$  of the wing for each combination of flap and slat deflection based on the calculated  $\Delta C_{L_{max}}$ . Although each flap setting typically specifies a particular slat setting in order to raise the stall angle, these values would be useful in estimating the optimal pairing of flap and slat deflection for the lift coefficients that are required.

**Table 12: Wing Maximum Lift Coefficient for each Flap and Slat Combination.**

$C_{L_{max}}$		Fowler Flap Deflection				
		$0^\circ$	$10^\circ$	$20^\circ$	$30^\circ$	$40^\circ$
Slat Deflection	$0^\circ$	1.247	1.899	2.117	2.280	2.334
	$10^\circ$	1.412	2.064	2.281	2.445	2.499
	$20^\circ$	1.576	2.228	2.445	2.609	2.663
	$30^\circ$	1.740	<b>2.392</b> (Takeoff)	2.610	2.773	<b>2.827</b> (Landing/Payload Drop)

For takeoff, the slats are deflected to  $30^\circ$  and the flaps are deflected to  $10^\circ$ . During retardant drop and landing, the slats and flaps are fully deflected for maximum lift. Figure 14 to Figure 16 show the different flap and slat deflections, with Figure 17 showing the deployment of ground spoilers as well.



**Figure 14: Slats extended to 30 degrees.**



**Figure 15: Rear view with flaps extended to 40 degrees (full extension).**



**Figure 16: Side view of flaps extended to 40 degrees (full extension). Note inboard nacelle deflects together with flaps.**



**Figure 17: Extension of ground spoilers together with full flaps and slats deflection. Ground spoilers aid in dumping lift after landing and shortens landing distance.**

## 6 Drag Estimation

### 6.1 Parasite Drag

The total parasite drag coefficient of the aircraft excluding propellers was estimated to be 0.013065 using OpenVSP Parasite Drag Tool and Torenbeek Form Factor equations [48]. Table 13 shows the  $C_f$ , FF and  $S_{wet}$  values used and the breakdown of parasite drag for the major aircraft components.

**Table 13: Breakdown of Parasite Drag (Excluding Propellers)**

Component	$S_{wet}/ft^2$	FF	$C_f$	$C_d$	% Total
Vertical Stabiliser	551.99	1.280061	0.002425	0.000903	6.91
Ventral Fin	78.20	1.280061	0.002342	0.000123	0.94
Fuselage	1632.11	1.062286	0.001918	0.001752	13.40
Inner Engine	450.46	1.153358	0.002259	0.000618	4.73
Outer Engine	388.89	1.27432	0.002355	0.000615	4.71
Wing	3896.46	1.455749	0.002504	0.007482	57.27
Horizontal Stabiliser	861.82	1.344845	0.002574	0.001571	12.03

The parasite drag coefficients of the propellers and landing gear were calculated using equations from Raymer [46]. The total parasite drag coefficient for all four propellers was thus found to be 0.009576. Using the frontal areas of the nose landing gear wheels and strut as well as the two main landing gear wheels and strut, the total parasite drag coefficient for the landing gear was found to be 0.002913.

Flap deflection also results in an increase in parasitic drag. Equations from Raymer were used to calculate the change in parasite drag at different deflections of flaps and shown in Table 14.

**Table 14: Increase in Parasite Drag Coefficient due to Flaps**

	10°	20°	30°	40°
$\Delta C_{D0}$	0.0138	0.0276	0.0414	0.0552

### 6.2 Leakage and Protuberance Drag

The leakage and protuberance drag comes about as a result of holes and gaps in the airframe as well as items such as antennas, vents, hinges and rivets. It was estimated to be 5% of the aircraft's total parasite drag, as suggested by Raymer for propeller aircraft [46].

### 6.3 Induced Drag

Induced drag is produced as a result of lift. The induced drag coefficient is equal to the square of the lift coefficient multiplied by a factor K. K can be found from Raymer [46], where it is a function of the Oswald efficiency factor,  $e$ . The Oswald efficiency factor was estimated using several methods and the average value was used in order to ensure better accuracy.

Using the Oswald Span Efficiency method from Raymer [46],  $e$  was found to be 0.6633. Using the leading edge suction method from Raymer [46] which incorporates the aspect ratio, lift curve slope and leading edge suction factor,  $e$  was found to be 0.755. Equations from Howe were also used to find  $e$  [49]. Using the flight Mach number, aspect ratio, thickness to chord ratio of airfoil, sweep angle and number of engines on each wing, the  $e$  was found to be 0.763. The average value of 0.727 for  $e$ , thus produces a value of 0.03178 for K.

Flaps also contribute to the induced drag. Using the sweep angle,  $k_f$  and the increase in  $C_{Lmax}$  at different deflections, the increase in induced drag coefficient was calculated using equations from Raymer. Table 15 shows the increase in  $C_{Lmax}$  and induced drag coefficient at different deflections of the flap.

**Table 15: Increase in Lift and Induced Drag Coefficients due to Flaps**

	10°	20°	30°	40°
$\Delta C_{Lmax}$	0.6522	0.8696	1.033	1.087
$\Delta C_{Di}$	0.02675	0.04755	0.06710	0.07430

## 6.4 Trim Drag

For stable flight, the tail exerts a downward force in order to trim the aircraft. To compensate, the wing has to generate additional lift, resulting in additional induced drag known as trim drag. To calculate the trim drag, the total cruise  $C_L$  is required. This was found to be 0.3439.

The contributions of the wing and tail to the total lift coefficient can then be plotted against angle of attack. Then, the angle of attack can be found from equating total lift coefficient to total cruise  $C_L$ . Figure 18 shows the tail, wing and total lift coefficient plotted against angle of attack.

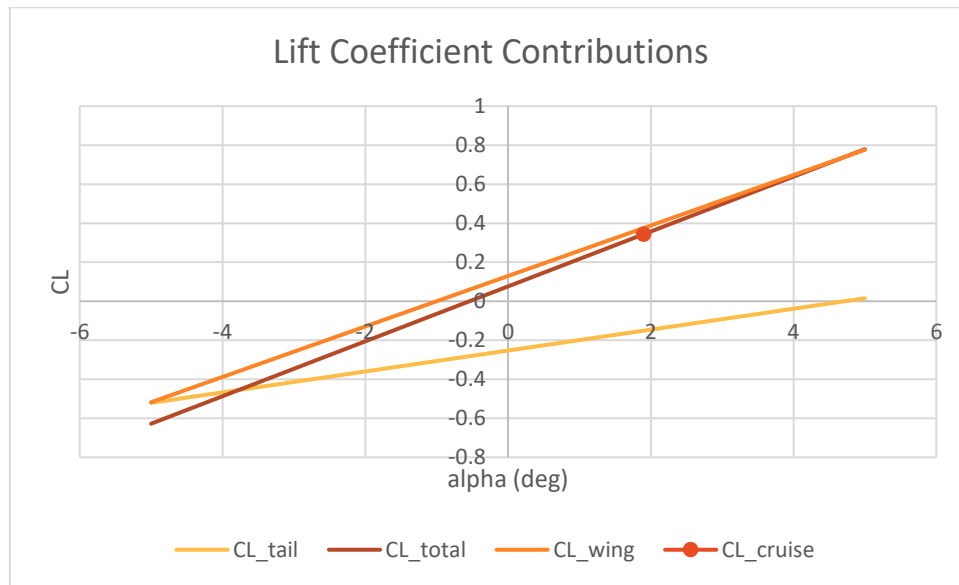


**Figure 18: Graph of Tail, Wing and Total Lift Coefficients Against Alpha**

Table 16 shows the angle of attack and wing and tail  $C_L$  at cruise  $C_L$  found from Figure 18.

**Table 16: Angle of Attack and Wing and Tail Lift Coefficients at Cruise Lift Coefficient**

$\alpha/^\circ$	Wing $C_L$	Tail $C_L$
1.9	0.37526	-0.1509

Using the aspect ratio, Oswald efficiency factor, lift coefficient for the tail and wing, as well as the tail area and horizontal stabiliser efficiency, the trim drag coefficient was found to be 0.004942.

## 6.5 Drag Polar

The total drag coefficient for different configurations can thus be found using the equation:

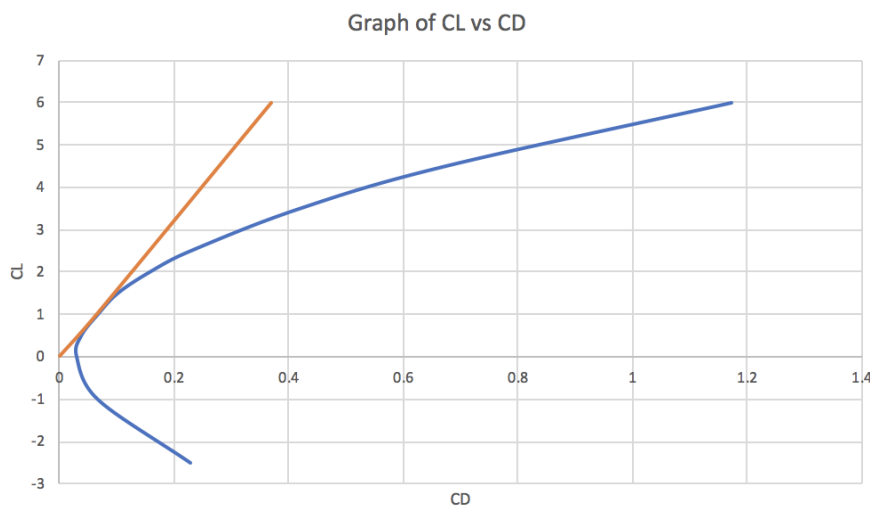
$$C_D = C_{D0} + KC_L^2 + \Delta C_{D_{flaps}} + C_{D_{trimmed}}$$

Table 17 shows the values used and the total drag coefficients calculated for different configurations. As the additional induced drag due to flaps is calculated separately, the  $C_L$  values used are the contributions from the wing excluding flaps. Leakage and protuberance drag was included in the estimation for zero-lift drag  $C_{D0}$ .

**Table 17: Total Drag Coefficient for Different Configurations**

Configuration	$C_{D0}$	$C_L$ (Excl. Flaps)	$\Delta C_{Di}$ due to Flaps	$C_D$
Takeoff (Landing gear extended, 10 °flaps and full slats)	0.04132	1.740	0.02675	0.1692
Cruise (Landing gear, flaps, and slats retracted)	0.02377	0.3439	-	0.03247
Retardant Drop (Landing gear retracted, full flaps and slats)	0.08173	1.740	0.07430	0.2571
Landing (Landing gear extended, full flaps and slats)	0.08479	1.740	0.07430	0.2602

Figure 19 shows the drag polar curve at cruise conditions. The maximum aerodynamic efficiency was found to be 16.22 by calculating the gradient of the line drawn from the origin to the steepest point on the drag polar curve.



**Figure 19: Drag Polar Curve at Cruise Conditions**

## 7 Propulsion

### 7.1 Engine and Propeller

Based on the constraint diagram, each engine must provide a minimum of 4527 hp to meet the performance requirements. Engines currently in the market that meet this power requirement are summarised in Table 18, along with the propeller they are paired with. As these propellers are tailor made to suit the performance characteristics of each engine, the same propeller pairing will be used together with the selected engine.

**Table 18: Shortlisted Engines and Propellers.**

Engine	AE 2100 D2 <sup>1</sup>	PW150A <sup>2</sup>	AI-20D Series 4 <sup>3</sup>	T56-A-15 <sup>4</sup>
Aircraft	Alenia C-27J, Saab 2000 (A variant), C-130J (D3 variant)	DHC-8-400, An-132 (Cancelled), Y8F600 (B variant, cancelled)	AN-12, Il-18, Shaanxi Y-8, Y-9 (As the WJ-6), AVIC TA-600 (As the WJ-6)	P-3 Orion, C-2 Greyhound, C-130H
ESHP (h)	4637	5071	5180	4591
Dry Weight (lbs)	1776.93	1582.92	2292.81	1847.47
Specific Fuel Consumption (lbs/ESHP*hr)	0.461	0.432	0.432	0.540
Propeller	R391	R408	-	54H60-91
Diameter (ft)	13.50	13.45	14.76	13.68
Number of Blades	6	6	4	4
Weight of Propeller (lbs)	718.71	555.57	-	-

<sup>1</sup> [50] <sup>2</sup> [51] <sup>3</sup> [52] <sup>4</sup> [53] [54] <sup>5</sup> [55]

From Table 18, the AI-20D turboprop has the highest equivalent shaft horsepower as well as lowest specific fuel consumption. However, it is not the most suitable engine due to the high weight as well as a small commercial market (largely Eastern Europe and China), which would make maintenance costly. Thus, the PW150A together with the R408 from Dowty Rotol was selected, as it has a high equivalent shaft power, low specific fuel consumption, and good aftermarket support for parts and maintenance.

### 7.2 Bypass Doors

Unlike a turbojet, the air intake of a turboprop engine need not be in line with the engine. Typically, the airstream entering the engine encounters a bend before entering the engine, an example of which is shown in Figure 20. When there is ice or debris, the bypass door opens, and the air-particle mixture is deflected downwards. Due to the inertia of the heavier particles, it will continue and leave the engine while the air swirls and enters the engine compressor. This feature is especially beneficial for the firefighting aircraft as ashes or light debris may be carried upwards due to updraft and it may enter the inlet as the aircraft is performing a payload drop.



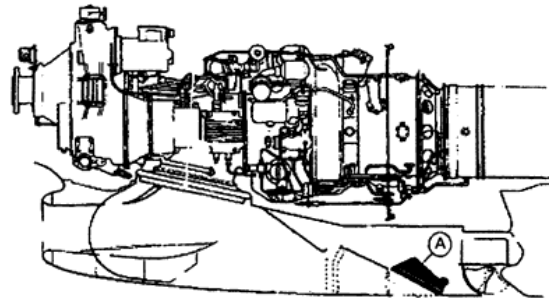


**Figure 20: Bypass door of a DHC-8 in the open position, labelled 'A' [56].**

### 7.3 Full Authority Digital Engine Control (FADEC)

Fireflyer is equipped with FADEC, which is an autonomous system which can self-monitor and operate with multiple redundancy. FADEC has similar advantages with electronic ignition and EEC systems, but with greater power management. FADEC is a combination of throttle, prop and mixture control. Regardless of flight altitude, a throttle setting done with FADEC will result in the optimum power, propeller RPM and mixture combination. This enables the aircraft to realize fuel economy for a greater range performance [57].

### 7.4 Maintenance Access

Maintenance Access to the Engines are provided through a series of panels on the sides and lower surface of the nacelles as shown in Figure 21 to Figure 23. This enables easy inspection and replacement of the engines, reducing maintenance costs and downtime.



**Figure 21: Open maintenance panels on both sides and lower part of the nacelle. Engine truss structure can also be seen.**

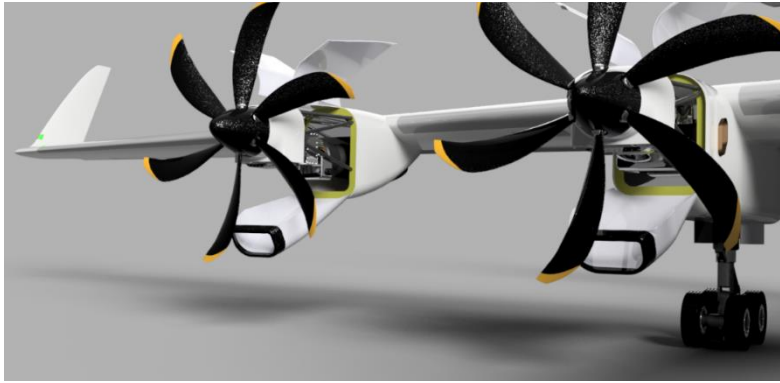


**Figure 22: Front view of open maintenance panels.**

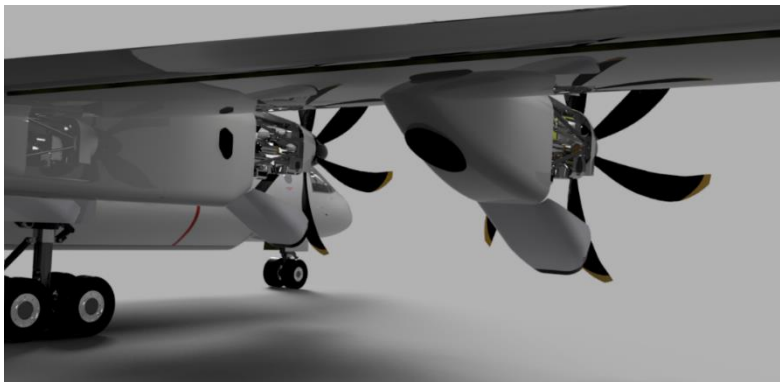


**Figure 23: Rear view of open maintenance panels.**

### 7.5 Fuel System

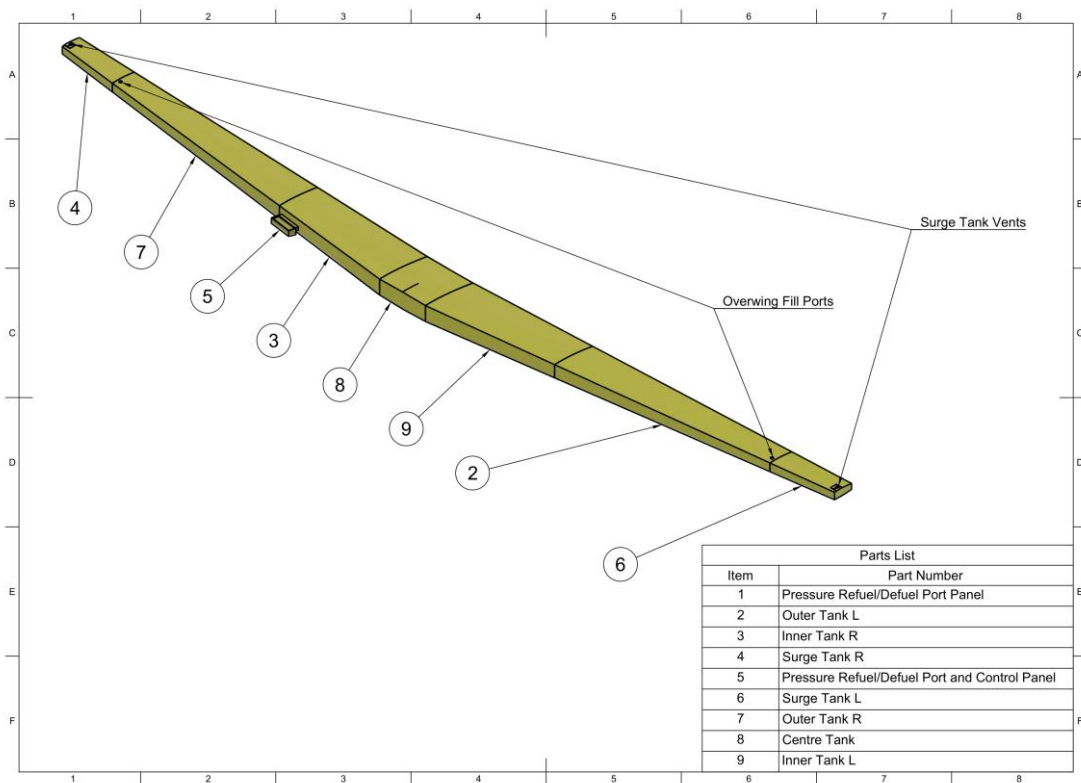


**Figure 24: Layout of fuel tanks.**

As the fuel weight required for the design and ferry missions differ slightly in the initial sizing, the higher fuel weight was used to calculate the required fuel tank size. Since turboprop engines are able to run on a variety of fuels, including Jet A, A-1/JP8, JP4, and JP5/JP1 [58], the lowest density of 6.4 lb/gallon, which corresponds to JP4 at a temperature of 100°F was taken as the density of fuel in order to ensure that sufficient volume is catered for. After accounting for 5% expansion under warmer temperatures, the required tank volume is 7995 gallons, which is rounded to 8000 gallons of total fuel volume required.

This fuel capacity is divided into 5 integral tanks, 4 within the wing and the last within the wing box structure. This ensures that there is minimal shift in the centre of gravity of the aircraft as fuel is consumed throughout the flight. To calculate the available fuel tank volume within the wing, semi-empirical equations from Torenbeek [59] were used, together with 85% of the measured volume bounded by the wing skin, front spar, rear spar, and wing ribs as suggested by Raymer, since an integral fuel tank is used. This results in a final fuel capacity as shown in Table 19.

**Table 19: Capacities of each fuel tank.**

Fuel Tank	Capacity	
	ft <sup>3</sup>	Gallons
Outer Tank L (Wing Tank 1)	233.96	1750
Inner Tank L (Wing Tank 2)	262.21	1961
Centre Tank	128.72	963
Inner Tank R (Wing Tank 3)	262.21	1961
Outer Tank R (Wing Tank 4)	233.96	1750
Total	1121.07	8385

The tanks can be filled from two overwing fill ports on wing tanks 1 and 4 or via a pressure refuel/defuel receptacle located on the right wing between the engine nacelles, as shown in Figure 25. As the maximum landing weight is equal to the maximum takeoff weight, no fuel dumping system is required under FAA regulations.

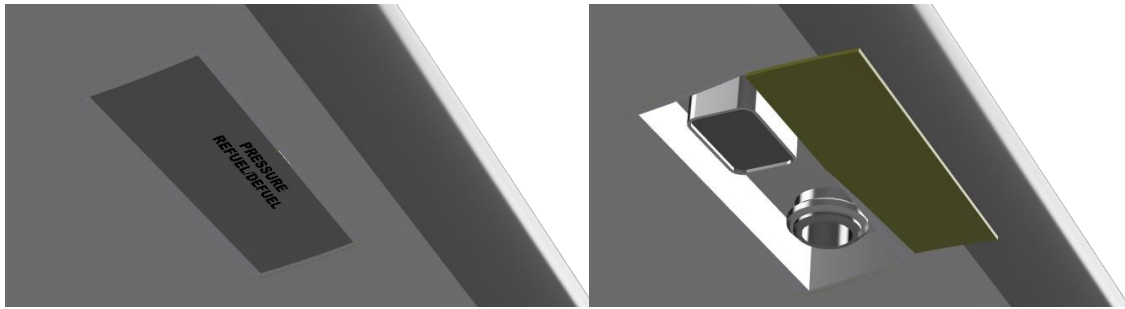


**Figure 25: Pressure refueling port on the underside of the right wing.**

## 8 Retardant Tank

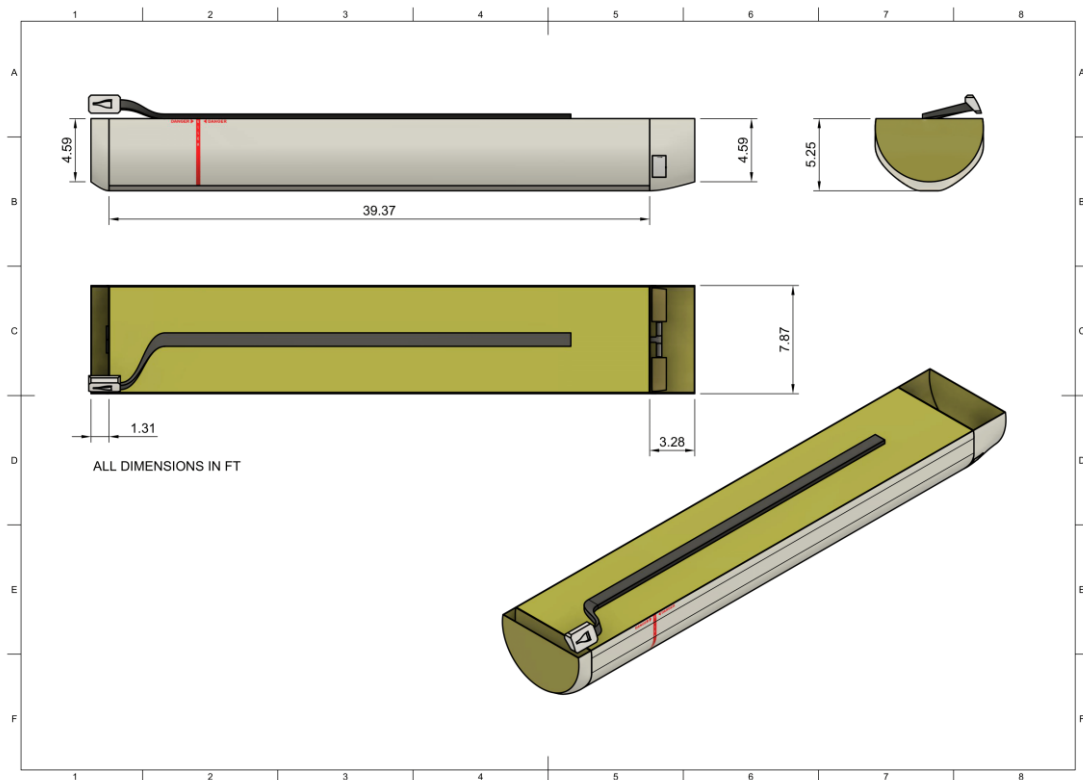


**Figure 26: Retardant tank overall dimensions.**

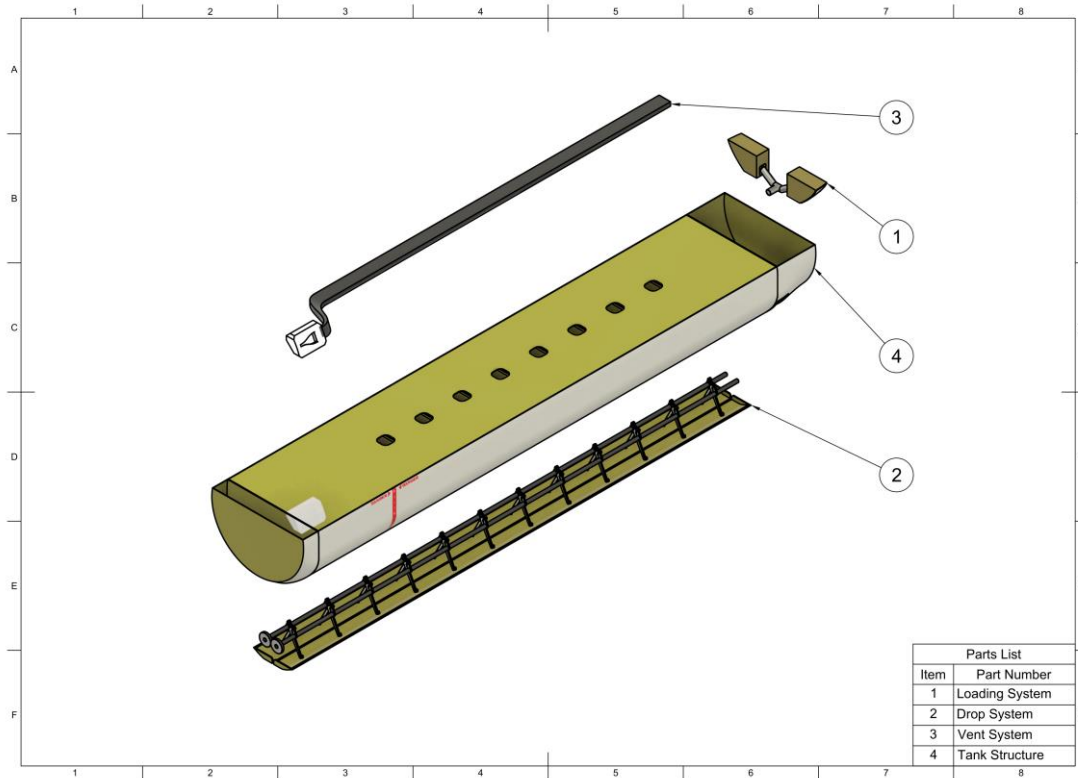


**Figure 27: Retardant tank with labelled subcomponents.**

### 8.1 Selection of Retardant Delivery System

The retardant delivery systems that are commonly used in firefighting operations can be categorised into several types: Discrete versus integral and external versus internal systems. These tanks can be further categorised by their drop mechanisms. The first drop mechanism, widely used amongst firefighting aircraft, is the gravity-drop system. In this system, the retardant or water is released through the tank doors and allowed to fall with the influence of gravity. The second mechanism is a pressurised tank system, in which compressed air is pumped into the tanks and retardant is discharged through nozzles with controlled flow.

Therefore, four existing system variations were chosen to be analysed in order to determine the most suitable system for use in a purpose-built firefighting aircraft. They are internal discrete tanks, external discrete tanks, integral tanks as well as internal pressurised tanks. The internal discrete tank is a modular tank that can be loaded through the aircraft's ramp and fitted within the fuselage of the aircraft, such as the RADS-CCL used on the C-130. These tanks commonly discharge retardant or water with the help of gravity. The external discrete tank is similar to an internal discrete tank but is fitted onto the outer body of the aircraft instead of within the fuselage, and is used on the DC-10 Air Tanker. The integral retardant tank is one where the retardant fluid is contained directly by the airframe structure instead of in a separate tank, in the same way that integral fuel tanks work. This is commonly used by purpose-built firefighting aircraft such as the CL-415. The internal pressurised

tank system is similar to an internal discrete tank but operates and discharges via pressurisation instead of via gravity and is used on the 747 SuperTanker.



**Figure 28: Types of retardant delivery systems. From top left, clockwise: Internal Discrete Tank in a C-130 [60], External Discrete Tank on a DC-10 [61], Integral Tank on a CL-415 [62], Internal Pressurised Tank in the 747 SuperTanker [63].**

To select the optimal type of retardant tank system to be used, three factors were chosen to evaluate the practicality and suitability of the retardant tank: complexity, weight, and mission flexibility. Weightings were allocated to these characteristics, with mission flexibility being the most crucial factor and thus given the highest weighting. This is because with wildfires occurring worldwide at different locations of various terrains, modern firefighting aircraft need to be able to accommodate different payloads and mission profiles. Therefore, a retardant system that is able to operate with greater flexibility, such as being able to be unloaded to reconfigure the cargo bay, would enable the aircraft to adapt to the needs of different operations.

The factor next in line of importance is complexity. The retardant system's complexity is described in terms of two aspects: the operating complexity of the system and the mounting complexity. The operating complexity includes the ease of the system's use by the operator, as well as the complexity of system operations. The ease of usage is important because it will lessen crews' workload and allow them to work efficiently during missions.

Mounting complexity is the difficulty level of installing or mounting the system onto the aircraft and the effect of the system on the aircraft's structure. Having a retardant system of minimal effect or changes to the aircraft structure will help to maximise the aircraft's mission performance and reduce costs.

Lastly, weight is weighted the lowest amongst all the factors. The weight of the system would often influence the operating and maintenance cost of the system as well as the structural load distribution of the aircraft, thus affecting its flight performance. However, the weight of the retardant tank system is small compared to the empty weight of the aircraft, and thus has lower weightage compared to the other factors.

The Pugh matrix in Table 20 summarises how each of the retardant tank systems fare amongst the three functionality factors. As the integral tank system has the highest score, it is chosen as the retardant system to be installed.

**Table 20: Pugh matrix showing the score of each tank system with reference to the factor weightings.**

Factor	Weighting	Retardant Tank System Type			
		Internal Discrete	External Discrete	Integral	Internal Pressurised
Mission Flexibility	5	5	4	4	3
Complexity	4	4	3	5	3
Weight	3	3	3	4	2
Total Score:	-	50	41	52	33



## 8.2 Tank Structure

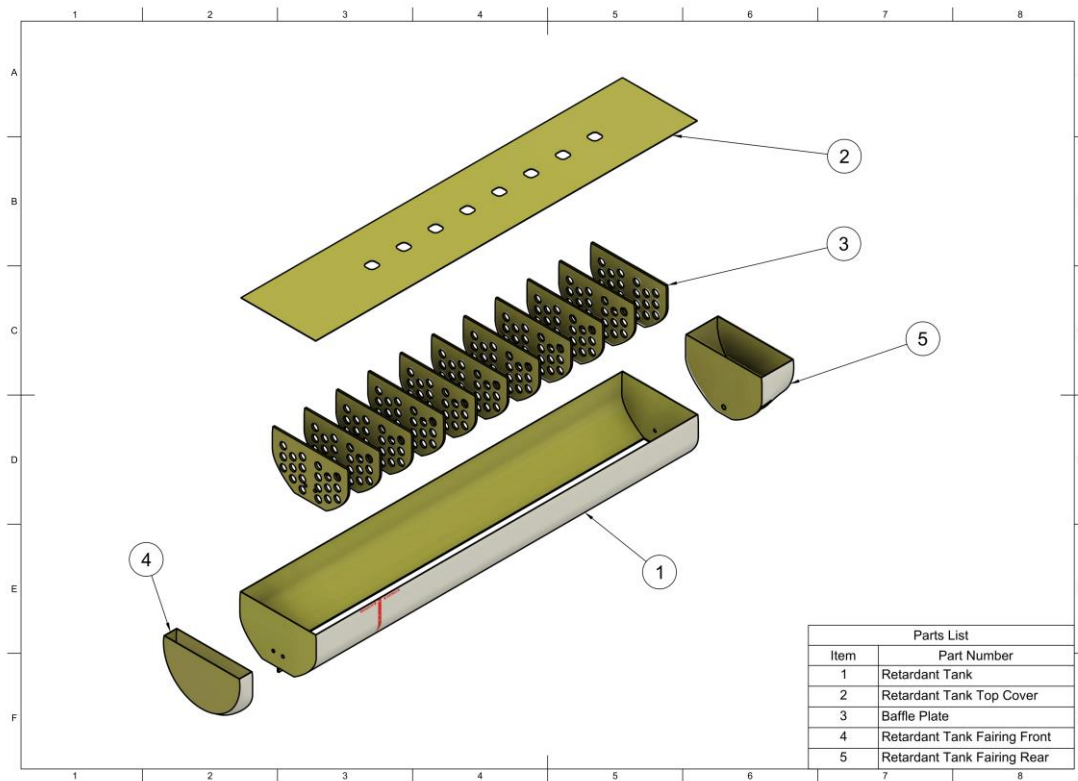


**Figure 29: Retardant tank design.**

The retardant tank design is shown in Figure 29. The cross-sectional profile is with high sides that taper steeply toward a set of drop doors, similar to designs of current retardant tanks. This allows the tank to carry a large volume of liquid while still being able to rapidly discharge its contents, achieving a high coverage level. Since the retardant tank is integral to the fuselage structure, the fuselage profile transitions from circular cross sections at the nose and tail to a tapered section at the centre. A set of fairings before and after the centre section helps to avoid sharp changes in the fuselage profile that would result in increased drag. In addition, baffle plates are installed to prevent sloshing of the fluid in the retardant tank, which would adversely affect the aircraft centre of gravity. To prevent corrosion from the fire retardant, the interior of the retardant tank is also coated with a polyurethane topcoat and AV-30, a corrosion inhibiting compound used in the CL-415 [64]. Regular inspections must also be made to prevent undetected corrosion that could lead to material failure.



### 8.3 Drop System

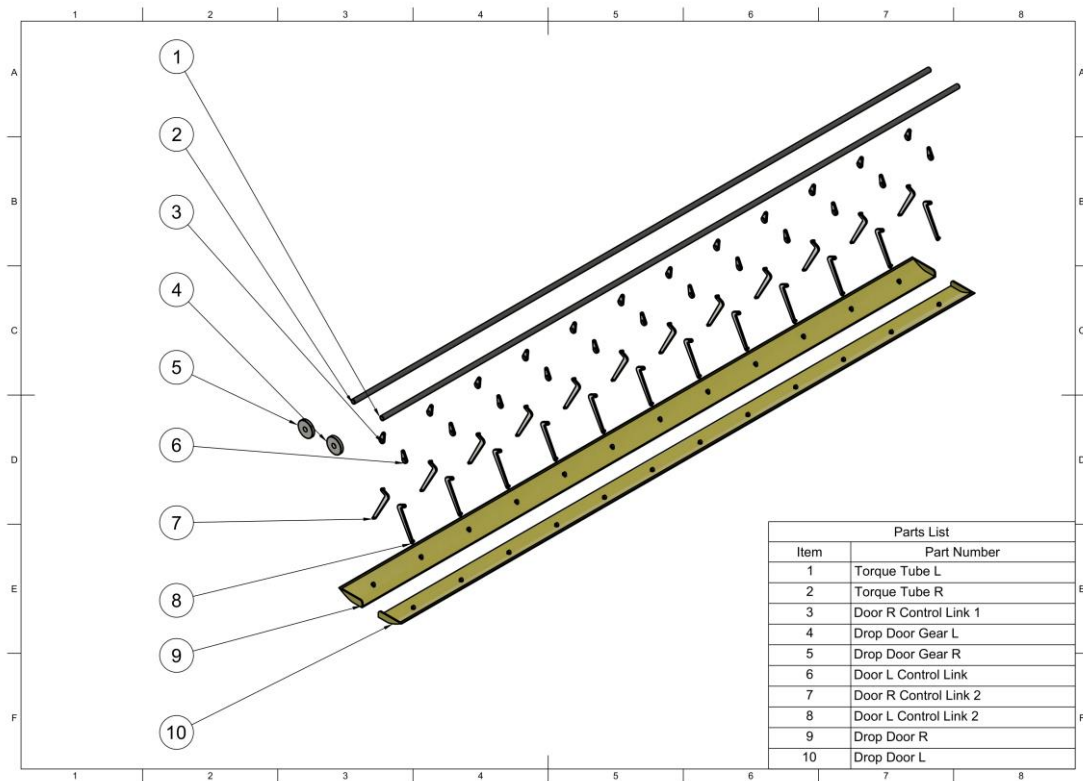


**Figure 30: Exploded view of drop system.**

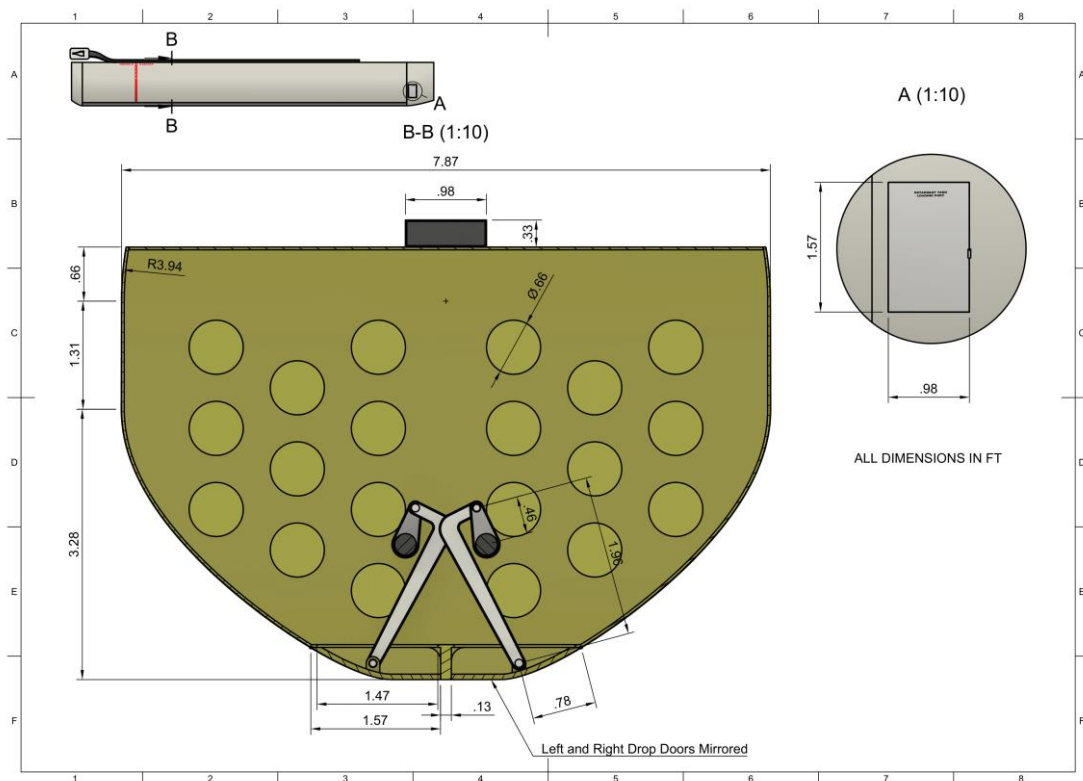


**Figure 31: Dimensioned drawing of drop doors, torque tubes and control links.**

The drop system consists of two doors hinged longitudinally at the bottom of the retardant tank. The doors can be partially opened to control the discharge rate and volume of fluid dropped. Thus, long, thin lines of retardant can be created to act as a firebreak, while large volumes can also be dropped over a small area in a decisive attack. This system, called the constant flow tank, allows for multiple drops to occur on a single mission and is one of the most reliable and effective delivery systems that is widely used in firefighting tankers [65].

The doors are electronically controlled and hydraulically operated. A set of rotary gears operate two torque tubes that control the opening of the tank doors through a set of control links. The doors and control links thus forms a 4-bar linkage with an over-centre lock that prevents the doors from opening even if the hydraulic system is unpressurised, as shown in Figure 31. In this way, the retardant tanks can be safely filled.

With the electronic control system, the pilots only need to select the drop volume as well as desired coverage level, with a microprocessor calculating the how wide and for how long the drop doors will open, taking into account multiple factors such as the volume remaining in the tank and the speed of the aircraft. The predicted point of impact for the dropped retardant is also continuously computed and projected onto the head-up display in the cockpit, allowing the pilots to adjust the flight path and release point to hit the desired target point.

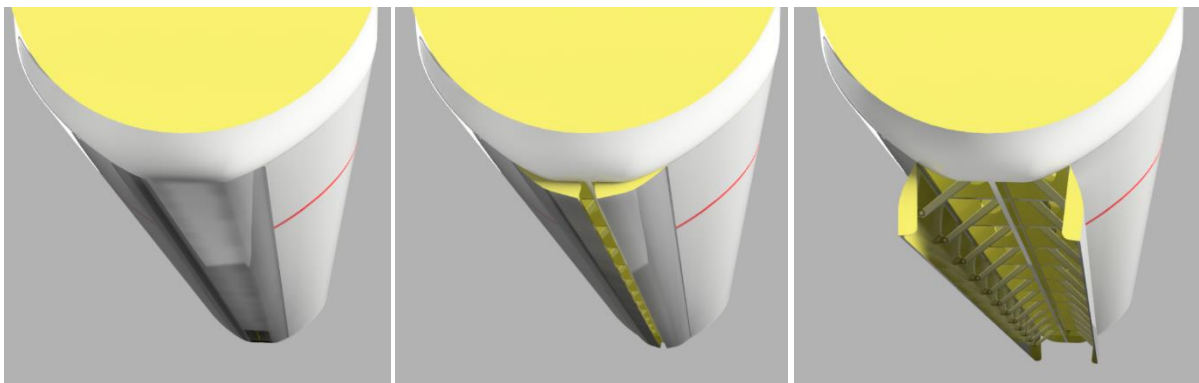


**Figure 32: Retardant tank doors in the closed, one-third open, and fully open positions.**

## 8.4 Loading System

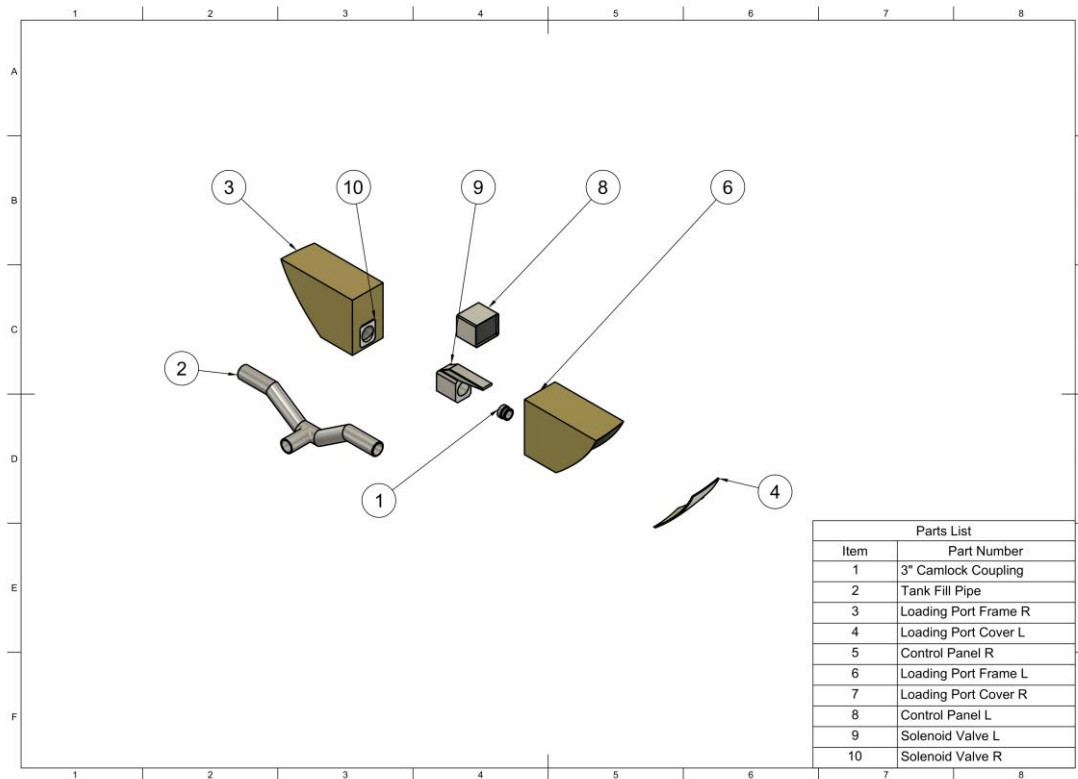


**Figure 33: Exploded view of loading system.**

The retardant tanks are filled from two loading ports located in the rear tank fairing, one on each side of the aircraft. Each loading port has a standard 3-inch male Camlock coupling and is equipped with a control panel and solenoid valve. The valve opens during filling and automatically closes once a pre-selected level is met or when the tank is full. Using the DC-10 as a reference point, which has a 12,000 gallon capacity and can be filled from three filling ports in eight minutes [66], each loading port is capable of filling the retardant tank with a 500 gallon per minute fill rate. This allows the Fireflyghter's 8,000 gallon retardant tank to be filled in eight minutes using both loading ports or 16 minutes if only a single side is used, meeting the RFP requirements.

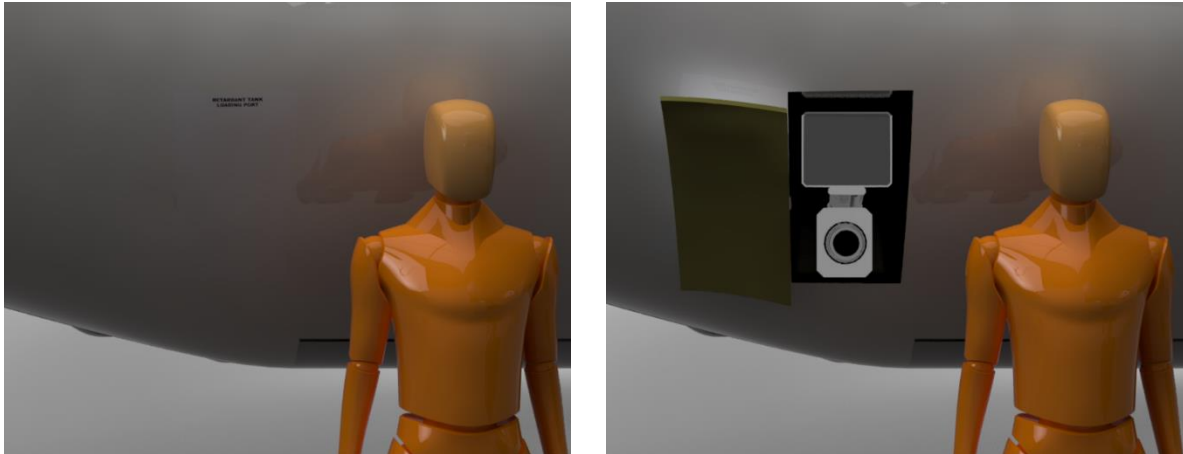


**Figure 34: Loading port showing Camlock coupling and control panel.**

### 8.5 Vent System

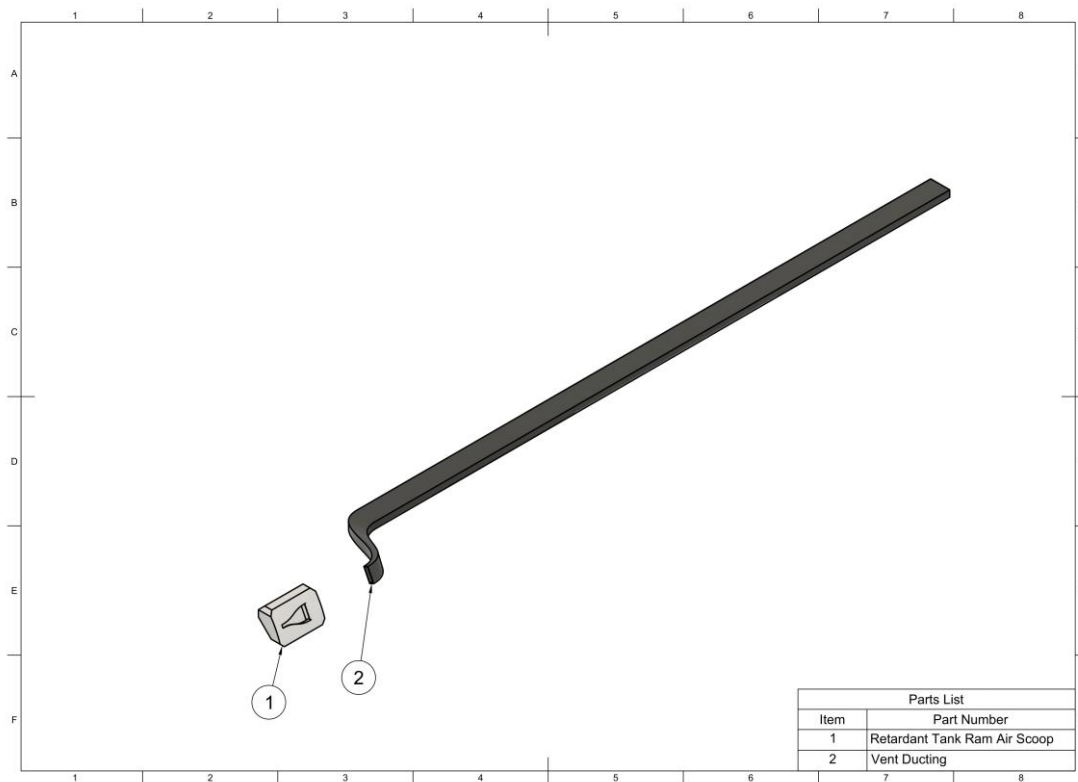


**Figure 35: Retardant tank vent system.**

The retardant tank is vented to allow air to exit the tank during filling as well as enter the tank when the payload is dropped. A ram air scoop on the left of the aircraft also adds additional air pressure to the top of the fluid in the tank, helping to force the payload downwards through the drop doors. This is a feature seen on existing firefighting aircraft such as the P-3 Orion [67].

## 9 Weight and Balance

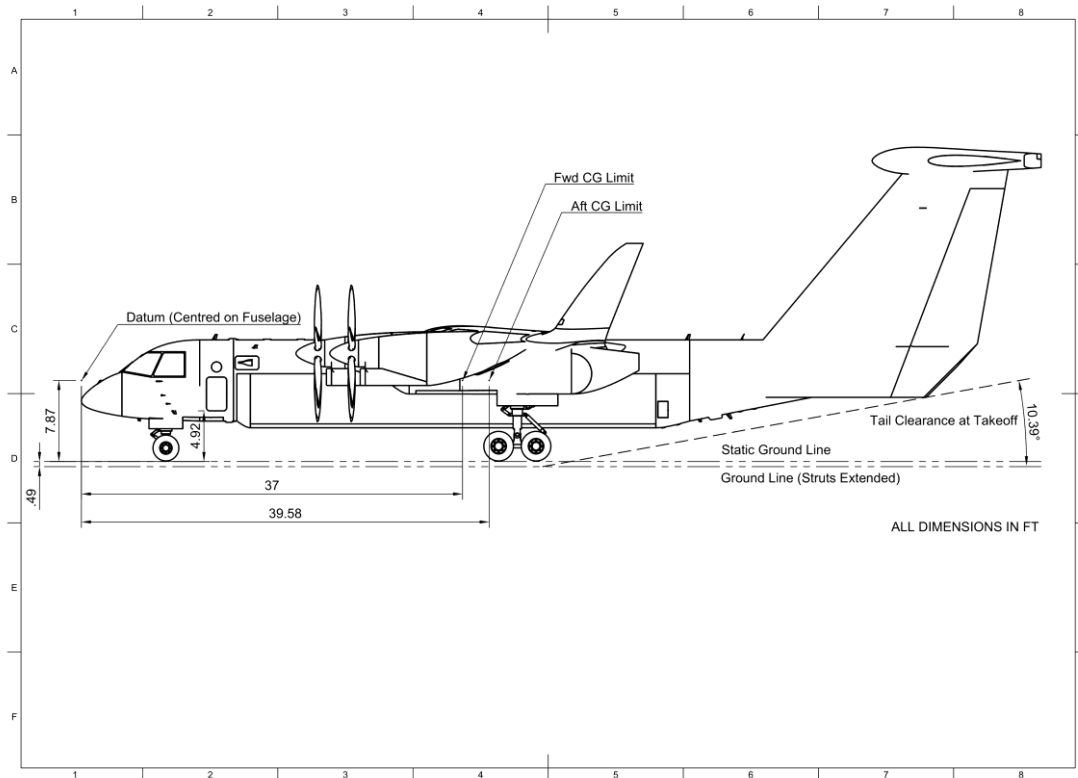


**Figure 36: Aircraft datum and centre of gravity limits.**

### 9.1 Weight Estimation

The method from Raymer Chapter 15 was used to calculate the final weights taking into account the design load factor and final dimensions of the various structural components.

To calculate the centre of gravity, the component weights are multiplied by CG locations of each component, then divided by the total weight. The component weights are given in Table 21.

**Table 21: Component weights and positions.**

Component	Weight (lbs)	Position (ft)	
		x	z
Wing (including winglets)	20966	41.83	3.94
Horizontal tail	1647	84.97	19.69
Vertical tail	2278	76.28	3.28
Fuselage	12660	38.39	0
Main landing gear	9275	41.01	-6.89
Nose landing gear	947	8.20	-7.22
Engine Inboard (2x)	3165	26.90	2.62
Propeller Inboard (2x)	1111	22.97	2.62
Engine Outboard (2x)	3165	30.18	2.62
Propeller Outboard (2x)	1111	26.25	2.62

Engine Inboard Nacelle (2x)	1545	36.09	2.62
Engine Outboard Nacelle (2x)	1474	36.09	2.62
Fuel system	2110	41.83	3.94
Flight controls	1514	4.92	-1.97
Instruments	318	4.92	-1.97
Hydraulics	265	42.65	0
Electrical	1305	42.65	0
Avionics	2141	4.92	-1.97
Furnishings	1280	8.20	-1.97
Anti-ice	377	41.83	3.94
Handling gear	57	42.65	0
Retardant Tank (8000 gal)	72000	36.75	0
Fuel (Max)	50000	41.83	3.94
Crew	500	8.20	-1.97
Empty Weight	68711		-

## 9.2 CG Location

The CG locations for the different loading conditions can be calculated, as shown in Table 22.

**Table 22: CG Position for each loading condition.**

Loading Condition	CG Position	
	X (ft)	Z (ft)
Empty	38.19	1.18
Full Fuel No Payload	39.59	2.32
Full Fuel Full Payload	38.27	1.45
Zero Fuel Full Payload	37.01	0.57

Thus, the most forward CG location is with full payload and zero fuel, and the most aft CG location is with full fuel and no payload, such as during a ferry flight. These positions can be plotted on a weight and balance diagram, as shown in Figure 37. The CG travel of the aircraft for different fuel and payload carried thus falls within these boundaries.

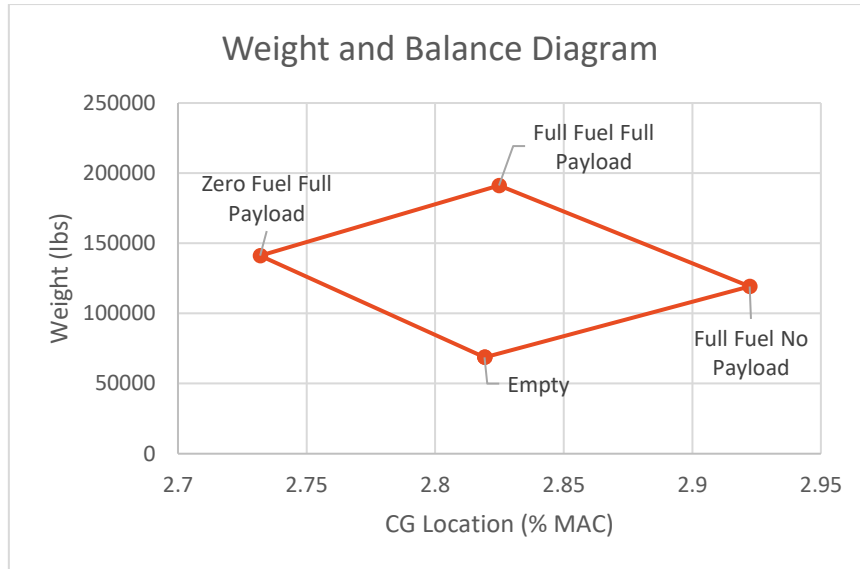


**Figure 37: Weight and balance diagram.**

## 10 Structural Layout

### 10.1 Materials

Aluminium alloy Al-7075-T651 is chosen as the airframe material, with the material properties shown in Table 23. This is due to its common use in modern civil aircraft with good strength-to-weight ratio and well-understood material properties. As a result, a large portion of the aerospace industry already possess the tools and processes to work with this alloy, reducing manufacturing costs. Although composite materials such as carbon fibre reinforced plastic may seem to be superior in terms of strength-to-weight ratio, they are much more costly to fabricate, especially for a large aircraft. In addition, a firefighting aircraft is expected to spend much of its time forward deployed at airtanker bases where specialised maintenance facilities may not be available. As aluminium alloys are easier and less costly to repair, they are the preferred material choice, especially since there is a higher risk of damage during low-altitude payload drops.

**Table 23: Material properties of Al-7075-T651 [68].**

Al-7075-T651	
Density	0.102 lb/in <sup>3</sup>
Young's Modulus	10,400 ksi
Shear Modulus	3,900 ksi
Poisson's Ratio	0.33
Yield Strength (Tensile)	73,000 psi
Ultimate Strength (Tensile)	83,000 psi

## 10.2 Wing Structural Design

The wing consists of two spars with ribs spaced at approximately 18 inches, taking reference from the C-130. Together with the upper and lower skin panels, these spars make up the wing torsion box. The upper and lower skin panels are reinforced with stringers that run across the span of the wing, as shown in Figure 38. The spars are capped with a T-section, while the stringers are made with a Z-section,

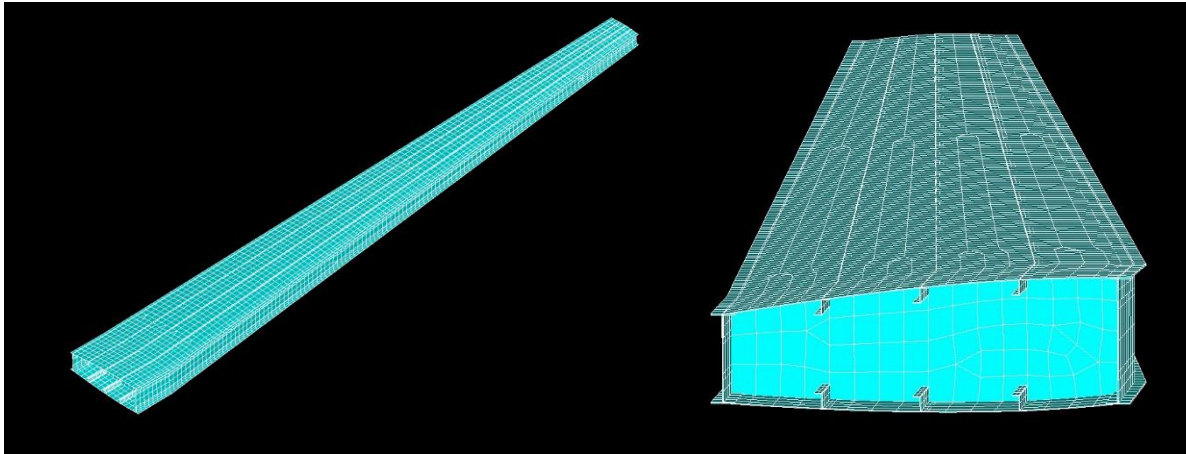


**Figure 38: Wing structure showing spars and stringers for left wing**

The dimensions of the stringers are shown in Figure 39, Table 24, and Table 25. The skin thickness is 0.2 inches.

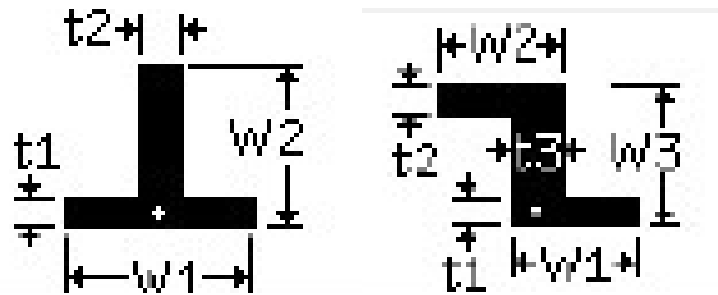


**Figure 39: Stringer sections**

**Table 24: Dimensions of T-section**

t1/inch	t2/ inch	W1/ inch	W2/ inch
0.59	0.59	11.81	5.91

**Table 25: Dimensions of Z-section**

t1/ inch	t2/ inch	t3/ inch	W1/ inch	W2/ inch	W3/ inch
0.39	0.39	0.39	1.97	1.97	3.94



To analyse the deformation and stress experienced by the wings during flight, A CAD model of the wing was designed and the loading on the wing was simulated using ANSYS Mechanical Software. The loading at different ribs was obtained by applying the spanwise lift distribution from a VSPAERO simulation at different load factors, as shown in Figure 40.

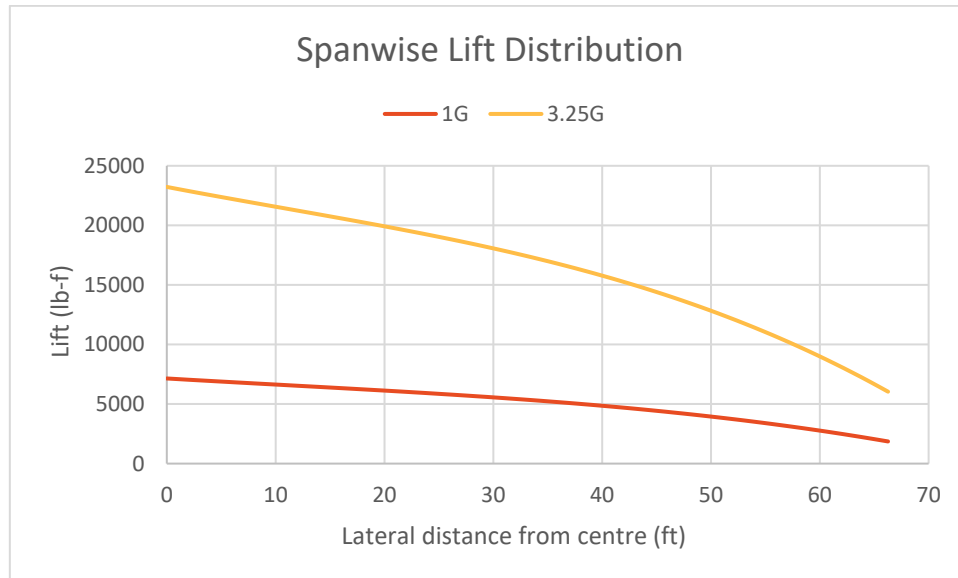


**Figure 40: Spanwise lift distribution at different load factors**

The estimated deformation and stress experienced by the wing was obtained at 1G loading and 3.25G loading. The wing was found to experience a deformation at the wingtip of 8.85 ft at 1G loading and 28.77 ft at 3.25G loading. These numbers were found to be acceptable given the loading conditions and hence helped to validate the structural design of the wing.

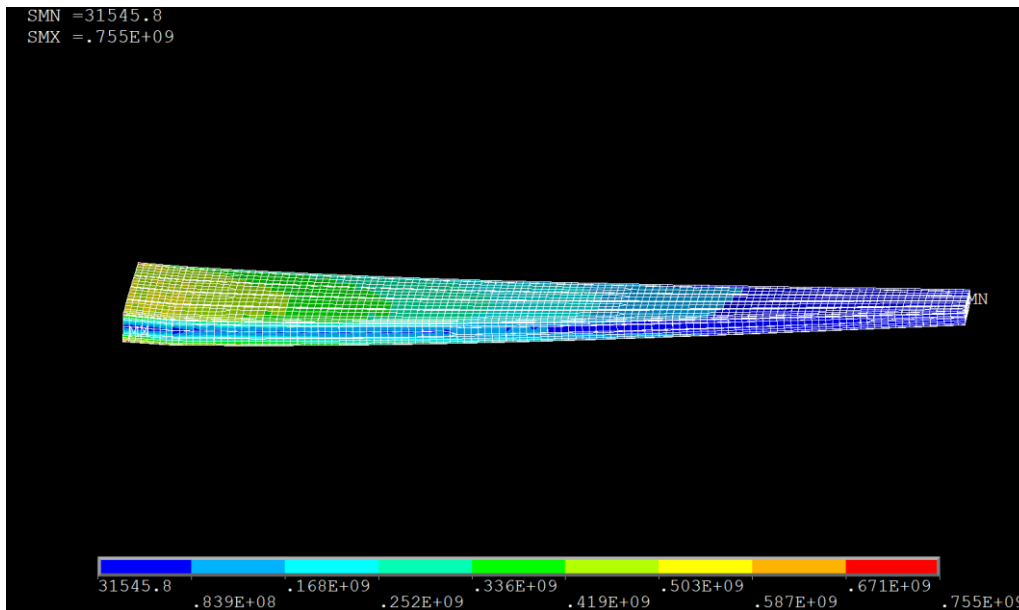


**Figure 41: Stress distribution at 1G loading**

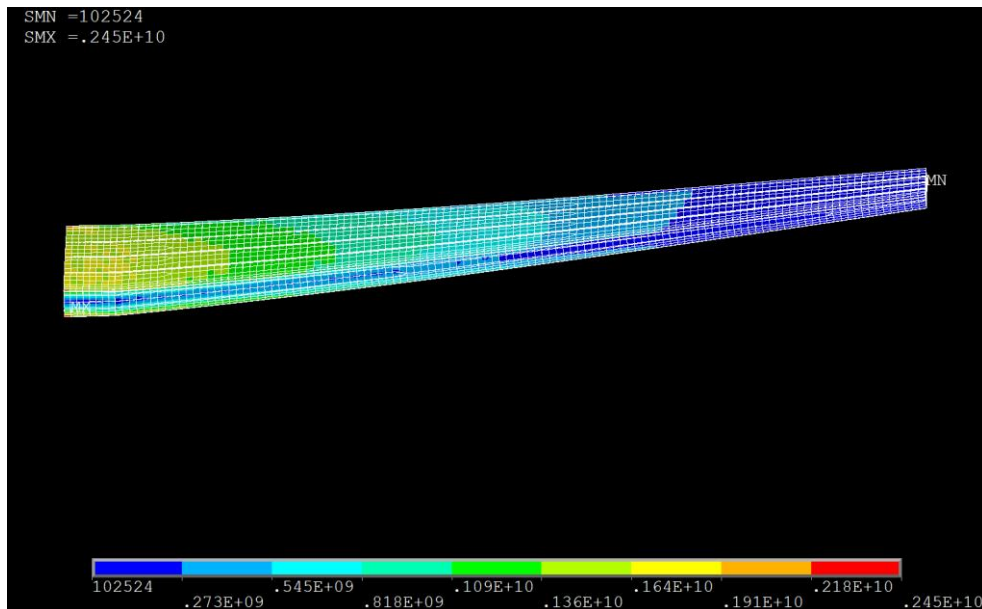


**Figure 42: Stress distribution at 3.25G loading**

The stress distribution around the wing was also found to be acceptable as shown in Figure 41 and Figure 42.

The FEM analysis thus helped to verify the structural design of the wing and that it will be able to safely withstand the highest estimated load on the structure.

## 11 Empennage

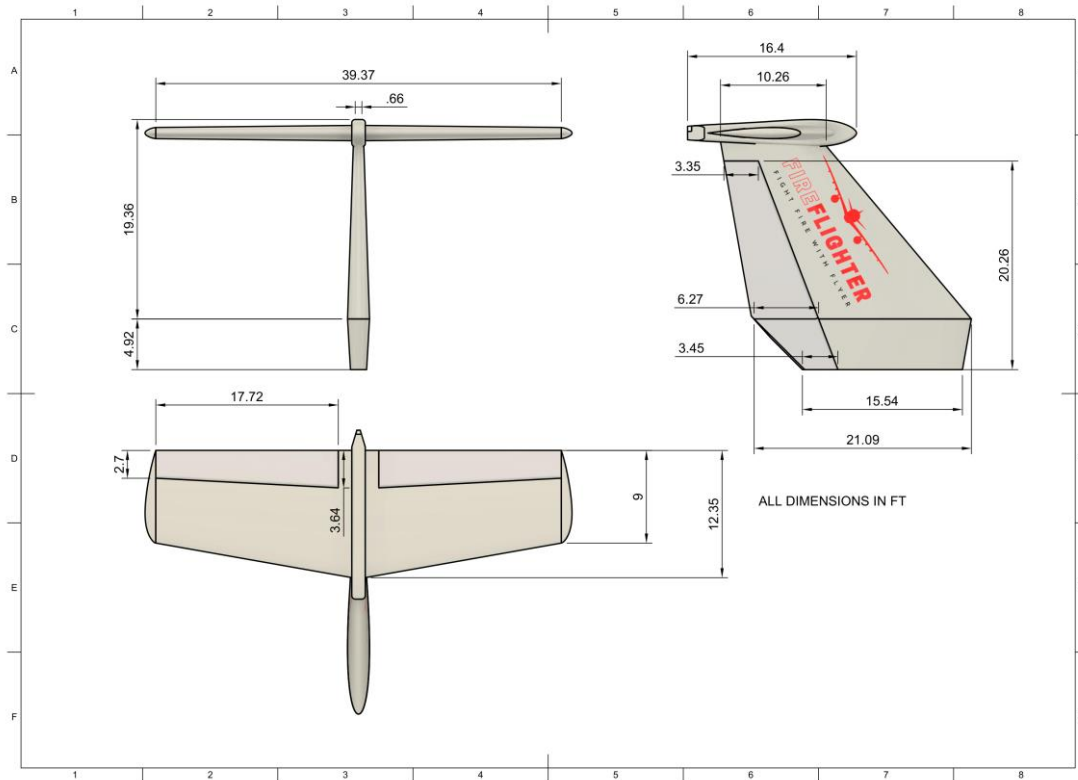


**Figure 43: Dimensioned drawing of empennage.**

**Table 26: Parameters of horizontal and vertical stabilisers.**

Component	Horizontal Stabiliser	Vertical Stabiliser	Ventral Fin	
Moment Arm (ft)	53.54	42.65	42.65	
Area (ft <sup>2</sup> )	422.48	276.85	100.64	
Span (ft)	39.37	18.04	4.92	
Root Chord (ft)	12.47	21.33	21.33	
Aspect Ratio	3.668	1.175	0.240	
Sweep (°)	10	40	10	
Taper Ratio	0.721	0.439	0.918	
Airfoil	NACA0012	NACA0010		
Incidence Angle	-3° (Variable)	0°	0°	
Control Surface	Span Ratio	0.9	0.85	1.0
	Chord Ratio	0.3	0.3	0.3
	Deflection Angle	±20°	±25°	

Weight (lbs)	1647	2278
--------------	------	------

### 11.1 Empennage Design

The empennage of the aircraft serves to provide stability and control in the yaw and pitch axes. There are several possible arrangements of the empennage surfaces, with around 70% of aircraft designed with a conventional tail due to its simplicity and relatively lower weight [69]. For the Firefly, however, the short fuselage length necessitates a large surface area on the stabilisers. On the vertical tail, this may result in a large span that contributes significantly to the height of the aircraft. An alternative configuration, the H-tail, splits the vertical stabilisers into two surfaces at the end of the horizontal stabiliser, allowing the overall height of the aircraft to be reduced. Another arrangement is the T-tail, which is commonly used on regional turboprop aircraft such as the Q400 and ATR72. The T-tail reduces the required surface area of the vertical stabiliser through the end plate effect, while also placing the horizontal stabiliser in clean air, away from the wake of the wing and increasing the effectiveness of the horizontal stabiliser.

To determine the optimal empennage configuration, a trade study on the three layouts was conducted. The weights of the respective components were estimated using the component weight approach from Raymer Chapter 15, with the sizing of the H-tail performed by reducing the horizontal tail volume coefficient by 5%. The volume coefficients of both the horizontal and vertical stabiliser were also reduced by 5% in the T-tail, as suggested by Raymer. Since no information was available to estimate the increased weight of a H-tail, a fudge factor of 1.168 from the T-tail was applied to the weight of the horizontal stabiliser in the H-Tail.

The H-tail and T-tail both reduce the wetted area of the aircraft but increases the structural weight. On the H-tail, there was a 0.7% increase in empty weight for a 0.7% reduction in wetted area, while the T-tail on the other hand, reduces the wetted area by 1.28% for only a 0.2% increase in empty weight. Thus, given the considerations for weight and wetted area, the chosen configuration is a T-tail.

### 11.2 Horizontal Stabiliser Sizing

The size of the horizontal stabiliser is determined through two main requirements. Firstly, the stability requirement, where the tail must be large enough to provide enough force to ensure a sufficient static margin for longitudinal static stability at the most-aft CG location; Secondly, a control requirement, which ensures that horizontal stabiliser provides enough force to stall, and thus control the aircraft, at the most-forward CG location

as well as when the nose-down pitching moment from the wing is the highest when flaps are deployed. These requirements are calculated using equations from Torenbeek.

Plotting the  $\frac{S_h}{S_w}$  ratio against the distance between the centre of gravity and aerodynamic centre divided by mean chord length  $\frac{x_{cg}-x_{ac}}{c}$ , the stability requirement produces an upward-sloping line representing the forward CG limit and the control requirement produces a downward-sloping line representing the aft CG limit. This is because a larger horizontal stabiliser area provides greater static margin for a more aft centre of gravity, with more downforce available to counteract a forward shift in the centre of gravity.

Besides accounting for the CG operational range, the aircraft also has to be balanced such that the CG locations fall within the forward and aft limits. This can be achieved by shifting the location of the wing, although this will result in changing the tail arm, which affects the size of the tail and thus the weights. The position of the payload will also need to be adjusted to avoid excessive CG travel under different loading conditions. Thus, the balancing is performed using an iterative process by adjusting the positions of the different components, recalculating the size and weight of the horizontal and vertical stabilisers until the criteria for minimum tail area and CG limits are achieved. Figure 44 shows the final scissor plot for the aircraft, with a minimum  $\frac{S_h}{S_w}$  ratio of 0.1813 and thus a minimum  $S_h$  of 344.12 ft<sup>2</sup>. Table 27 shows the forward and aft CG limits based on this sizing.

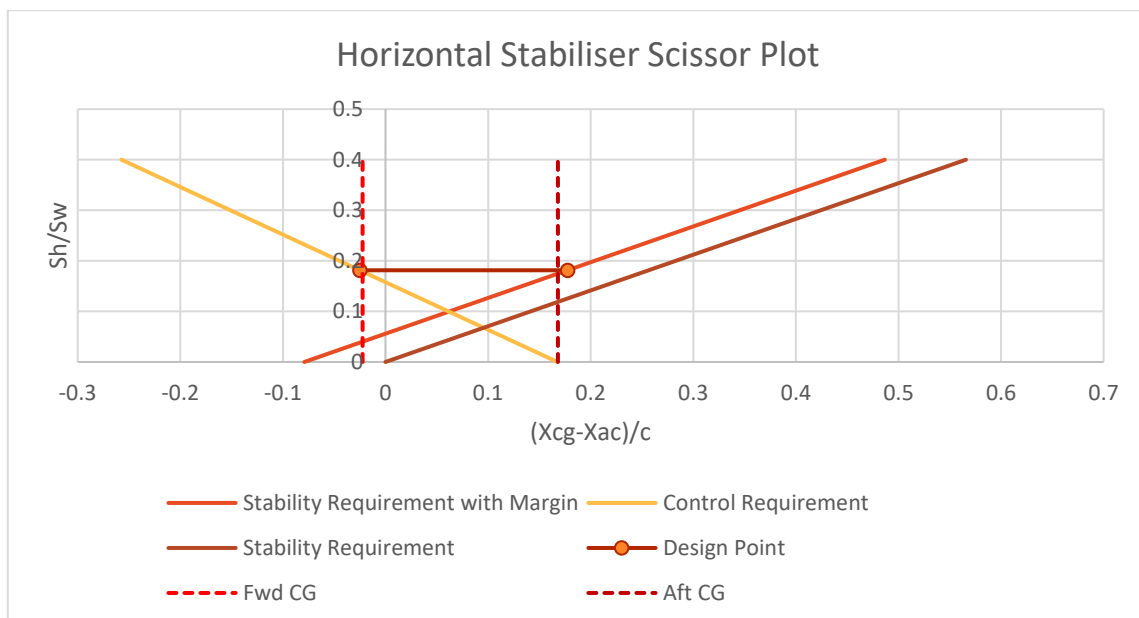


**Figure 44: Scissor plot for horizontal stabiliser sizing.**

**Table 27: CG Limits.**

Parameter	Fwd CG Limit	Aft CG Limit
$X_{CG}$	37.3 ft	39.6 ft
$\bar{X}_{cg}$	2.63	2.79

### 11.3 Vertical Stabiliser Sizing

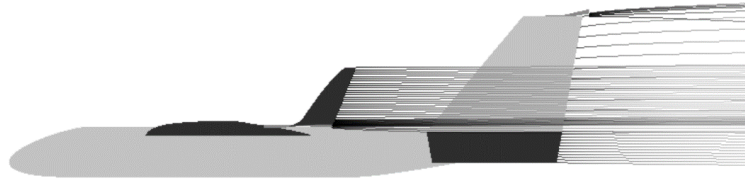
The vertical stabiliser provides lateral-directional stability to the aircraft and is sized for the following two conditions: controllability after engine failure during take-off and lateral stability during flight.

The critical condition for a 4-engined aircraft is the failure of two engines on the same side, which produces a yawing moment from the thrust of the remaining active engines as well as drag from the failed engines. Since the aircraft is equipped with variable pitch propeller, the failed engines can be feathered, which reduces the drag. The vertical stabiliser must be large enough to provide sufficient rudder authority to counter this yawing moment. This is achieved by modelling the rudder as a plain flap with a maximum deflection of  $25^\circ$  and using a minimum control speed of 1.2 times the stall speed. Equations from Scholz were used to thus calculate a required vertical tail area is  $321.41 \text{ ft}^2$ .

The vertical stabiliser also needs to provide sufficient directional stability during cruise conditions. Accounting for the stabilising moment contributions from the fuselage and vertical stabiliser together with  $C_{N,\beta} \geq 0.0571 \text{ rad}^{-1}$  as recommended by Roskam II for sufficient static directional stability, equations from Scholz and Raymer gives a minimum  $\frac{S_v}{S_w}$  ratio and minimum  $S_h$  of 0.1423 and  $270.17 \text{ ft}^2$  respectively. Between the two values, the higher value from the engine failure criteria is taken to be the minimum vertical stabiliser area, with the required area shared between the vertical stabiliser and ventral fin.

### 11.4 Moment Coefficient Slope

Based on the tail geometry, the lift and moment coefficients at different angles of attack can be obtained. Figure 46 shows the moment coefficient slopes at cruise conditions,  $x_{CG} = 37.73 \text{ ft}$ , and different elevator deflection angles, obtained from the VSPAERO simulation module of OpenVSP. An example is shown in Figure 45. The elevator deflection angle  $\delta_e$  maintains the convention of positive downwards (nose-down pitch). The horizontal line at  $C_m = 0$  are the points at which the aircraft is trimmed.



Mach: 0.600, Beta: 0.00000000, Alpha: 0.000  
Vehicle CG: 11.500000, 0.000000, 0.500000

Figure 45: VSPAERO simulation using vortex lattice method with elevator deflection  $\delta_e = -10^\circ$ .

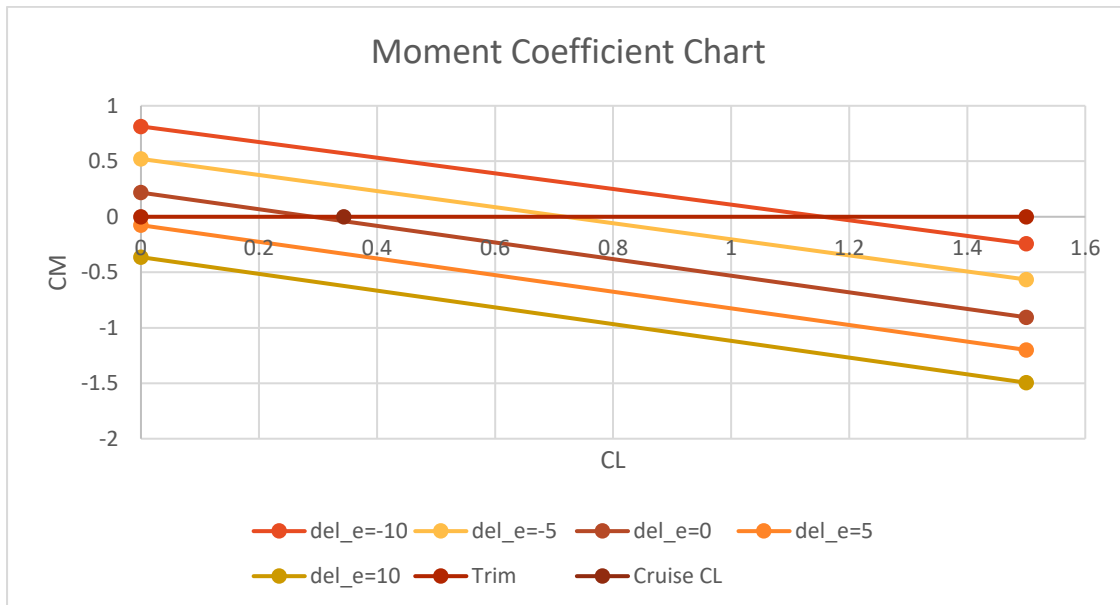


Figure 46: Moment Coefficient Chart.

Table 28: Parameters of moment coefficient chart.

Parameter	$\delta_e$				
	$-10^\circ$	$-5^\circ$	$0^\circ$	$5^\circ$	$10^\circ$
$\frac{dC_m}{dC_L}$	-0.7046	-0.7243	-0.7487	-0.7491	-0.7540
$C_{mL=0}$	0.8140	0.5212	0.2175	-0.0760	-0.3640

Since the slope of the moment coefficient chart  $\frac{dC_m}{dC_L}$  is negative, the aircraft has static pitch stability. Plotting the cruise lift coefficient on the chart also shows that the aircraft can be trimmed at cruise conditions with a set tail incidence angle of  $-3^\circ$  with minimal elevator deflection. Since the aircraft is equipped with a variable incidence

horizontal stabiliser, similar to most transport category aircraft, the incidence angle can be adjusted throughout all flight phases such that no elevator deflection is required.

The elevator control power  $C_{m\delta_e}$  can also be calculated from the moment coefficient chart, resulting in an average value of  $C_{m\delta_e} = -0.05932 \text{ deg}^{-1}$ .

### 11.5 Deep Stall

One problem of a T-tail configuration is the possibility of a deep stall, where the wake from the wing at high angles of attack blankets the horizontal stabiliser and results in the loss of pitch authority. The inclusion of stall prevention devices such as a stick pusher system allows these aircraft to fulfil ICAO stall safety requirements. The stick pusher system pushes forward automatically on the elevator if the angle of attack reaches a critical value, reducing the angle of attack and preventing the aircraft from entering a stall [70].

### 11.6 Stability Derivatives

The stability derivatives were obtained from running P, Q, R analyses in VSPAERO and shown in Table 29.

**Table 29: Stability derivatives.**

Stability Derivatives	P	Q	R
$C_{M_l}$	-48.7871	0.139484	6.643978
$C_{M_m}$	5.327572	67.17651	-9.82505
$C_{M_n}$	0.017434	1.678247	-3.99677

These stability derivatives can be used to calculate the dynamic stability properties of the aircraft, allowing the control systems such as the yaw damper to be designed and tuned.



## 12 Landing Gear

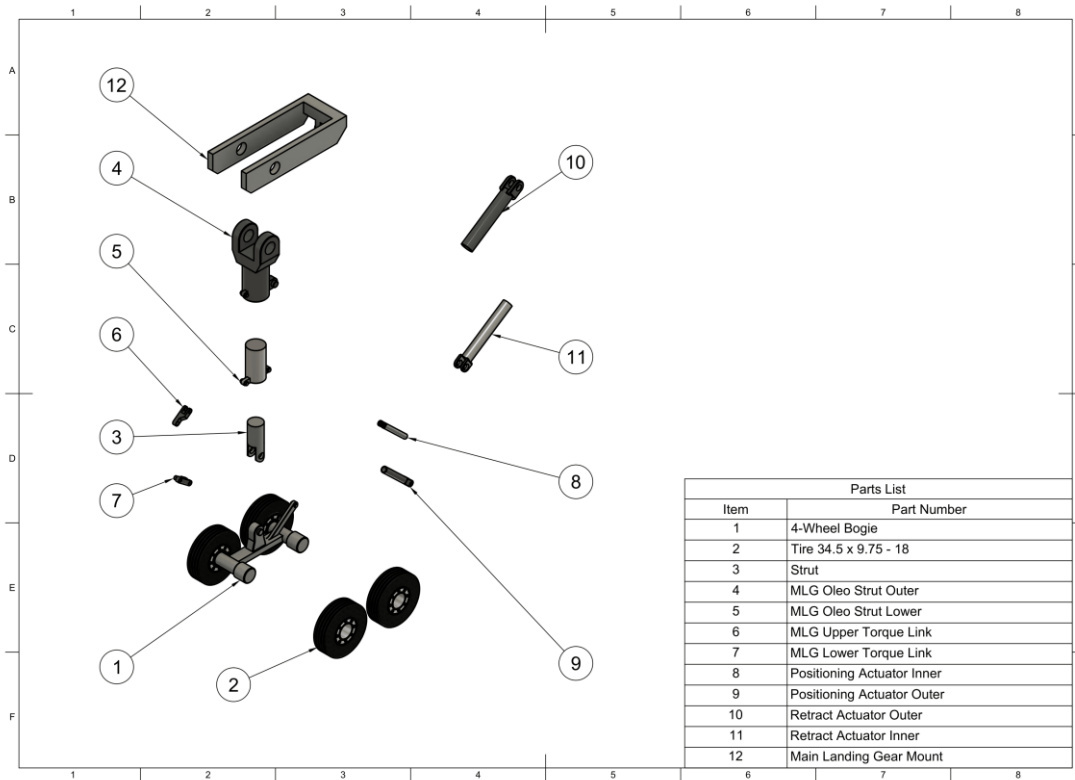


**Figure 47: Labelled diagram of main landing gear**

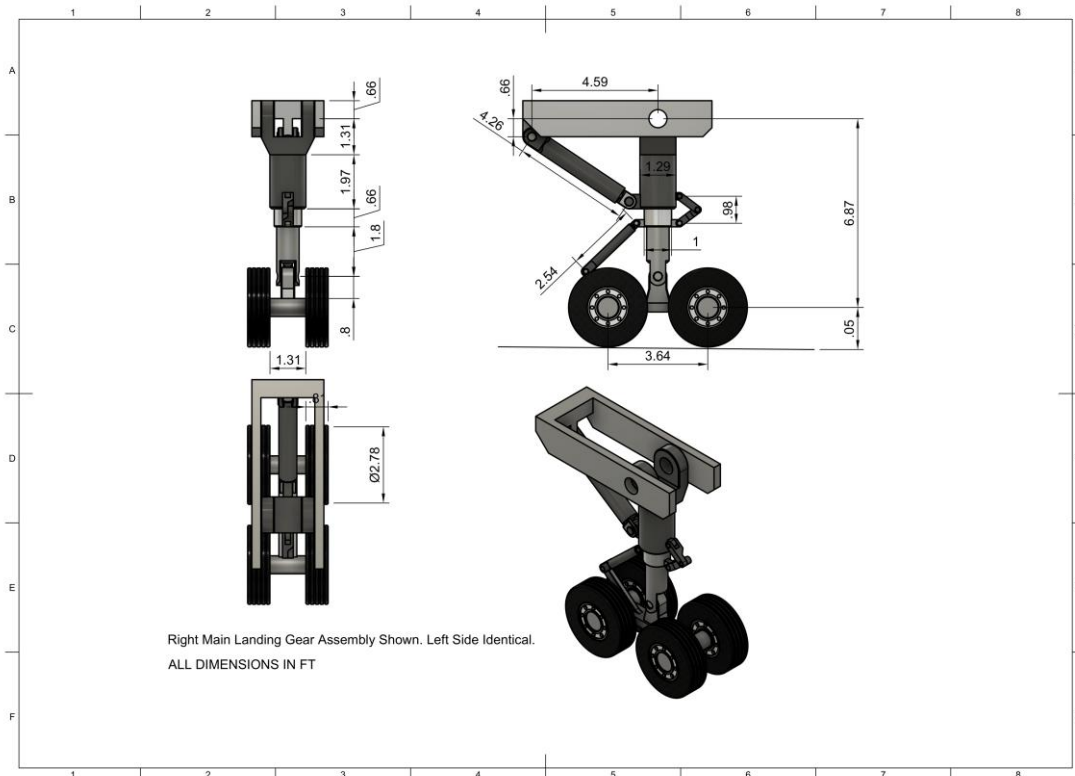


**Figure 48: Dimensioned drawing of main landing gear**

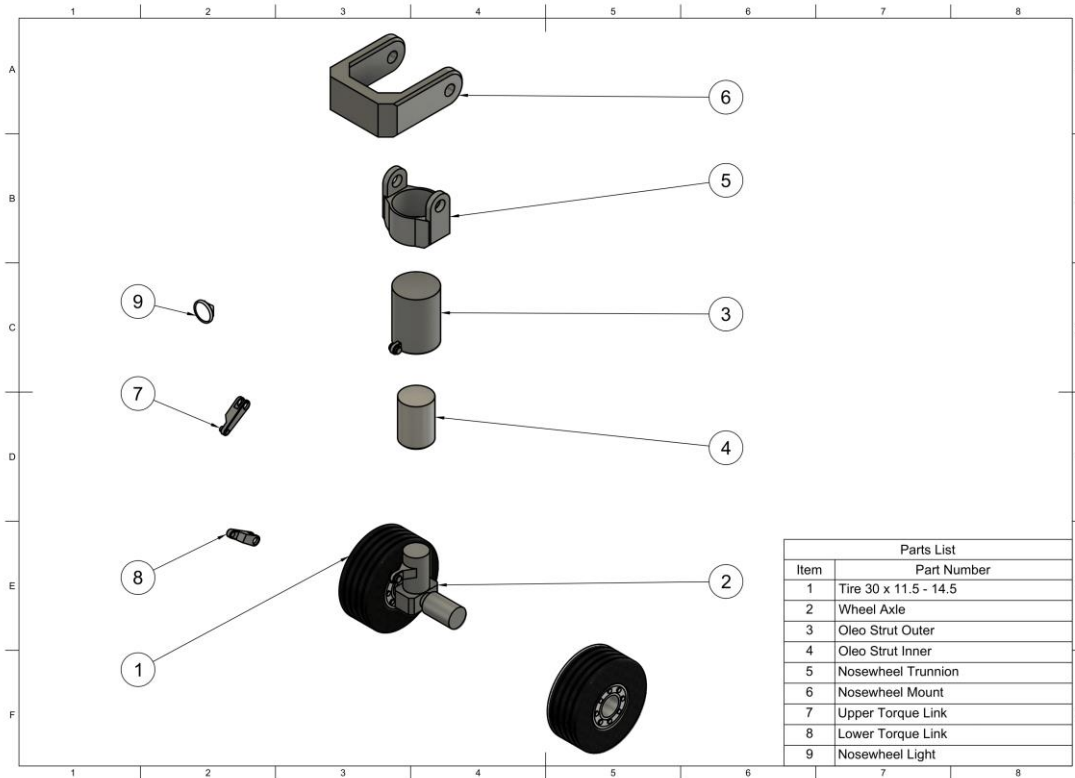


**Figure 49: Labelled diagram of nose landing gear**

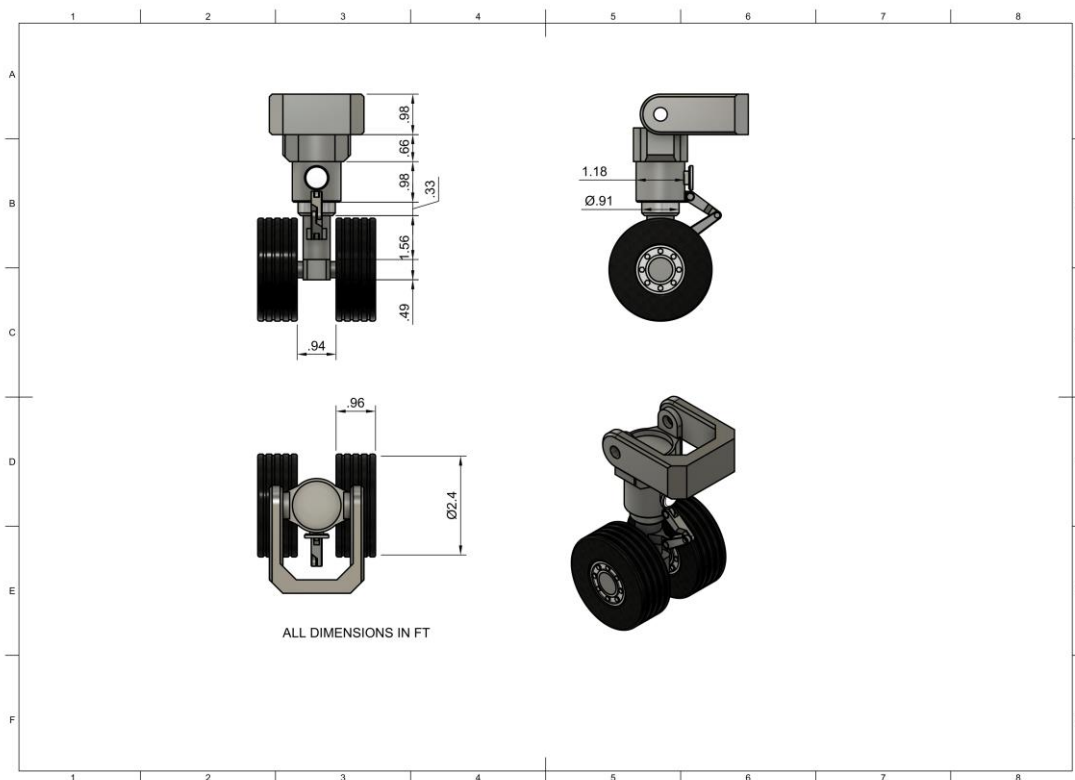


**Figure 50: Dimensioned drawing of nose landing gear**

### 12.1 Tire and Wheel Sizing

The Firefighter makes use of a tricycle landing gear. To ensure an appropriate loading distribution between the nose and main landing gear, Raymer suggests for the values for  $\frac{M_a}{B}$  to be greater than 0.05 and  $\frac{M_f}{B}$  should be less than 0.20, as seen from Figure 51.

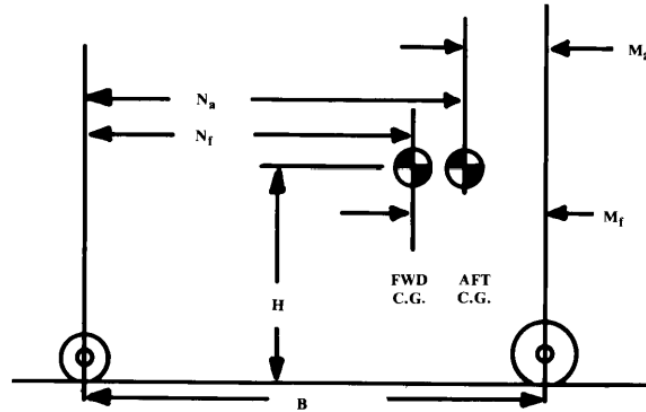


**Figure 51: Wheel load geometry**

Table 30 shows the calculated location of each parameter given the ideal distance ratio for  $\frac{M_a}{B}$  to be 0.08 and  $\frac{M_f}{B}$  to be 0.15, with the nose tire is 8.202 ft away from the nose.

**Table 30: Values for wheel load geometry**

Parameter	Distance/ft
$M_a$	0.26
$M_f$	2.53
$N_a$	31.38
$N_f$	29.11
B	34.11
H	10.66

With these values, the main landing gear is thus calculated to be located 42.35 ft away from the nose gear. Then, the tires are sized to carry the weight of the aircraft under static and dynamic loading conditions during operation. For the main landing gear, only the static loading was considered in the tire selection. However, for the nose tire both the static loading and the dynamic loading was taken into consideration and the larger sized tire was selected. Additionally, the calculated static load requires an additional 7% margin to comply with FAR 25 provision and another 25% to account for later growth of the aircraft design. Using the datasheet from

Michelin Aircraft Tire [71] and their respective static loads, the appropriate tire is selected as shown in Table 31. Two configurations for the main landing gear wheels were considered at this point, a tandem twin wheel configuration and a 4-wheel bogey arrangement.

**Table 31: Selected tires for landing gear**

Landing Gear	Nose (Twin)	Main (Twin)	Main (4-wheel bogey)
Load per tire/lbs	24,304	58,822	29,411
Tire Selected	30x11.5-14.5	50x20-20	34.5 x 9.75-18
Outer Diameter/inches	30	50.0	34.5
Width/inches	11.5	20.0	9.75
Rim Diameter/inches	14.5	20	18

### 12.2 Oleo Sizing

The landing gear oleo struts absorb the shock from the landing and is sized by determining the stroke and diameter of the piston. The method from Raymer was used to determine the size of the oleo struts. Stroke can be determined using the conservation of kinetic energy during landing. As the oleo only absorb shock vertically, only the vertical kinetic energy was taken into calculation, yielding a stroke of 0.485 ft.

The oleo diameter is determined by the load it carries. The main wheel oleo is the static load of the main gear divided by the number of oleos, which is 2, while the nose gear oleo load is the system total dynamic load of the nose gear. 1800psi was used as the oleo operating pressure to yield the internal diameter of piston, with the external diameter 30% larger than the piston diameter. The outer diameters of the nose and main gear oleo are calculated and given in Table 32.

**Table 32: Oleo outer diameter**

Landing Gear	Diameter/ inches
Nose	10.78
Main	11.86

### 12.3 Gear Retraction and Storage

The nose landing gear of the Firefly retracts rearwards into the nose landing gear wheel bay below the flight deck, as shown in Figure 52.

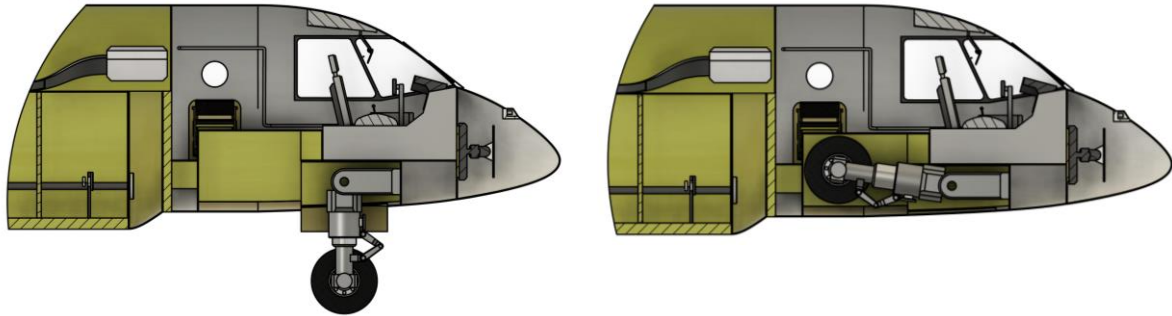


**Figure 52: Nose landing gear in extended and retracted positions**

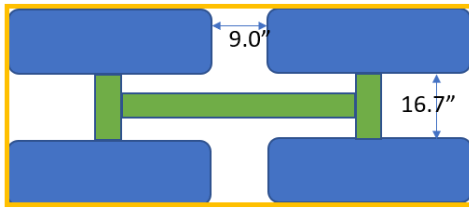
The main landing gear of the Firefly retracts into the inboard engine nacelle, similar to the Bombardier Q400. A trade study was conducted to determine the configuration of the main landing gear that results in the smallest storage volume. This would avoid unnecessary increases to the size of the inboard engine nacelle, which would increase drag and worsen the performance of the aircraft. The average storage volume of a 4-wheel bogey configuration and a tandem twin wheel configuration based on the selected tires above were calculated.

The main consideration in the design of a bogey is that there should be sufficient spacing between each wheel. This is to ensure that the wheels do not touch each other during operation and there should be sufficient space to house the brake device, brake control system, antiskid system, actuators, shock absorber and other structural components. The expansion of the tire when it is loaded must also be considered when designing the bogey, with the method to do so taken from reference [72].

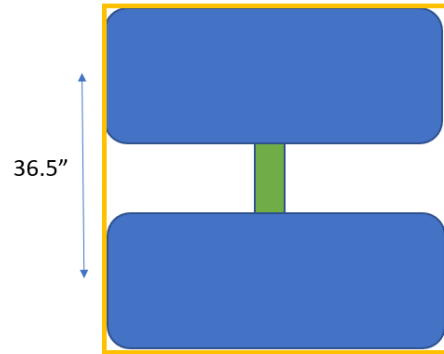
For the twin design, the expanded dimensions are used to calculate the storage volume as well. Spacing between the twin wheels was approximated from the main landing gear of A321 and spacing between bogey wheels was approximated from the main landing gear of A380. The results of the calculation are shown in Table 33 and Figure 53.

**Table 33: Expanded dimensions**

Wheel Configuration	Exp Width/inches	Exp Diameter/inches	Exp Height/inches
4-Wheel Bogey	10.4	36.8	9.4
Twin	20.8	51.7	15.8



$$\begin{aligned} \text{Approximate area} &= (9'' + 2 * D_{\text{expanded}}) * (16.7'' + 2 * W_{\text{expanded}}) \\ &= 82.72 * 37.5 \\ &= 3102 \text{ inches}^2 \\ \text{Approximate volume} &= 2947.31 * D \\ &= 2947.31 * 36 \\ &= 111672 \text{ inches}^3 \end{aligned}$$



$$\begin{aligned} \text{Approximate area} &= D_{\text{expanded}} * (36.5'' + W_{\text{expanded}}) \\ &= 51.73 * 57.3 \\ &= 2965.85 \text{ inches}^2 \\ \text{Approximate volume} &= 2965.85 * D \\ &= 2965.85 * 50 \\ &= 148292.4 \text{ inches}^3 \end{aligned}$$

**Figure 53: Storage volume estimation (left) 4-wheel bogey, (right) twin**

As the 4-wheel bogey arrangement has a smaller approximate volume, it was chosen as the arrangement for the main landing gear, with the stowage position within the engine nacelle shown in Figure 54.

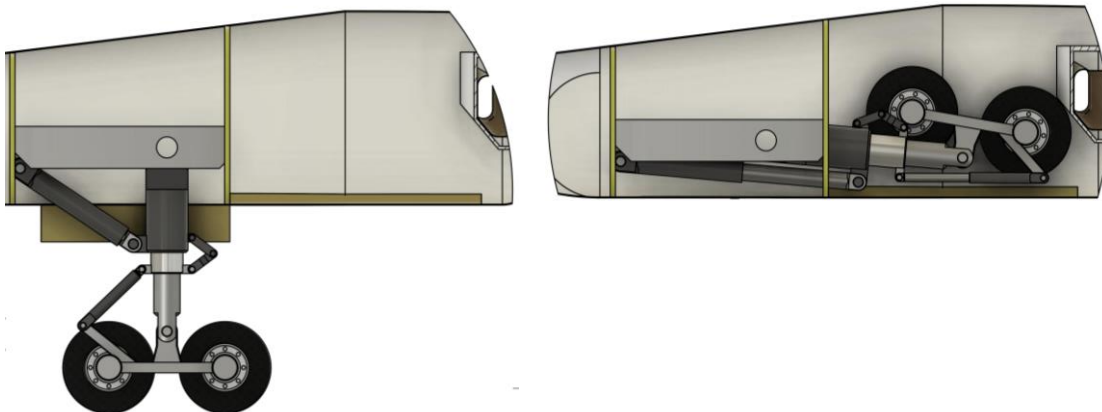


**Figure 54: Main landing gear in extended and retracted positions**

#### 12.4 Turnover Angle

The turnover angle is determined by the ground clearance and the lateral location of the main gear, as shown in Figure 55 [73].

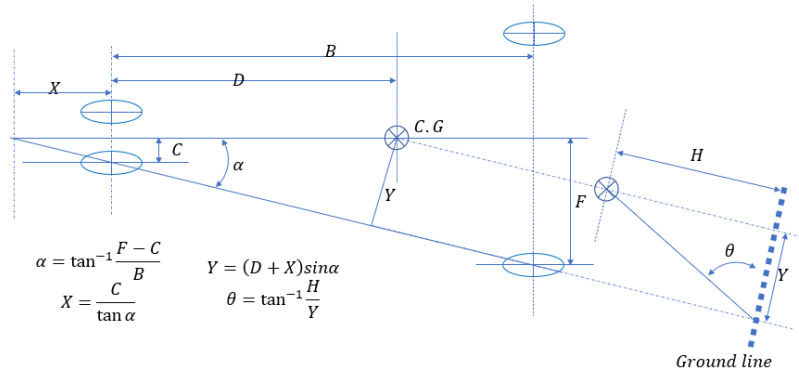


**Figure 55: Turnover angle calculation**

The nose tire separation given by  $2 \cdot C$  is the data extracted from A321-200 handbook. As suggested by Raymer, the turnover angle should never exceed  $63^\circ$ . Using the equations and the parameters where CG is the most forward CG, a graph was plotted in MATLAB as shown in Figure 56 to show the relationship between turnover angle and lateral distance between the main landing gear and aircraft centreline. From the graph the main landing gear must be placed at least 7.09 ft away from the fuselage centreline for the turnover angle to be below  $63^\circ$ . As the main landing gear is mounted to the inboard engine nacelle, which is 13.12 ft from the aircraft centreline, the turnover angle requirement is met.

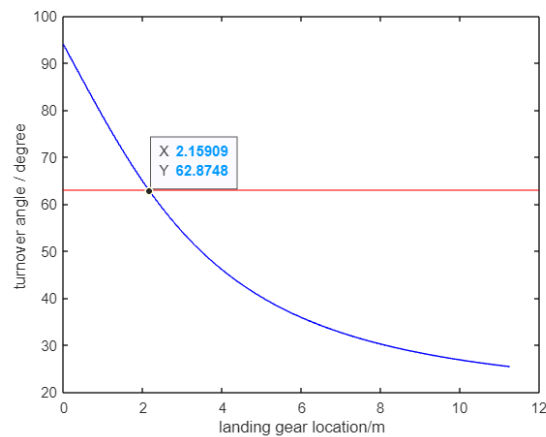


**Figure 56: Graph of main gear location against turnover angle**

### 12.5 Aircraft Classification Number (ACN)

ACN is defined by a number which expresses the relative effect of an airplane at a given weight on a pavement structure for a specified standard subgrade strength [74]. Using the COMFAA 3.0 software available on FAA website, the ACN for Fireflyer was computed for different pavement types. As shown in Table 34, the CAN of Fireflyer at maximum payload is comparable if not lower than existing firefighting aircraft. Thus, Fireflyer is able to utilise the same airports and bases as current firefighting aircraft, enhancing operational flexibility in firefighting operations.

**Table 34: ACN comparison**

Aircraft	Rigid/Flexible	A	B	C	D
C-130	Rigid	29.7	32.2	34.9	37.5
	Flexible	26.7	30.2	32.3	37.6
DC10 Airtanker	Rigid	40.6	47.0	55.9	65.4
	Flexible	43.5	46.8	54.1	75.0
747 Supertanker	Rigid	52.6	63.0	74.6	85.3
	Flexible	53.2	59.3	72.6	94.2
Fireflyter	Rigid	25.6	30.3	35.1	39.4
	Flexible	24.1	27.4	31.8	39.0

### 12.6 Turning Radius

With the geometry of the landing gear, the turning radius can also be calculated with the nosewheel at its maximum steering angle as shown in Figure 57. This allows the crew to plan for operations at different airtanker bases.

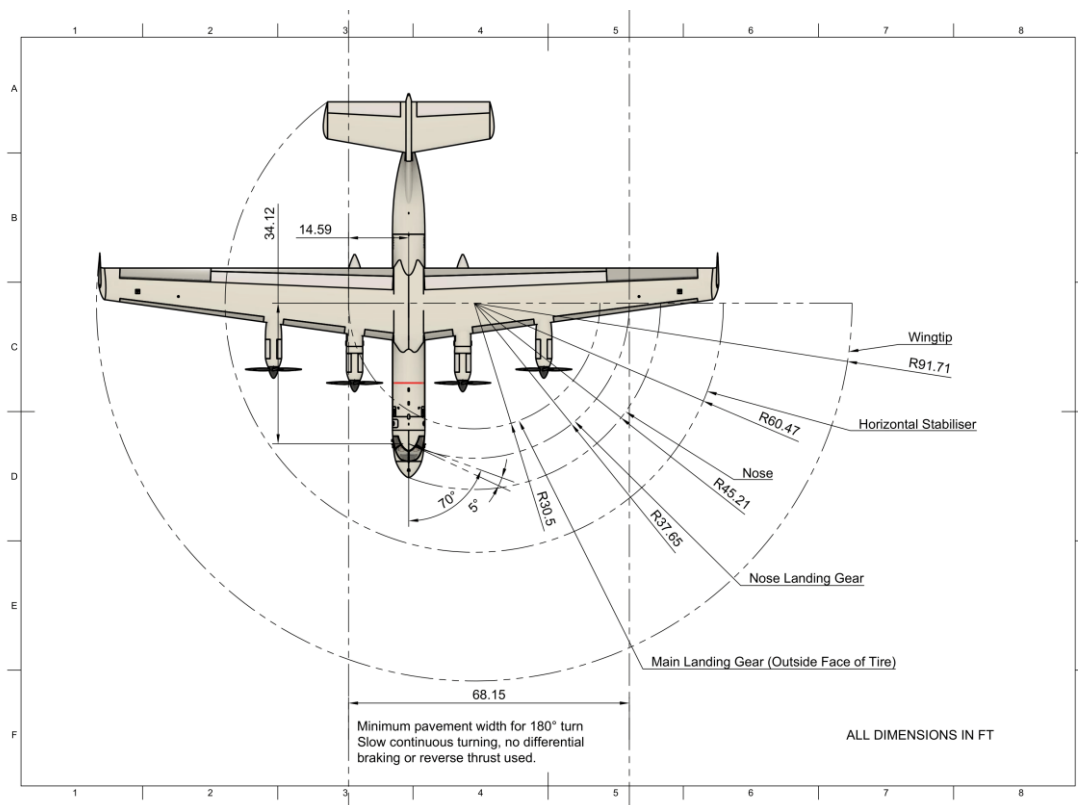


**Figure 57: Turning radius diagram**



## 13 Flight Performance

### 13.1 Methodology

Using the final weights and aerodynamic characteristics of Firefly, the flight performance of the aircraft vis-à-vis the mission profiles were calculated using equations from Raymer Chapter 17. In this way, the design of the aircraft was validated in its ability to meet all requirements set out in the RFP.

### 13.2 Design Mission

Table 35 below tabulates the specific mission segment weight fractions, fuel consumed, as well as flight performance values in each mission segment of the design mission.

**Table 35: Fuel Fraction and Fuel Consumed for Mission Segments (Design Mission)**

Mission Segment		Fuel Fraction		Fuel Consumed (lbs)	Assumptions
1	Warmup, taxi and takeoff	$W_1/W_0$	0.9896	1858.91	5,000 ft elevation
2	Climb to 20,000 ft	$W_2/W_1$	0.9925	1333.06	Min Power Climb $V_{average} = 3359.3 \text{ ft/min}$
3	Cruise for 400 nm	$W_3/W_2$	0.9650	6138.97	$V = 368.61 \text{ knots}$ $M_{cruise} = 0.6$
4	Descent	$W_4/W_3$	0.9950	845.91	-
5	Manoeuvring for payload drop (Sea level conditions)	$W_5/W_4$	0.9245	12703.31	4 drops taking 10 minutes each $V = 1.2V_{stall} = 102.11 \text{ knots}$
6	Climb to 20,000ft	$W_6/W_5$	0.9831	1413.49	Min Power Climb $V_{average} = 7657.2 \text{ ft/min}$
7	Dash at 400 knots for 400 nm	$W_7/W_6$	0.9298	5770.37	$V = 400 \text{ knots}$
8	Descent	$W_8/W_7$	0.9950	382.24	-
9	Landing and Taxi	$W_9/W_8$	0.9920	608.53	5,000 ft elevation
10	[Reserve] Climb to 20,000ft	$W_{10}/W_9$	0.9866	1009.89	Min Power Climb $V_{average} = 8498.4 \text{ ft/min}$
11	[Reserve] Cruise 100 nm to divert field	$W_{11}/W_{10}$	0.9822	1323.14	$V = 368.61 \text{ knots}$ $M_{cruise} = 0.6$

12	[Reserve] Descent	$W_{12}/W_{11}$	0.9950	365.62	-
13	[Reserve] Climb to 5,000 ft	$W_{13}/W_{12}$	0.9946	391.09	Min Power Climb $V_{average} = 8820.4 \text{ ft/min}$
14	[Reserve] 45 minutes at cruising speed	$W_{14}/W_{13}$	0.9876	894.13	$V = 102.49 \text{ knots}$

### 13.3 Ferry Mission

Table 36 below tabulates the specific mission segment weight fractions, fuel consumed, as well as flight performance values in each mission segment of the ferry mission.

**Table 36: Fuel Fraction and Fuel Consumed for Mission Segments (Ferry Mission).**

Mission Segment		Fuel Fraction		Fuel Consumed (lbs)	Assumptions
1	Warmup, taxi and takeoff	$W_1/W_0$	0.9843	1839.49	5,000 ft elevation
2	Climb to 20,000 ft	$W_2/W_1$	0.9904	1100.08	Min Power Climb $V_{average} = 5420.4 \text{ ft/min}$
3	Cruise for 3000 nm	$W_3/W_2$	0.6762	36938.15	$V = 307.17 \text{ knots}$ $M_{cruise} = 0.5$
4	Descent	$W_4/W_3$	0.9950	385.67	-
5	Landing and Taxi	$W_5/W_4$	0.9920	613.99	5,000 ft elevation
6	[Reserve] Climb to 20,000ft	$W_6/W_5$	0.9867	1010.36	Min Power Climb $V_{average} = 8419.2 \text{ ft/min}$
7	[Reserve] Cruise 100 nm to divert field	$W_7/W_6$	0.9824	1323.12	$V = 368.58 \text{ knots}$ $M_{cruise} = 0.6$
8	[Reserve] Descent	$W_8/W_7$	0.9950	369.01	-
9	[Reserve] Climb to 5,000 ft	$W_9/W_8$	0.9947	391.15	Min Power Climb $V_{average} = 8736.6 \text{ ft/min}$
10	[Reserve] 45 minutes at cruising speed	$W_{10}/W_9$	0.9876	902.45	$V = 102.98 \text{ knots}$

### 13.4 Performance Summary

The flight performance for a variation of the design mission with no payload drop was also calculated. This could be because weather conditions do not permit a safe drop, resulting in an aborted mission and the payload being kept throughout the entire mission. As fire retardant can be costly, the ability to complete the mission without jettisoning the payload is thus a desirable. Table 37 shows the summary of aircraft performance values across the design and ferry missions. The fuel requirements are within the total fuel tank capacity, with the BFL and landing distance meeting RFP requirements.

**Table 37: Summary of aircraft performance.**

Performance	Design Mission (Payload drop)	Design Mission (No payload drop)	Ferry Mission
$W_e$ (lbs)	68,712		
$W_{crew}$ (lbs)	500		
$W_{payload(Takeoff)}$ (lbs)	72,000		0
$W_{payload(Landing)}$ (lbs)	0	72,000	0
$W_f$ (lbs)	37,300	41,500	47,800
$W_0$ (lbs)	178,512	182,712	117,012
Take-off distance (ft)	3,756	3,849	3,117
Balanced Field Length (ft)	4,533	4,762	2,014
Landing distance (ft)	2,839	4,101	2,559
Mission Duration (Including Reserve) (hr)	4.16	4.20	11.12

The maximum velocity of the aircraft, absolute ceiling, and service ceiling were also calculated, and given in Table 38.

**Table 38: Maximum Velocity, Absolute and Service Ceilings**

<b>Maximum Velocity</b>	713 ft/s (20,000 ft, MTOW)
<b>Absolute Ceiling</b>	34,500 ft
<b>Service Ceiling</b>	33,200 ft

Although the RFP specifies a desired dash speed, that may not be the most optimal speed for every firefighting mission. For example, an extended operation to lay down extensive retardant lines may opt for a more

economical mission profile to generate a greater number of sorties, as opposed to maximising the sortie rate.

Thus, the best cruise velocities at different altitudes were calculated based on the Breguet range equation for propeller aircraft and shown in Figure 58.

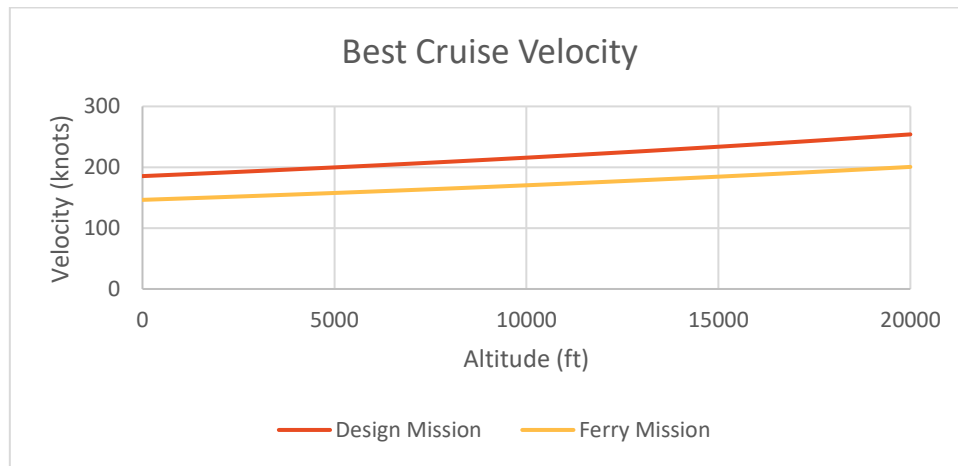


**Figure 58: Best cruise velocity at different altitudes**

### 13.5 V-n Diagram

A V-n diagram is a chart of load factor versus flight speed, and shows the limits of an aircraft’s performance at different airspeeds. The V-n diagrams are constructed based the guidelines from Federal Aviation Regulation (FAR) Part 25. Although a transport category aircraft of this size only requires a limit load factor of 2.5g, a higher limit load factor of 3.25g was used, based on the purpose-built CL-415. This is because of the larger loads encountered during low-altitude payload drops. A sufficiently high limit load factor is critical not just for the operational safety of the airframe but for the aircrew as well, as French pilots in the Sécurité Civile voiced concerns in 2006 over insufficient load factors (2.1g fully loaded and 3g empty) of converted Dash 8 aircraft used in a firefighting role [75]. The negative limit load factor used is -1, together with the design cruise speed of 400 knots.

A gust V-n diagram indicates the safe operating limits of an aircraft in gusty conditions. The gust speeds used were 20 m/s, 15.25 m/s, 7.5 m/s for conditions at 5,000 ft altitude, and 11.6 m/s, 7.6 m/s, 3.8 m/s for conditions at 20,000 ft altitude, based on FAA requirements. Figure 59 shows the gust V-n diagram for the design mission at sea level, while Figure 60 shows the diagram for the ferry mission at sea level. In both plots, the green lines represent the gust diagram, while the red lines represent the V-n diagram.

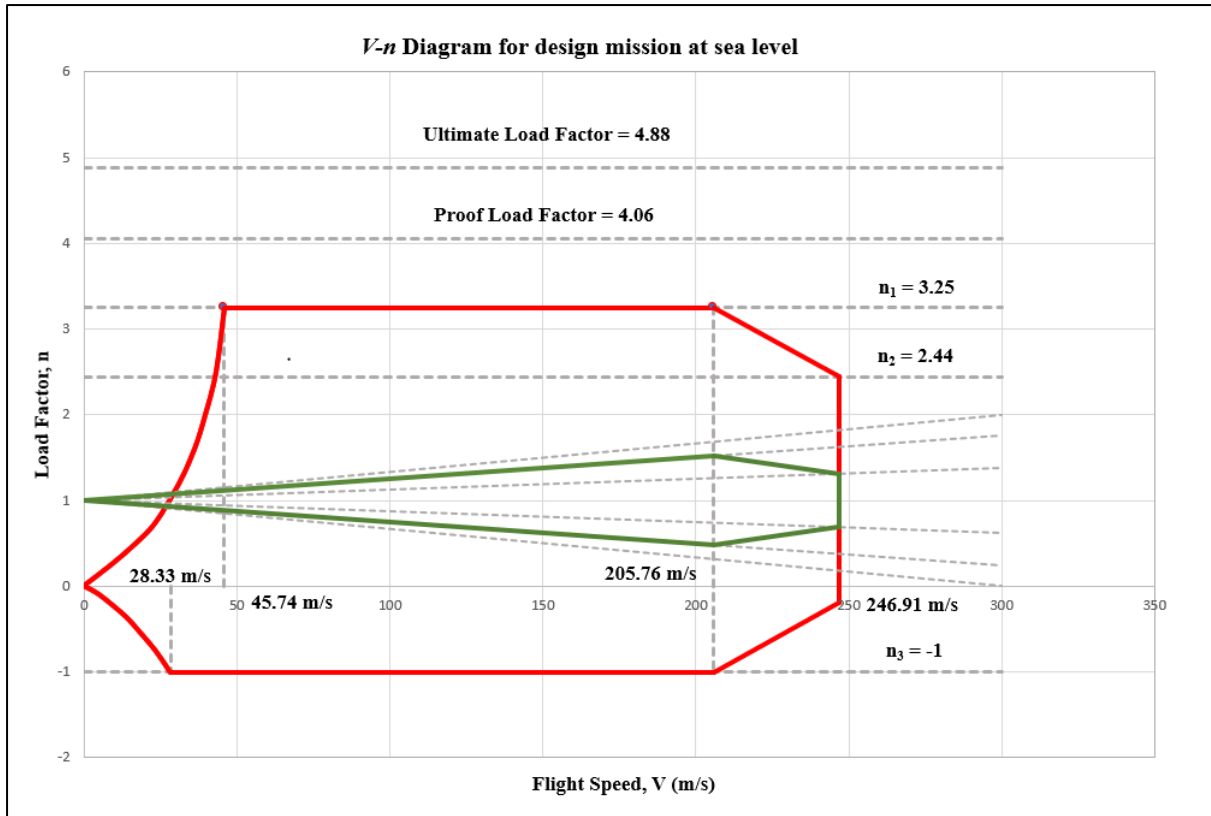


Figure 59: V-n diagram of design mission at sea level

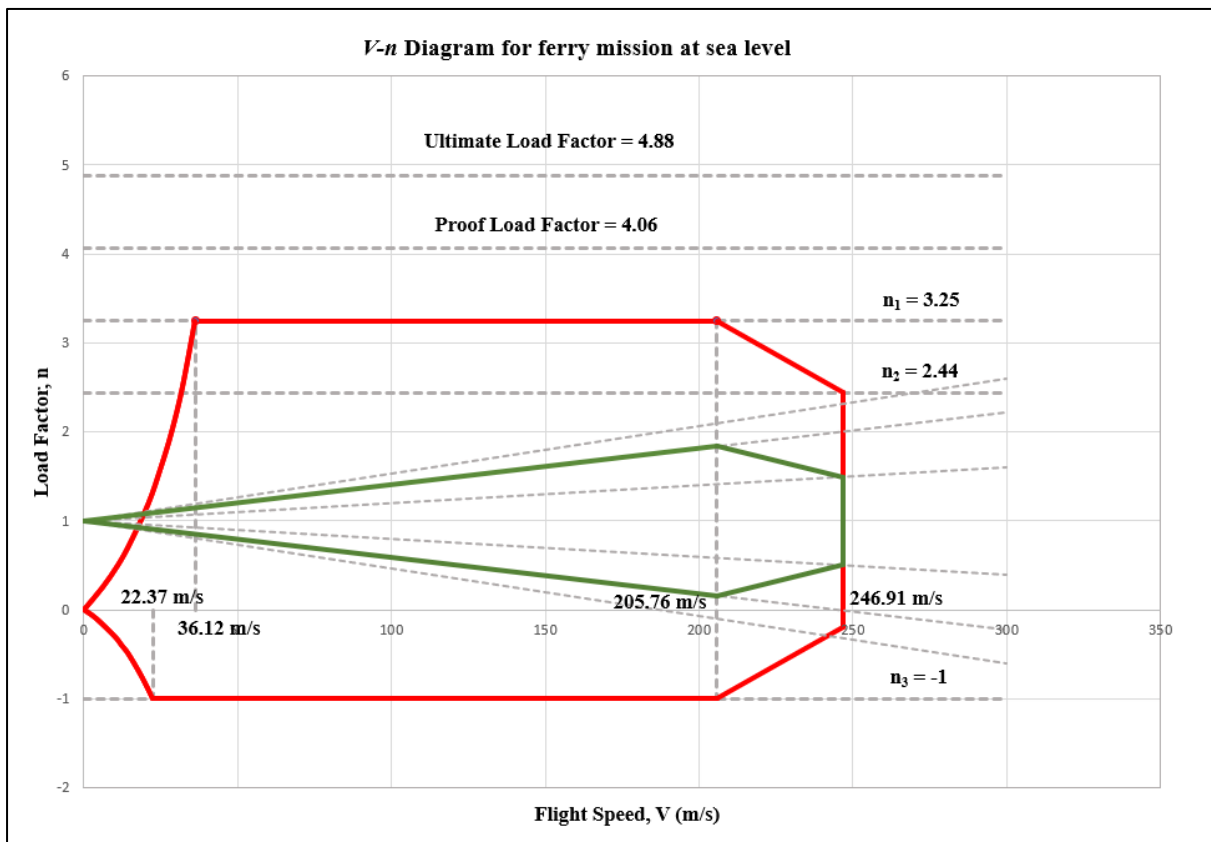
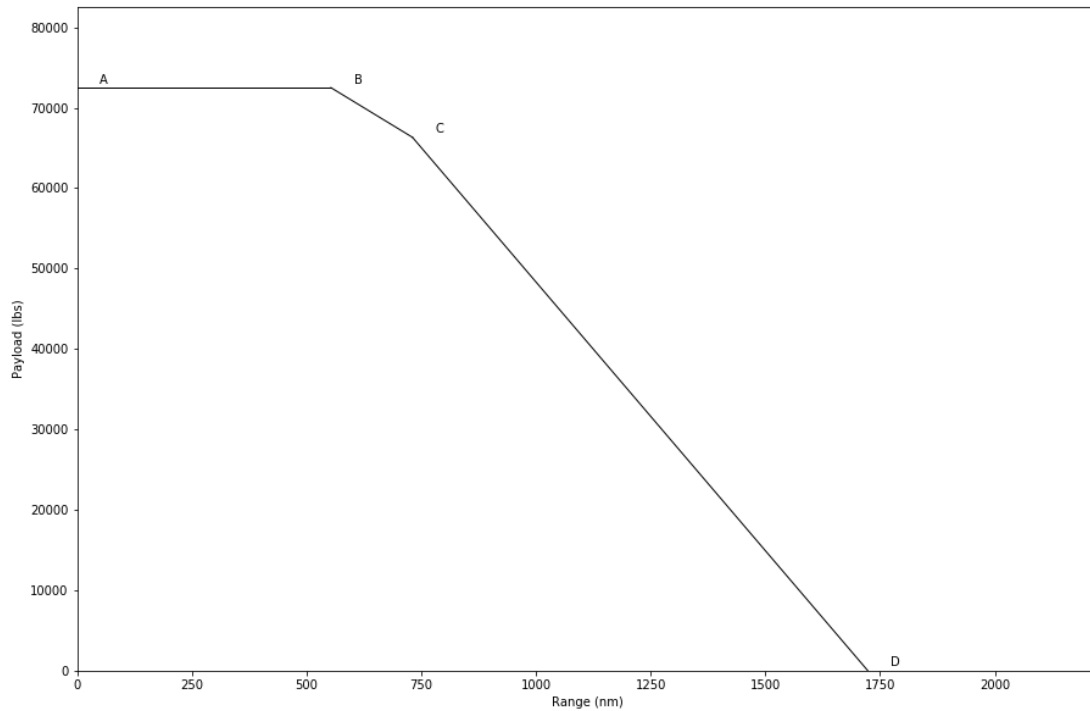


Figure 60: V-n diagram of ferry mission at sea level

### 13.6 Payload Range Diagram

The payload range diagram illustrates the trade-off relationship between the payload and the range of one single aircraft. The payload refers to all the mass that is taken by an airplane, excluding fuel. The structure of an aircraft is designed to sustain a certain amount of load.



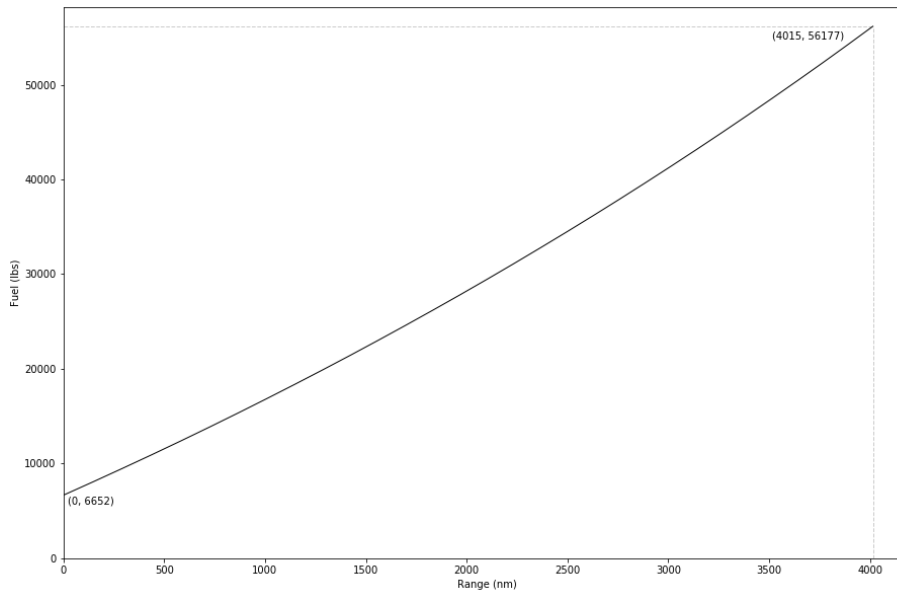
**Figure 61: Payload Range Diagram for Design Mission without Payload Drop**

Figure 61 above represents the payload range diagram for the design mission, assuming it does not drop its payload. The diagram measures the trip both ways. This means that a range of 400 nm will represent the airplane travelling 400 nm to the firefighting site, and 400 nm back to its take-off airport. Table 39 below represents the payload weight and range corresponding to the points A to D, where the slope joining points B and C represents the trade-off between payload and fuel under the constraint of maximum take-off weight, point D represents the maximum range of the aircraft (no payload and maximum fuel), and the slope joining points C and D represents the reduction of payload to maximize range.

**Table 39: Payload and Range Calculated for Design Mission without Payload Drop**

Point	Payload Weight (lbs)	Range (nm)
A	72,500	0
B	72,500	553
C	66,322	730
D	0	1723

### 13.7 Fuel Range Diagram



**Figure 62: Fuel Range Diagram for ferry mission**

Figure 62 above represents the fuel range diagram for the ferry mission. The longest range achievable is approximately 4000 nm at maximum fuel capacity, exceeding the 3000 nm range requirement and enabling the aircraft to be deployed more flexibly across various locations worldwide. It should be noted that this excess range is a by-product of the large fuel tank capacity as a result of the wing geometry, which was determined based on other operational requirements.

## 14 Aircraft Systems

### 14.1 De-icing System

De-icing and Anti-icing systems are extremely vital in modern aircraft to protect important operating components on the aircraft such as the wing leading edge, pitot tubes, and stall warning systems from structural icing, which may lead to a loss of lift or poor instrument readings. Firefly is equipped with Electro-Thermal blankets similar to those use on the 787, which is energised directly from the electrical system compared to traditional pneumatic heating systems that rely on engine bleed air. This greatly reduces the power consumption as compared to the traditional bleed-air de-icing technique, from a range of 150-200kW to less than half, 45-75kW [76].

## 14.2 Crew Oxygen Supply System

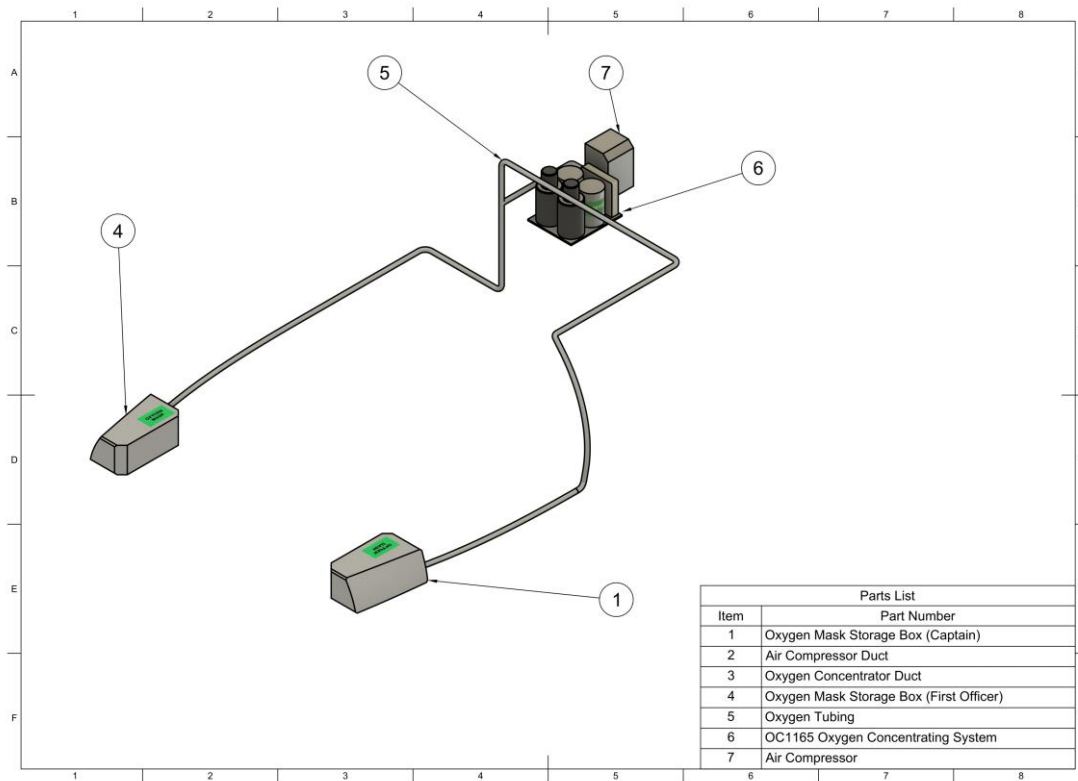


**Figure 63: Oxygen supply system**

The fuselage of Firefly is designed to be unpressurised, in order to reduce weight and the structural fatigue that comes with accumulated pressure cycles. Thus, an oxygen supply system for the 2-man crew is necessary, as FAA regulations require continuous oxygen to be supplied for flights that are above 10,000 feet for a duration of more than 30 minutes. Firefly is equipped with a Molecular Sieve Oxygen Generator (MSOG), also used on the C-130 [77], taking in ambient air and extracting oxygen, supplying it to the crew. This installation requires minimal modification to the aircraft, and it weighs much lesser than a liquid oxygen storage system. Using this oxygen generator, the life cycle cost is reduced, and there is no need for repeated refilling of oxygen in storage cylinders, reducing the turnaround time of the aircraft. Although the use of oxygen generators on non-military or commercial aircraft has not yet been certified, its capabilities have been well proven in its application on military aircraft [78], thus making it a optimal choice in supplying oxygen to the crew.

## 14.3 Weather and Terrain-Following Radar

A weather radar system is crucial for pilots to detect and assess the weather conditions ahead in the flight. This enables the pilot to plan the flight route and navigate through the skies safely and strategically. The radar is also often used to detect the presence of cumulonimbus clouds, as these clouds could be an indicator to the common threats to an aircraft during flight, which includes turbulence, hail and windshear.



As the aircraft performs its payload drop at a low altitude across varying terrain such as hills and canyons, the installation of a terrain-following radar is desired to enhance mission effectiveness. Terrain-following radar is commonly used in the military to enable aircraft to execute terrain hugging flights. With the automation of terrain navigation, the pilots will also be able to execute other flight tasks with better focus, and the release of the retardant can also be more precisely controlled for more effective payload drops. The weather and terrain-following radar is installed in the nose of the aircraft, as shown in Figure 64.



**Figure 64: Weather and terrain radar in the nose of the aircraft**

14.4 Electrical System

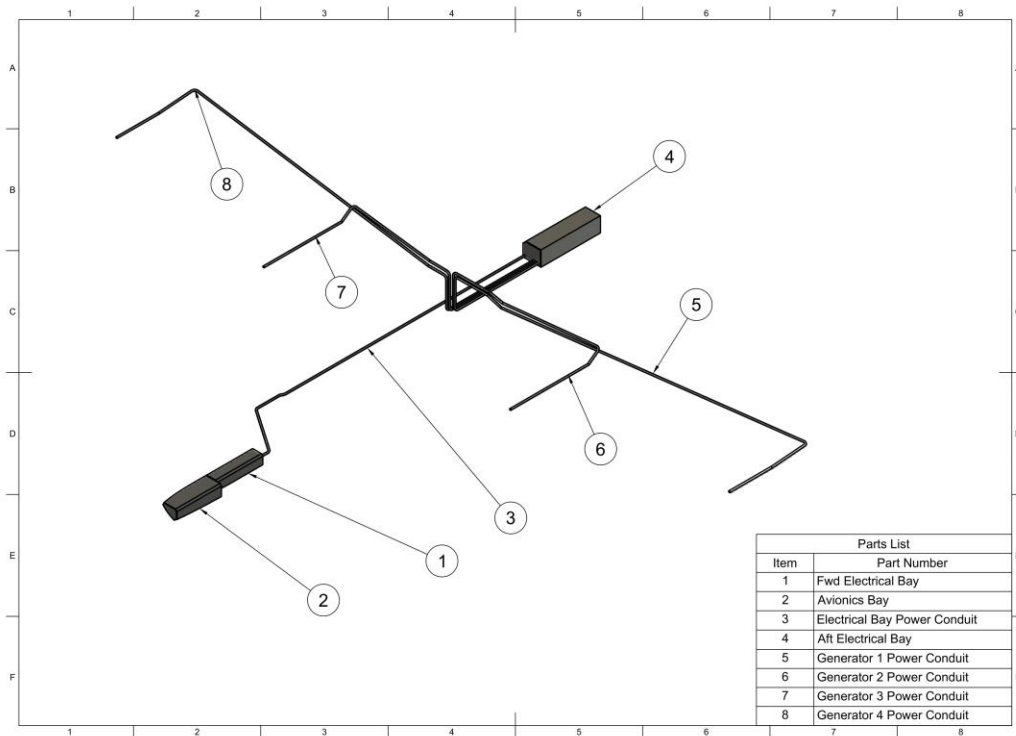


Figure 65: Physical layout of electrical system

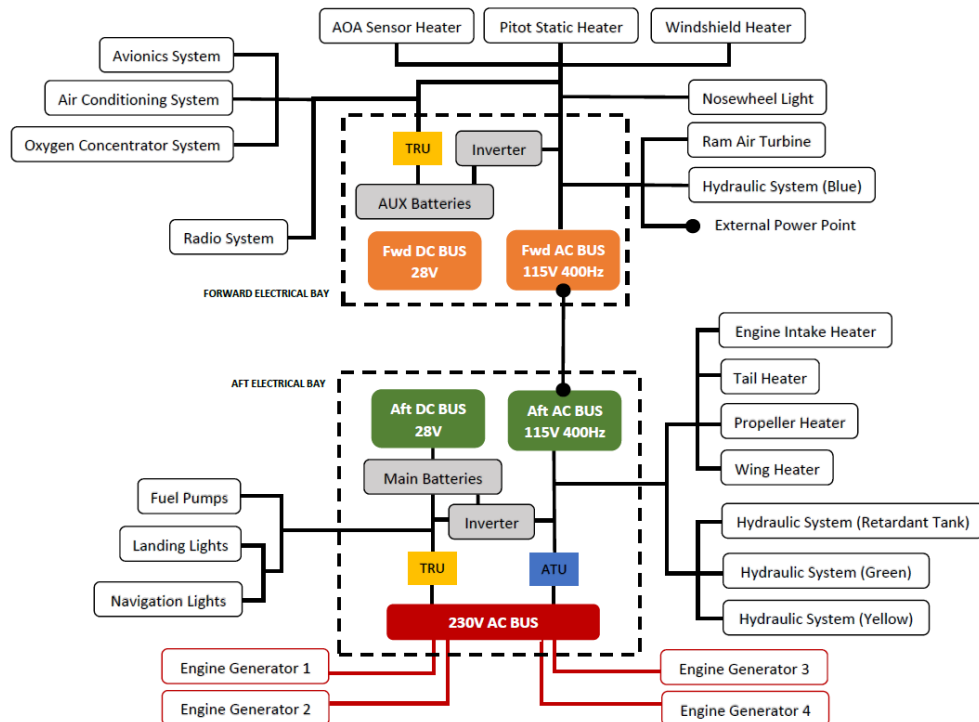


Figure 66: Electrical System Schematic Diagram

The electrical system consists of a 230V AC electrical bus that is powered by the engine generators in the 4 turboprop engines. The generators can also serve as the electrical starters for the PW150A engines [79], eliminating the need for maintenance-intensive bleed air systems in the aircraft and improving the aircraft's reliability. An Auxiliary Power Unit (APU) is also thus not necessary and omitted to save weight. The system relies on having remote distribution systems at the front and aft of the aircraft to power the aircraft control systems in different sections of the aircraft, similar to the electrical layout of a 787. Each distribution system includes a 28V DC bus unit and a 115V AC bus unit. An inverter is connected between these 2 units to spontaneously invert the power output from one unit to another, in the case where the components of a unit require higher power input. In comparison to the 787's electrical system, this proposed system does not have an additional 270V DC distribution system as the electrical load from the environmental control system pressurisation is not required.

In the aft of the aircraft, there is an auto-transformer unit (ATU) attached to the Aft AC Bus and a transformer rectifier unit (TRU) attached to the Aft DC Bus. The ATU serves to convert the power output from the 230V AC Bus to a power input of 115V AC in the Aft AC bus. Similarly, the TRU has both a transformer and a rectifier installed to convert the 230V AC power to 28V DC power to be supplied to the Aft DC bus [80]. The Aft AC bus will supply power to the main hydraulic systems in the aircraft as well as the heaters in the aft components. The Aft DC bus supplies power to the exterior lighting system and the fuel pumps.

The forward electrical bay is subsequently connected to the aft electrical bay via the Aft AC bus. The Forward AC bus serves as the main power source for the heaters in the cockpit area and the sensors. The Forward DC bus will supply electrical power to the various aircraft systems such as the avionics system, air-conditioning, oxygen concentrator, and the radio communications system. When the engines are turned off, electrical power can be supplied to the aircraft via the external power port, which is located in the forward electrical bay and shown in Figure 67.



**Figure 67: External power door open**

### 14.5 Hydraulic System

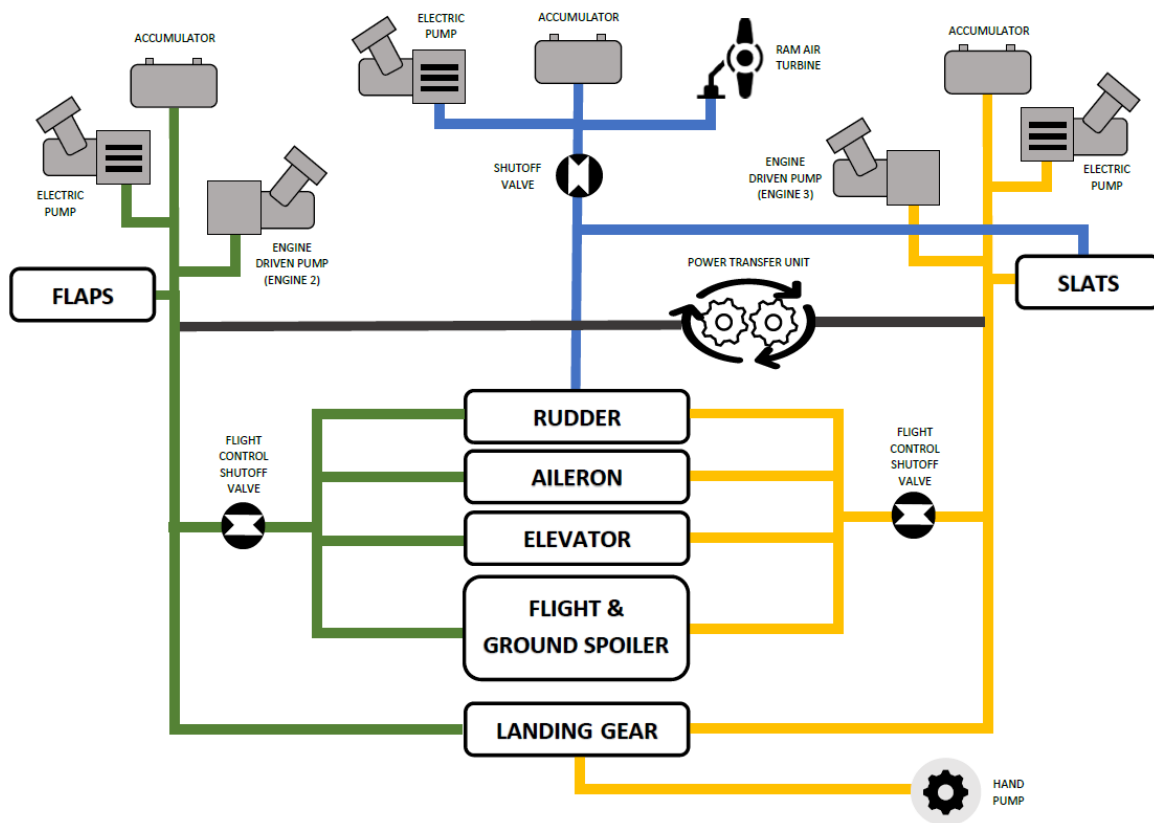


**Figure 68: Hydraulic System Schematic Diagram**

The proposed hydraulic system consists of 2 main hydraulic lines (Green and Yellow) and 1 backup line (Blue). Each main hydraulic line is operated by an engine driven pump as well as an electric pump. The reserve hydraulic line is powered by an electric pump and the ram air turbine. For redundancy, every hydraulic line is also fitted with an accumulator that serves to regulate the pressure of the system.

Each of the control surfaces operated by hydraulics is connected to 2 different hydraulic lines. This would ensure that the control surfaces continue to stay operational even when one of the connecting hydraulic lines is faulty. This is supported by the installation of the power transfer unit between the 2 main hydraulic lines, which

allows the transferring of hydraulic power from one system to another with having the need to share the hydraulic fluid.

Shutoff valves are connected within each hydraulic system to act as safety valve, controlling the flow of hydraulic fluid in the system. When the system is operating, hydraulic pressure is exerted on the valve and the valve will be kept open. When the system is not in use, the pressure will be removed and the valve at rest will remain closed [81].

### 14.6 Fire Protection System

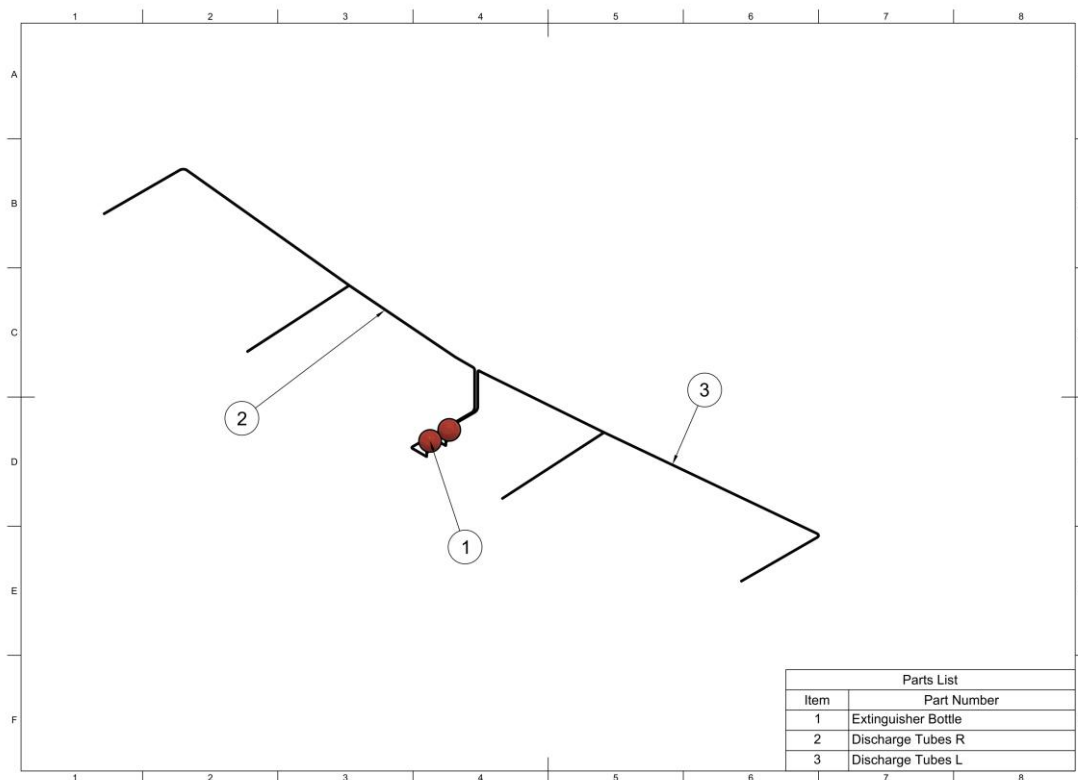


**Figure 69: Fire protection system**

Fire is one of the most common threats onboard an aircraft, especially when it is concerning certain vital aircraft operating systems. The FAA has outlined several fire protection regulations in the Federal Aviation Regulations Part 25, which includes the requirements for the fire detection and fire extinguishing systems, as well as the mandatory testing methods of the protection systems. Different regulations have been listed for specific fire zones to apply for different aircraft components and all the requirements must be proven to be achieved through either actual or simulated flight tests [82]. Thus, Firefly is equipped with a Halogenated Hydrocarbons Fire Extinguishing System with Halon 1301 as the inert extinguishing agent.

## 15 Crew Compartment

### 15.1 Flight Deck

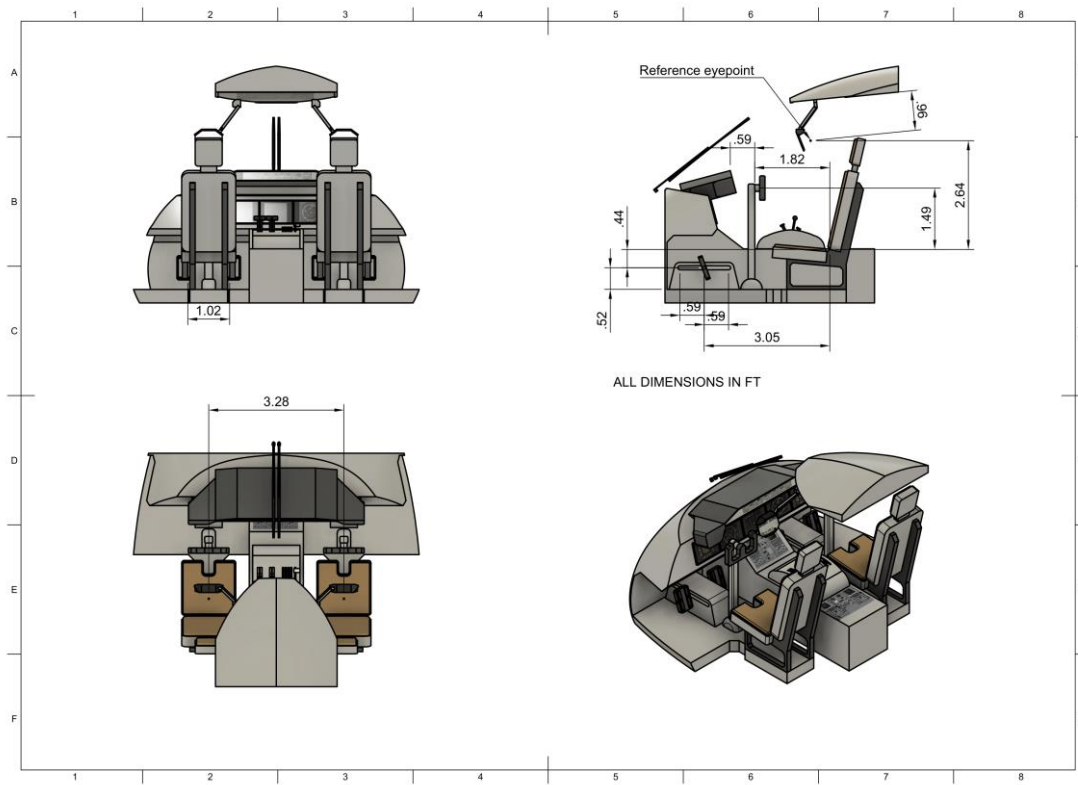


**Figure 70: Dimensioned drawings of flight deck**

The flight deck is designed such that the flight controls and instruments are easily accessible, a clear view is provided of the outside, and it can be adjusted for pilots of varying dimensions. This is crucial during firefighting missions as good situational awareness of the terrain and other aircraft is essential when operating at low altitudes. The reference eye point method from Torenbeek was used to define the positions of the seat, controls, instrument panels, and windows, using the recommended flight deck dimensions for transport aircraft with wheel controls. The dimensions of the various components are shown in Figure 70.

The visibility from the cockpit is essential during ground movement, takeoff, landing, as well as during the payload drop. The flight deck windows of Firefly were designed to meet minimum required clear angles of vision for VFR flight using the reference eye point from Torenbeek, as shown in Figure 71 to Figure 73. This enables the flight crew to have excellent visibility when flying close to the ground at high angles of attack, such as during landing or during a retardant drop. The designed view angles also facilitate ground taxiing at airtanker bases since the wingtips can be easily seen.

15.2 Cockpit Visibility

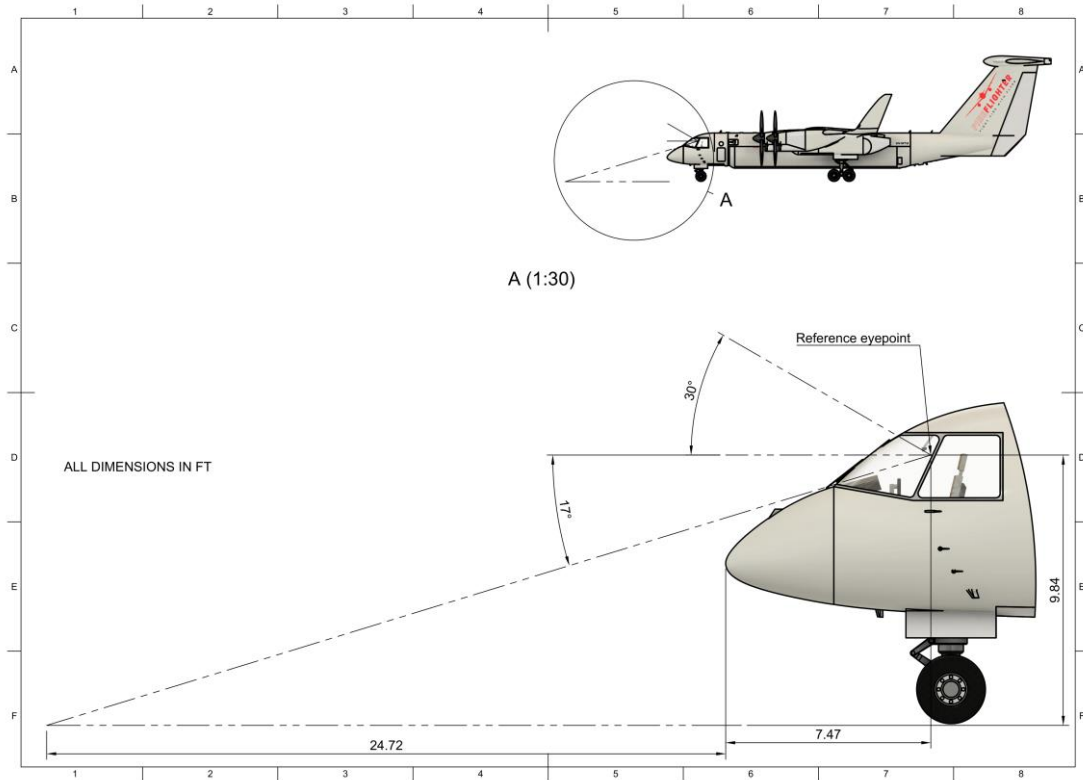


Figure 71: Cockpit view angles (elevation)

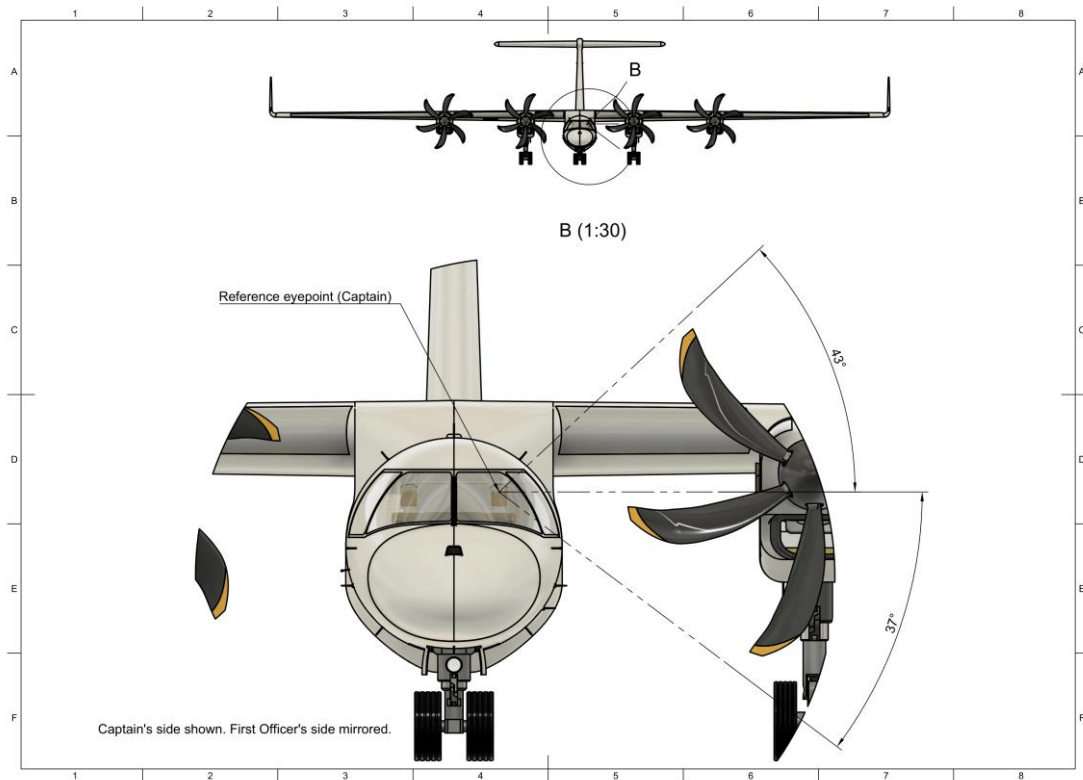
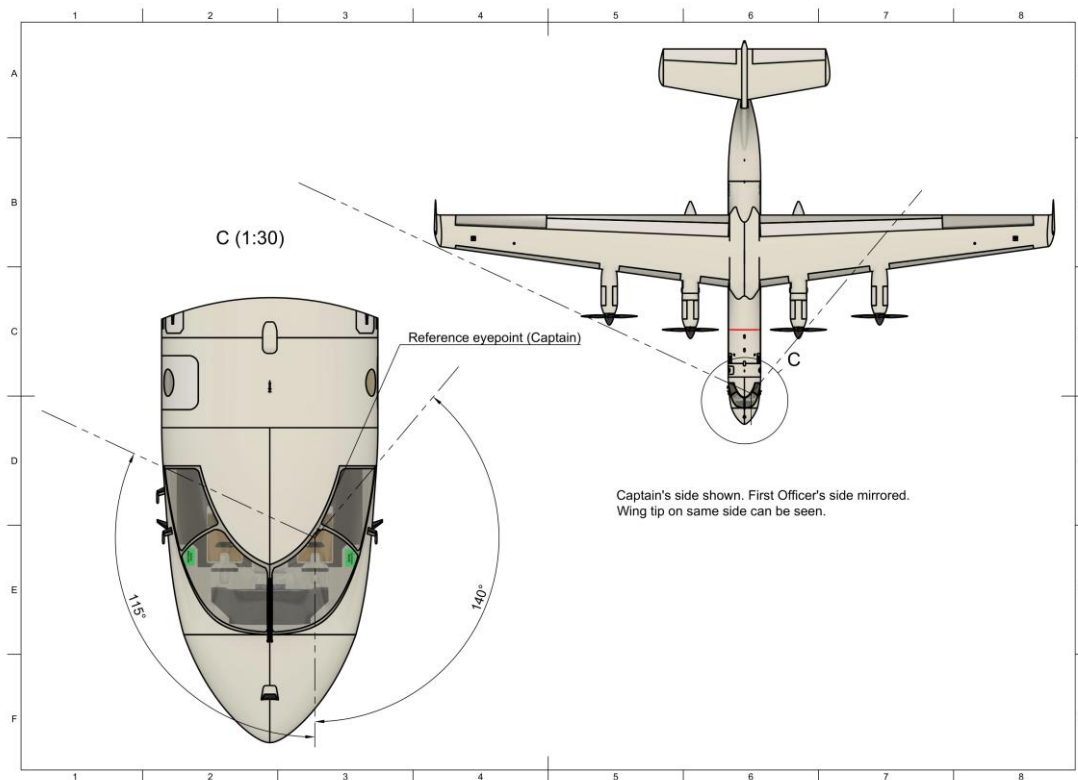


Figure 72: Cockpit view angles (side, vertical)



**Figure 73: Cockpit view angles (side, horizontal)**

### 15.3 Main Entrance Hatch and Emergency Exit

The main entrance hatch provides access from the exterior to the crew compartment and is located on the left side of the fuselage. As passenger comfort when boarding is not a factor in the design, smaller doors can be used, which also reduces the amount of structural reinforcement needed in the fuselage as a result of the smaller cutout. A set of integral stairs on the main entrance hatch facilitates boarding, and allows the crew to enter and exit without the need for dedicated support equipment which may not be available on airfields used as airtanker bases.

An emergency exit is also located in the crew compartment opposite the main entrance hatch. The dimensions of the emergency exit together with the main entrance hatch meets the FAR 25.807 requirement for aircraft with a capacity of less than 11 people.



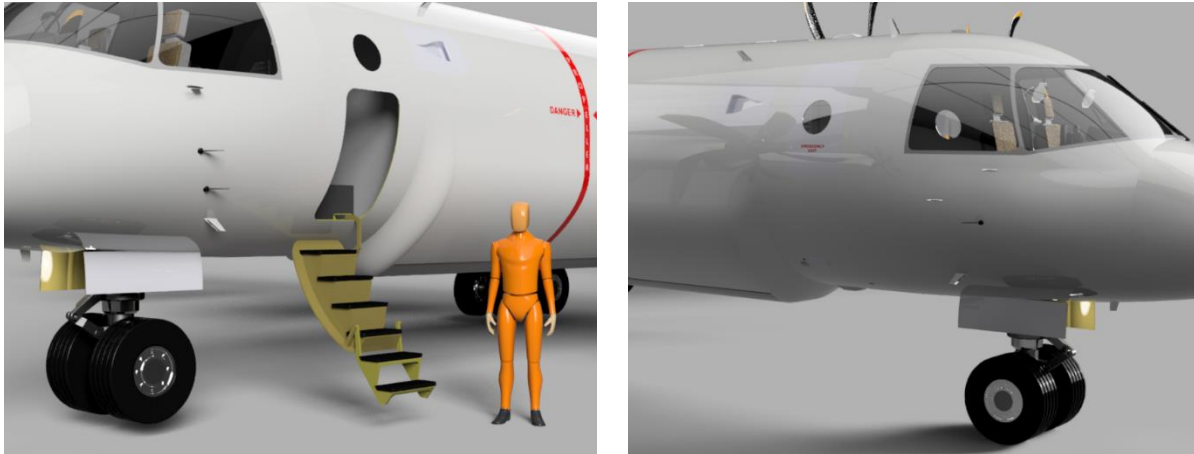


**Figure 74: Main Entrance Hatch and Emergency Exit**

#### 15.4 Air Conditioning

Although the crew compartment is unpressurised, air-conditioning is still a desirable feature in order to improve crew comfort and reduce fatigue. This is especially important as firefighting aircraft typically operate in hot weather and under intense operating conditions. For this reason, even older firefighting aircraft such as the CL-215 can be modified by installing a flight deck cooling system. The selected air conditioning unit is the FlyCool air conditioning system, which is a lightweight hermetically sealed R-134a vapour cycle system. It can be powered from a standard 28V power supply and weighs 22 lbs [83]. Although designed to cool the cabins of light sport aircraft, this air conditioning system is suitable for the Firefly due to the small cabin size. The cabin ventilation ram air scoop on the right side of the aircraft supplies fresh air to the air conditioning unit, and also supplies external air to a small compressor of the oxygen system for the onboard oxygen generator.

## 16 Avionics

### 16.1 Avionics Systems

A glass cockpit is used in Firefly, where flight data is shown on Electronic Flight Displays (EFDs) rather than separate gauges for each instrument. Examples of EFDs are the Primary Flight Display (PFD) which combines data from several instruments and is the pilot's primary source of flight information and the multi-function display (MFD) which allows data to be presented on multiple pages that are convenient to switch between. Another common name for these displays is Electronic Flight Instrument System (EFIS). Both seats are also equipped with a head-up display unit as shown in Figure 75 to facilitate low-level missions where awareness of the terrain is especially crucial.



**Figure 75: Glass cockpit and head-up display unit.**

Honeywell Aerospace was chosen as the primary avionics vendor as their avionics architecture provides key features that can serve the specialised needs of firefighting missions. A general Honeywell Avionics architecture, which includes Electronics Flight Instrumentation System (EFIS), Integrated Flight Deck (IFD) (Honeywell Primus Apex) and Flight Management System (FMS), integrates seamlessly with additional systems that are necessary for the safety and success of firefighting missions, such as Synthetic Vision System (SVS), which essential for navigation, and Onboard Maintenance System, which provides vital information about avionics health and can greatly reduce turn-around time.

Additional systems that can be sourced from Honeywell include the Navigation and Communication Radio System (Honeywell Primus II) and its corresponding modules, namely VOR, ILS, MKR, ADF, DME and the Radio Altimeter (Honeywell AA-300). Further potential advantages of this procurement strategy are the reduced cost from the low number of vendors, and the support Honeywell engineers can provide on integrating their different products which can also reduce costs and time of the manufacturing-assembly stage.

The onboard sensors of Fireflyer are summarized in Table 40 below and the locations shown in Figure 76.

**Table 40: Onboard sensors and their purpose**

<b>Name of Sensor</b>	<b>Purpose</b>
Pitot-Static Probe	Determines airspeed of aircraft by measuring stagnation pressure of the fluid in the pitot tube.
AOA Sensor	Provides Angle of Attack (AOA) or Sideslip by sensing the direction of local airflow.
TCAS	A Traffic Collision Avoidance System (TCAS) monitors the airspace around an aircraft for other aircraft equipped with a corresponding active transponder. It warns pilots of the presence of other transponder-equipped aircraft which may present a collision threat.
VHF Antenna	To communicate with air traffic control using radio frequencies in the Very High Frequency (VHF) band.

DME Transponder Antenna	The Distance Measuring Equipment (DME) measures the slant range between an aircraft and a ground station by timing the propagation delay of radio signals in the frequency band between 960 and 1215 MHz.
ATC Transponder Antenna	The Air Traffic Control (ATC) transponder antenna is used to enhance surveillance radar monitoring and separation of air traffic.
GPS	The Global Position System (GPS) determines the current position of the aircraft with the use of satellites.
Marker Beacon Antenna	It is a type of VHF radio beacon used, usually in conjunction with an Instrument Landing System (ILS), to give pilots a means to determine position along an established route to a destination such as a runway.
Radio Altimeter	It is used to measure the absolute height of the aircraft above the terrain.
ELT Antenna	The Emergency Locator Transmitter (ELT) is used to transmit a distress signal on 121.5 and 243.0 MHz frequencies in the event of an aircraft accident.
Glideslope Antenna	It broadcasts radio signals to guide an aircraft vertically to the runway. It is part of the Instrument Landing Systems (ILS)
VOR/LOC Antenna	Very high frequency omni-directional range (VOR) is a type of short-range radio navigation system for the aircraft, enabling it with a receiving unit to determine its position and stay on course by receiving radio signals transmitted by a network of fixed ground radio beacons.
Weather Radar	It determines certain weather conditions in the atmosphere by locating precipitation. It can estimate weather conditions such as rain and snow.

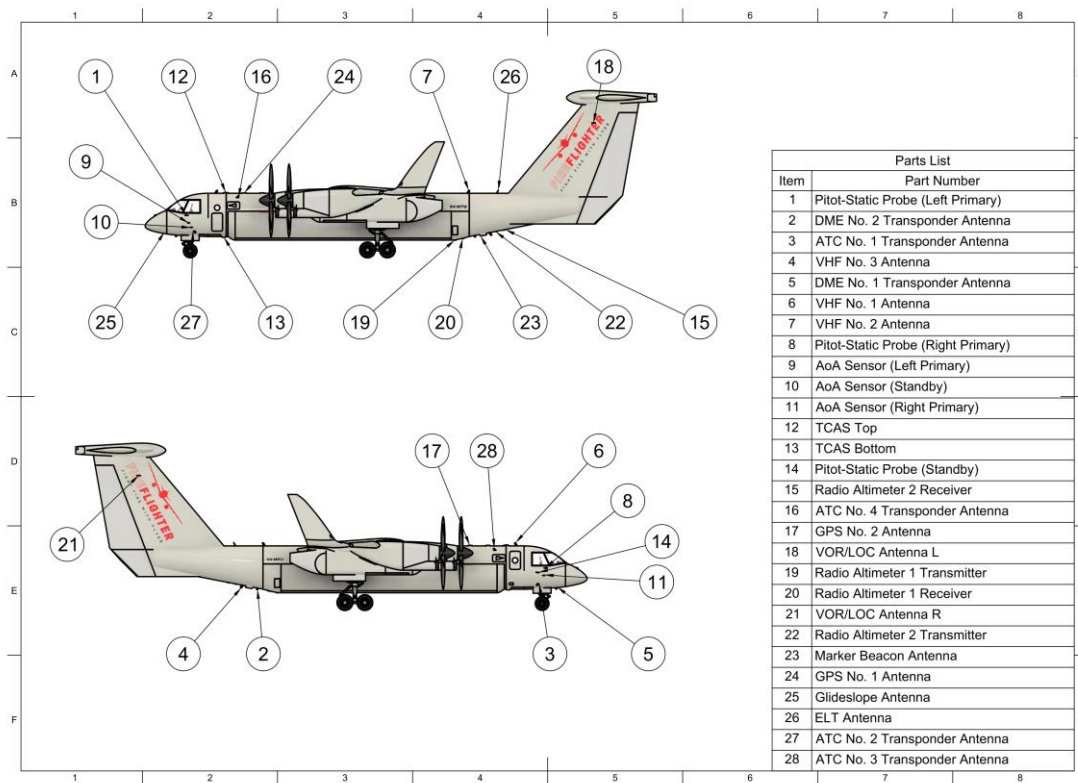


**Figure 76: Locations of antennas and probes.**

## 16.2 Autonomous Operations

Due to size of the highly dynamic environments and unpredictable circumstances common for firefighting missions, it was not viable to implement any mission-specific autonomous capability apart from the

conventional autopilot and instrument landing systems. Although significant progress has been made in autonomous aircraft, the state of current technology and legislative environment means that human adaptability and judgement of the flight and control crew must remain in place.

### 16.3 Aircraft Vision Systems

Firefly is equipped with both a Synthetic Vision System (SVS) and Enhanced Flight Vision System (EFV) for increased situational awareness in low visibility conditions, such as due to smoke. SVSs display computer generated graphical representation of the flight environment on a screen on the cockpit dashboard. SVS functionality is database reliant, gathering GPS and IMU data about the aircraft position and orientation, providing terrain, obstacle, and hydrological information accordingly. EFVs are navigation hardware that makes use of imaging sensors, cameras, and other navigation-aiding sensors to produce images of the environment. Unlike SVSs, EFVs use real-time environmental data gathered by on-board sensors, therefore they are not entirely weather independent. However, visual images provided by EFVs are more representative of the actual flight environment and serve as a complement for SVSs.



**Figure 77: Enhanced Vision System located on the nose of the aircraft.**

## 17 Cost Estimation

### 17.1 Research Development Test and Evaluation (RDT&E) and Flyaway Costs

The RAND DAPCA IV Model was applied to estimate the RDT&E and flyaway costs of Firefly. The required variables for model are defined in Table 41, and the wrap rates used in the model were obtained from Raymer Chapter 18. Values were adjusted for inflation wherever necessary using the U.S. Bureau of Labour Statistics CPI Inflation Calculator. With the expected expenditure on firefighting estimated to be around \$5 to \$30 billion annually in 2050 and more countries seeking to establish their own personal firefighting forces, the expected demand for a new model of firefighting aircraft can be estimated to be about 500 to 1000 across the next three decades assuming a steady demand [29]. Comparing the prices of similar aircraft, The Firefly as a tanker with an 8000-gallon capacity can be priced competitively at around \$75 million. The results of the DAPCA IV model are shown in Table 42 and Table 43.

**Table 41: DAPCA IV Model Parameters**

Required Variables	
Empty Weight, $W_e$	68,712 lbs
Maximum Velocity, $V$	414.039 knots
Production quantity (5 years), $Q$	300 (15 units per year over 20 years)
Number of Flight Test Aircraft, FTA	4 (typically 2-6)
Cost of Engine, $C_{eng}$	\$1,300,000 [84]
Cost of Avionics, $C_{avionics}$	\$4,282,000 (\$2000 per pound, 1986 dollars)

**Table 42: Results for RDT&E Costs**

Area	Cost (millions, 2022 dollars)
Engineering	2280.02
Tooling	1548.35
Development Support	319.64
Flight Test	87.93
Total RDT&E:	4235.95

**Table 43: Results for flyaway costs per aircraft**

Area (per aircraft)	Cost (millions, 2022 dollars)
Manufacturing Labour	20.37
Materials	10.51
Quality Control	1.71
Engine	5.20
Avionics	10.71
Total Flyaway:	48.49

Using these cost estimations, the production breakeven point was found to occur at 160 aircraft, just after the halfway point of the program. At the end of the production run, a profit of \$4.576 billion can be expected.

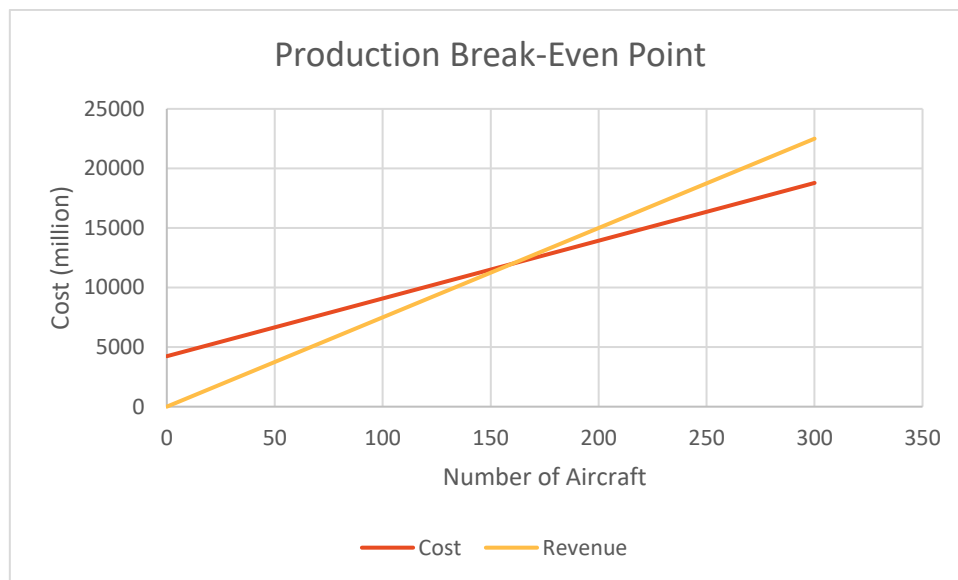


**Figure 78: Production break-even point**

## 17.2 Operating Cost Estimation

The operations and maintenance costs required for the aircraft was also estimated using Raymer Chapter 18. These include the Fuel Costs, Crew Costs, Maintenance Costs and Material Costs. From the total operating costs obtained, the competitiveness of the aircraft against the alternatives currently available in the market can be evaluated. The cost of the retardant (\$4.00 per gallon [85]) was omitted as it is usually not included when pricing the costs per gallon dropped of a firefighting aircraft.

### 17.2.1 Fuel and Oil Costs

The flight performance of the aircraft during the design mission was used to obtain the fuel consumption of the aircraft. The fuel burn was calculated to be 5668 lbs/hr during a payload drop mission which can be estimated to

be 845.97 gallons/hr. Similar values were obtained from a firefighting mission profile study done in Colorado.

The Bae-146, with an empty weight of 50400 lbs has a fuel consumption of 743 gallons/hr while the C-130H/Q with an empty weight of 75800 lbs has a fuel consumption of 944 gallons/hr [85]. As the fuel consumption of an aircraft is expected to be higher during a firefighting mission, the initial estimate of 845.97 gallons/hr is considered to be reasonably accurate. Using a fuel price of 170.8 cents per gallon, the resultant fuel cost was estimated to be \$144.92 per hour.

### 17.2.2 Crew Costs

Crew costs were estimated using a two-man crew model, as only a pilot and co-pilot is required to meet FAR 25 requirements for transport aircraft. The total crew cost was estimated to be \$340.53.

### 17.2.3 Maintenance Costs

The costs required for maintenance was estimated by first assuming 50 Maintenance Man Hours per flight hour, the value for military bombers as found in Raymer Chapter 18. This is because the low-level manoeuvring performed during a payload drop adds additional stress onto the airframe and components. Using a Manufacturing Wrap Rate of \$50.10 as estimated in the DAPCA Model, the maintenance costs per flight hour was estimated to be \$2505.

### 17.2.4 Material Costs

To estimate the material costs per flight hour, the cost of the aircraft less engines,  $C_a$  and the cost per engine,  $C_e$  were used. Using the equation in Chapter 18, the material costs per flight hour was estimated to be \$399.50.

## 17.3 Total Operating Cost and Comparison

After summing the individual components in Table 44, the total cost to operate the aircraft per flight hour was found to be \$4689.96. After accounting for inflation, the total cost per flight hour can be estimated to be \$11,724.89. Assuming each flight drop of 8000 gallons takes an hour, typical of current large air tankers, the cost per gallon dropped is calculated to be \$1.46.

**Table 44: Operating Cost Breakdown.**

Operating Cost Breakdown	
Fuel Costs/FH	\$1444.92
Crew Costs/FH	\$340.53
Maintenance Costs/FH	\$2505.00
Material Costs/FH	\$399.50
Total Cost/FH:	\$4689.95
Total Cost/FH (Accounting for Inflation):	\$11,724.89
Total Cost/Gallon Drop	\$1.46

The per flight hour as well as per gallon dropped cost metrics can then be compared to other contemporary firefighting aircraft to assess its competitiveness, as shown in Table 45.

**Table 45: Operating Cost Comparison with Commercially Available Firefighting Aircraft [86].**

Class	Aircraft	Max Tank Capacity	Availability	Cost/FH	Fills Per Hour	Gallons Per Hour	Cost Per Gallon
Scooper	Fire Boss	820	\$4,500	\$4,500	20	14,000	\$0.64
	CL-415	1,600	\$42,000	\$13,500	17	27,200	\$2.04
VLAT (Very Large Air Tanker)	DC-10	10,800	\$55,000	\$8,200	1	10,800	\$5.85
	BAe-146	3,000	\$29,000	\$8,000	1	3,000	\$12.33
	Firefighter	8,000	\$ -	\$11,724	1	8000	\$1.46

The availability cost refers to the cost of chartering the aircraft for firefighting missions. It is omitted in the proposed firefighting aircraft as pricing is subject to market conditions and together with the assumption that the firefighting aircraft is operated as a self-owned asset.

The cost comparison shows that using a dedicated firefighter as opposed to a converted aircraft can help firms and agencies save a significant amount on operating costs. This helps to substantiate the development of a dedicated firefighting aircraft and provides assurance that there will be a significant market demand for it.



## 18 Conclusion

The Firefly was designed to address the growing intensity of forest fires globally while being an affordable and cost-effective platform for government agencies and contractors. With a payload capacity of 8,000 gallons, terrain-following radar, SVS and EFV systems, a sizeable amount of retardant can be flexibly and precisely laid down in any weather and any terrain. Designed to a limit load factor of 3.25G, the airframe is purpose-built to withstand the stresses of low-level firefighting manoeuvres. Situational awareness during operations is also exceptional, with superb visibility, head-up displays and a full glass cockpit empowering crews to perform at their best. The low operating cost and excellent firefighting performance places the Firefly as one of the top choices for governments and agencies around the world for swift and efficient firefighting efforts.

## 19 References

- [1] C. f. C. a. E. Solutions, “Center for Climate and Energy Solutions,” [Online]. Available: <https://www.c2es.org/content/wildfires-and-climate-change/>.
- [2] D. Cave, “The New York Times,” 21 November 2019. [Online]. Available: <https://www.nytimes.com/2019/11/21/world/australia/fires-water-tankers-climate-change.html>.
- [3] S. DiGiovanna, “Firefly Safety around Air Drops,” 4 June 2021. [Online]. Available: <https://www.firerescue1.com/firefly-safety/articles/heads-up-and-clear-out-firefly-safety-around-air-drops-BYhADS9MxO0KP60h/>.
- [4] B. Gabbert, “What did we learn from the Aerial Firefighting Use and Effectiveness study?,” Fire Aviation, 16 April 2021. [Online]. Available: <https://fireaviation.com/2021/04/16/what-did-we-learn-from-the-aerial-firefighting-use-and-effectiveness-study/>. [Accessed 22 August 2021].
- [5] F. W. D. System, “Aerial Firefighters & Fire Fighting,” [Online]. Available: <https://www.frontlinewildfire.com/aerial-wildfire-fighting-how-effective-is-it/>.
- [6] S. R. Hall, “Consolidation and analysis of loading data in firefighting operations: Analysis of existing data and definition of preliminary air tanker and lead aircraft spectra,” Celeris Aerospace Canada, October 2005. [Online]. Available: <http://www.tc.faa.gov/its/worldpac/techrpt/ar05-35.pdf>. [Accessed 22 August 2021].
- [7] J. W. Jewel, G. J. Morris and D. E. Avery, “Operating Experiences of Retardant Bombers During Firefighting Operations,” November, 1974.
- [8] Viking Air Ltd, “Specifications,” Viking Air Ltd, 2021. [Online]. Available: <https://aerialfireflyer.vikingair.com/firefighting/specifications>. [Accessed 15 August 2021].

- [9] WinAir, “Everything that You Need to Know about the Canadair CL-415,” WinAir, [Online]. Available: <https://winair.ca/blog/everything-need-know-canadair-cl-415/>. [Accessed 15 August 2021].
- [10] D. Woods, E. G. Keating, A. R. Morral and D. M. Norton, “Investing in Firefighting,” Rand Corporation, 30 12 2013. [Online]. Available: <https://www.rand.org/blog/2013/12/investing-in-firefighting.html>. [Accessed 15 August 2021].
- [11] aerospaceweb.org, “DC10,” aerospaceweb.org, 2018. [Online]. Available: <http://www.aerospaceweb.org/aircraft/jetliner/dc10/>. [Accessed 27 August 2021].
- [12] McDonnell Douglas Corporation, “DC/MD-10 Airplane Characteristics for Airport Planning,” April 2004. [Online]. Available: <https://www.boeing.com/resources/boeingdotcom/commercial/airports/acaps/dc10.pdf>. [Accessed 27 August 2021].
- [13] Plane and Pilot, “Douglas DC-10,” Plane and Pilot, 6 February 2016. [Online]. Available: <https://www.planeandpilotmag.com/article/douglas-dc-10/>. [Accessed 27 August 2021].
- [14] J. Hart, “Ask Joe: How much do those firefighting planes cost to operate?,” News4, 30 July 2020. [Online]. Available: <https://mynews4.com/on-your-side/ask-joe/ask-joe-how-much-do-those-firefighting-planes-cost-to-operate>. [Accessed 27 August 2021].
- [15] aerospaceweb.org, “IL-76,” aerospaceweb.org, 2018. [Online]. Available: <http://www.aerospaceweb.org/aircraft/transport-m/il76/>. [Accessed 27 August 2021].
- [16] Ilyushin, “IL-76-TD-90,” Ilyushin, 3 November 2009. [Online]. Available: <https://web.archive.org/web/20091103142428/http://www.ilyushin.org/eng/products/cargo/76td90.html>. [Accessed 27 August 2021].
- [17] GlobalSecurity.org, “IL-76 Candid,” GlobalSecurity.org, 2021. [Online]. Available: <https://www.globalsecurity.org/military/world/russia/il-76-specs.htm>. [Accessed 27 August 2021].
- [18] L. Jenkinson, P. Simpkin and D. Rhodes, “Table 5: Douglas and Boeing (Douglas Products Division) Aircraft,” Civil Jet Aircraft Design, 2001. [Online]. Available: <https://booksite.elsevier.com/9780340741528/appendices/data-a/table-5/table.htm>. [Accessed 27 August 2021].
- [19] Skybrary, “McDonnell Douglas MD-87,” Skybrary, 13 October 2014. [Online]. Available: <https://www.skybrary.aero/index.php/MD87>. [Accessed 27 August 2021].
- [20] McDonnell Douglas, “MD-80 Series Airplane Characteristics for Airport Planning,” 1990. [Online]. Available: <https://www.boeing.com/resources/boeingdotcom/commercial/airports/acaps/md80.pdf>. [Accessed 27 August 2021].

- [21] Coulson Flying Tankers, “Martin Mars Specifications,” [Online]. Available: [https://en.wikipedia.org/wiki/Martin\\_JRM\\_Mars#cite\\_note-cftspecs-26](https://en.wikipedia.org/wiki/Martin_JRM_Mars#cite_note-cftspecs-26). [Accessed 7 August 2014].
- [22] K. Palt, “Martin JRM Mars,” Flugzeug info.net, 2019. [Online]. Available: [http://www.flugzeuginfo.net/acdata\\_php/acdata\\_jrmmars\\_en.php](http://www.flugzeuginfo.net/acdata_php/acdata_jrmmars_en.php). [Accessed 27 August 2021].
- [23] DH Vancouver Staff, “Province signs contract to use Martin Mars water bomber,” DH News, 19 December 2017. [Online]. Available: <https://dailyhive.com/vancouver/bc-wildfire-martin-mars-water-bomber>. [Accessed 27 August 2021].
- [24] WarbirdsNews, “Why is the Iconic Martin Mars Not Fighting Fires?,” Warbird Digest, 2 September 2021. [Online]. Available: <https://warbirdsnews.com/warbirds-news/why-is-the-iconic-martin-mars-not-fighting-fires.html>. [Accessed 14 September 2021].
- [25] B. Gabbert, “The 747 Supertanker is ceasing operations,” FireAviation, 23 April 2021. [Online]. Available: <https://fireaviation.com/2021/04/23/the-747-supertanker-is-ceasing-operations/>. [Accessed 11 September 2021].
- [26] M. B. O. J. M. L. Corey R. Butler, “Aviation-Related Wildland Firefighter Fatalities,” 31 July 2015. [Online]. Available: <https://www.cdc.gov/mmwr/preview/mmwrhtml/mm6429a4.htm>.
- [27] B. Gabbert, “10 years ago today, the second air tanker crash of 2002,” Wildfire Today, 18 July 2012. [Online]. Available: <https://wildfiretoday.com/2012/07/18/10-years-ago-today-the-second-air-tanker-crash-of-2002/>. [Accessed 27 August 2021].
- [28] B. Gabbert, “A-10 Warthog proposed, again as an air tanker,” Fire Aviation, 25 September 2014. [Online]. Available: <https://fireaviation.com/2014/09/25/a-10-warthog-proposed-again-as-an-air-tanker/>. [Accessed 27 August 2021].
- [29] J. Roman, A. Verzoni and S. Sutherland, “Greetings from the 2020 Wildfire Season,” 1 November 2020. [Online]. Available: <https://www.nfpa.org/News-and-Research/Publications-and-media/NFPA-Journal/2020/November-December-2020/Features/Wildfire>.
- [30] M. Langfield, “Aerial firefighting boost in Sweden,” AirMed&Rescue, 1 February 2021. [Online]. Available: <https://www.airmedandrescue.com/latest/news/aerial-firefighting-boost-sweden>. [Accessed 11 September 2021].
- [31] The North Africa Post, “Morocco to boost its aerial firefighting fleet,” The North Africa Post, 18 August 2021. [Online]. Available: <https://northafricapost.com/51789-morocco-to-boost-its-aerial-firefighting-fleet.html>. [Accessed 11 September 2021].

- [32] Conair Aerial Firefighting Stand, “Conair Expands with Purchase of Eleven Dash 8 Q400 Aircraft,” Conair Group, 15 January 2021. [Online]. Available: <https://www.aerial-firefighting-europe.com/exhibitor-press-releases/conair-expands-with-purchase-of-eleven-dash-8-q400-aircraft>. [Accessed 11 September 2021].
- [33] K. Papadopoulos, “Greece to recruit 3,000 firefighters, invests 1.76 billion euros in fire protection,” Greek City Times, 16 June 2021. [Online]. Available: <https://greekcitytimes.com/2021/06/16/greece-to-recruit-3000-firefighters-invests-1-76-billion-euros-in-fire-protection/>. [Accessed 11 September 2021].
- [34] Reuters Staff, “World's largest amphibious aircraft makes maiden flight in China,” Reuters, 24 December 2017. [Online]. Available: <https://www.reuters.com/article/china-defence-airplane-idUSL4N1000P>. [Accessed 12 September 2021].
- [35] R. Mason, “Mitigating America's Wildfire Threat,” AerialFire Magazine, 3 September 2021. [Online]. Available: <https://www.aerialfiremag.com/mitigating-americas-wildfire-threat/>. [Accessed 11 September 2021].
- [36] A. Mak, “The Reason We Don't Have Enough Airplanes to Put Out Wildfires,” Slate Magazine, 28 August 2021. [Online]. Available: <https://slate.com/business/2021/08/california-wildfires-airplanes-dc10-shortage.html>. [Accessed 11 September 2021].
- [37] J. Jorgensen, “Viking Air's New CL-515, Where Multi-Mission is the Watchword,” Kiakaha Media, 23 August 2020. [Online]. Available: <https://www.airattackmag.com/viking-airs-new-cl-515-where-multi-mission-is-the-watchword>. [Accessed 27 August 2021].
- [38] “Is a turboprop or a turbofan more eco-friendly?,” Aviation Stack Exchange, 17 June 2020. [Online]. Available: <https://aviation.stackexchange.com/questions/48221/is-a-turboprop-or-a-turbofan-more-eco-friendly>. [Accessed 24 August 2021].
- [39] D. E. Calkin, C. S. Stonesifer, M. P. Thompson and C. W. McHugh, “Large airtanker use and outcomes in suppressing wildland fires in the United States,” *International Journal of Wildland Fire*, vol. 23, no. 2, p. 259, January 2014.
- [40] Federal Aviation Administration, “14 CFR 91.151 Fuel requirements for flight in VFR conditions,” Legal Information Institute, 21 January 2000. [Online]. Available: <https://www.law.cornell.edu/cfr/text/14/91.151>. [Accessed 20 August 2021].
- [41] Federal Aviation Administration, “14 CFR 91.167 Fuel requirements for flight in IFR conditions,” Legal Information Institute, 21 January 2000. [Online]. Available: <https://www.law.cornell.edu/cfr/text/14/91.167>. [Accessed 21 August 2021].
- [42] P. Jackson, *Jane's All the World's Aircraft, 2003-2004*, Janes Information Group, 2003.
- [43] Airfoil Tools, 2001. [Online]. Available: <http://airfoiltools.com>. [Accessed 26 August 2021].

- [44] H. Riblett, "What are Wortman Airfoils?," 40 November 1988. [Online]. Available: [http://acversailles.free.fr/documentation/08~Documentation\\_Generale\\_M\\_Suire/Aerodynamique/Profils/Wortman/What%20are%20wortman%20airfoils.pdf](http://acversailles.free.fr/documentation/08~Documentation_Generale_M_Suire/Aerodynamique/Profils/Wortman/What%20are%20wortman%20airfoils.pdf). [Accessed 25 August 2021].
- [45] D. Scholz, "Definition and discussion of the intrinsic efficiency of winglets," in *Aerospace Europe CEAS 2017 Conference*, Bucharest, 2017.
- [46] D. P. Raymer, *Aircraft Design: a conceptual approach*, Reston, VA : American Institute of Aeronautics and Astronautics, 1999.
- [47] D. Scholz, "High Lift Systems and Maximum Lift Coefficients," [Online]. Available: [https://www.fzt.haw-hamburg.de/pers/Scholz/HOOU/AircraftDesign\\_8\\_HighLift.pdf](https://www.fzt.haw-hamburg.de/pers/Scholz/HOOU/AircraftDesign_8_HighLift.pdf). [Accessed 16 September 2021].
- [48] D. P. R. 3. ed., *Aircraft design : a conceptual approach*, Reston, VA : American Institute of Aeronautics and Astronautics, 1999.
- [49] M. F. Niță, "Aircraft Design Studies Based on the ATR 72," 2008.
- [50] AE-2100, VCOMB 3855 Defence Data sheet, <https://www.rolls-royce.com/~media/Files/R/Rolls-Royce/documents/defence/VCOMB%203855%20Defence%20Data%20sheet%20-%20AE%202100.pdf>.
- [51] "TYPE-CERTIFICATE DATA SHEET For R391 Series Propellers," in *European Aviation Safety Agency*, [https://www.easa.europa.eu/sites/default/files/dfu/TCDS%20P.087%20Issue%2003\\_11.12.18.pdf](https://www.easa.europa.eu/sites/default/files/dfu/TCDS%20P.087%20Issue%2003_11.12.18.pdf).
- [52] Bombardier Q400 Propeller - Dowty R408, <https://www.flyradius.com/bombardier-q400/propeller-dowty-r408>.
- [53] AI-20 specifications, <http://motorsich.com/eng/products/aircraft/tr/ai-20/>.
- [54] The Ilyushin Il-18 & Il-38, <https://www.airvectors.net/avil18.html>.
- [55] LOCKHEED C-130 "HERCULES", <https://aircraftreview.wordpress.com/2013/01/27/lockheed-c-130-hercules/>: AircraftReview.
- [56] Emerald Group Publishing Limited, "Double Engine Failure," *Aircraft Engineering and Aerospace Technology*, vol. 74, no. 3, 2002.
- [57] "Full Authority Digital Engine Control," FAA Aviation Safety.
- [58] Pratt & Whitney Canada, "EASA Type-Certificate Data Sheet PW 150 Series Engines," 19 November 2014. [Online]. Available: [https://www.easa.europa.eu/sites/default/files/dfu/TCDS%20PW150%20series%20issue%2001\\_20141119\\_1.0.pdf](https://www.easa.europa.eu/sites/default/files/dfu/TCDS%20PW150%20series%20issue%2001_20141119_1.0.pdf). [Accessed 23 August 2021].

- [59] D. Scholz, "Wing Design," Aircraft Design - an Open Educational Resource for Hamburg Open Online University, 27 May 2017. [Online]. Available: [https://www.fzt.haw-hamburg.de/pers/Scholz/HOOU/AircraftDesign\\_7\\_WingDesign.pdf](https://www.fzt.haw-hamburg.de/pers/Scholz/HOOU/AircraftDesign_7_WingDesign.pdf). [Accessed 17 September 2021].
- [60] L. Martin, "Lockheed Martin," 2020. [Online]. Available: [https://www.lockheedmartin.com/content/dam/lockheed-martin/aero/documents/LM-100J/20-00975%20FireHerc\\_Brochure\\_2020.pdf](https://www.lockheedmartin.com/content/dam/lockheed-martin/aero/documents/LM-100J/20-00975%20FireHerc_Brochure_2020.pdf).
- [61] M. Guilhem, "In California, Air Tanker Pilots Help Keep Wildfires At Bay," 29 October 2019. [Online]. Available: <https://www.npr.org/2019/10/29/774456972/in-california-air-tanker-pilots-help-keep-wildfires-at-bay>.
- [62] "staticflickr," [Online]. Available: [https://live.staticflickr.com/5699/30793168940\\_cbbe22ed4f\\_b.jpg](https://live.staticflickr.com/5699/30793168940_cbbe22ed4f_b.jpg).
- [63] B. Gabbert, "A tour through the 747's retardant delivery system," 24 October 2017. [Online]. Available: <https://fireaviation.com/2017/10/24/a-tour-through-the-747s-retardant-delivery-system/>.
- [64] Viking Air, "Corrosion Protection," Viking Air, 22. [Online]. Available: <https://aerialfirefighter.vikingair.com/firefighting/specifications/corrosion-protection>. [Accessed 11 May 2022].
- [65] F. Mee, "Fire Bombers Drop Systems," 09-27.fr, 2015 September 2015. [Online]. Available: <http://www.marsaly.fr/fred/fire-bombers-drop-systems/>. [Accessed 30 October 2021].
- [66] H. Biggs, "Very Large Air Tanker Operational Trial Project," State Aircraft Unit Victoria, February 2010. [Online]. Available: [https://firewebext.ffm.vic.gov.au/BurnsToday/sau/SAU\\_External/documents/VLAT/VLAT%20-%20Approved%20Draft%20Project%20Operations%20Program%20February%202010.pdf](https://firewebext.ffm.vic.gov.au/BurnsToday/sau/SAU_External/documents/VLAT/VLAT%20-%20Approved%20Draft%20Project%20Operations%20Program%20February%202010.pdf). [Accessed 30 October 2021].
- [67] Airstrike Firefighters LLC, "Firefighting," Airstrike Firefighters LLC, [Online]. Available: <http://www.airstrikefirefighters.com/fire-fighting.html>. [Accessed 30 October 2021].
- [68] MatWeb, "Aluminium 7075-T6; 7075-T651," MatWeb Material Property Data, 2001. [Online]. Available: <https://www.matweb.com/search/DataSheet.aspx?MatGUID=4f19a42be94546b686bbf43f79c51b7d&ckck=1>. [Accessed 11 May 2022].
- [69] D. Scholz, "Empennage General Design," Aircraft Design - an Open Educational Resource for Hamburg Open Online University, 27 May 2017. [Online]. Available: [https://www.fzt.haw-hamburg.de/pers/Scholz/HOOU/AircraftDesign\\_9\\_EmpennageGeneralDesign.pdf](https://www.fzt.haw-hamburg.de/pers/Scholz/HOOU/AircraftDesign_9_EmpennageGeneralDesign.pdf). [Accessed 8 September 2021].

- [70] Skybrary, “Stick Pusher,” Skybrary, 8 December 2020. [Online]. Available: [https://www.skybrary.aero/index.php/Stick\\_Pusher](https://www.skybrary.aero/index.php/Stick_Pusher). [Accessed 15 September 2021].
- [71] “Aircraft Tire Engineering Data,” MICHELIN AIRCRAFT TIRE.
- [72] Z. Li and T. Mu, “Study on Dimension of Landing Gear Bogie for Civil Aircraft,” in *IOP Conference Series: Materials Science and Engineering*, 2019.
- [73] N. S. Currey, *Aircraft Landing Gear Design-Principles and Practices*, 1988.
- [74] “Standardized method of reporting airport pavement strength-PCN,” U.S Department of Transportation Federal Aviation Administration, 2006.
- [75] T. Dubois, “Pilots stall delivery of 2nd Q400 to French fireguard,” AIN online, 19 September 2006. [Online]. Available: <https://www.ainonline.com/aviation-news/aviation-international-news/2006-09-19/pilots-stall-delivery-2nd-q400-french-fireguard>. [Accessed 1 November 2021].
- [76] C. L. R. S. D. Q. a. I. M. Ahmed Shinkafi, “AN INTELLIGENT ICE PROTECTION SYSTEM FOR NEXT GENERATION AIRCRAFT TRAJECTORY OPTIMISATION,” [Online]. Available: [http://icas.org/ICAS\\_ARCHIVE/ICAS2014/data/papers/2014\\_0395\\_paper.pdf](http://icas.org/ICAS_ARCHIVE/ICAS2014/data/papers/2014_0395_paper.pdf).
- [77] Cobham, “C-130 OBOGS,” [Online]. Available: <https://www.cobhammissionsystems.com/oxygen-systems/military-aerospace-oxygen-systems/on-board-oxygen-generation-systems-obogs/c-130-obogs/docview/>.
- [78] S. International, “On-Board Oxygen Generating Systems (Molecular Sieve),” 14 July 2020. [Online]. Available: <https://www.sae.org/standards/content/air825/6a/>.
- [79] “Dash 8 Q400 Electrical,” [Online]. Available: <https://www.smartcockpit.com/docs/Q400-Electrical.pdf>.
- [80] Skybrary, “Transformer Rectifier Unit (TRU),” [Online]. Available: [https://www.skybrary.aero/index.php/Transformer\\_Rectifier\\_Unit\\_\(TRU\)](https://www.skybrary.aero/index.php/Transformer_Rectifier_Unit_(TRU)).
- [81] Marlia, “Hydraulic Shutoff Valve,” [Online]. Available: [https://www.marlia-ing.com/en/brochures/shutoff\\_hydraulic\\_valve.pdf](https://www.marlia-ing.com/en/brochures/shutoff_hydraulic_valve.pdf).
- [82] L. I. I. (LII), “14 CFR § 25.1195 - Fire extinguishing systems.,” [Online]. Available: <https://www.law.cornell.edu/cfr/text/14/25.1195>.
- [83] FlyCool, “All-Electric Light Weight AC for the sport cruiser aircraft,” Air Management Technology Inc, [Online]. Available: <https://www.midwestsaexpo.com/wp-content/uploads/2018/07/Sport-Cruiser-FlyCool-flyer.pdf>. [Accessed 25 October 2021].

- [84] Forecast International, “Microsoft Word - F641 Cover Page,” December 2010. [Online]. Available: [https://www.forecastinternational.com/samples/F641\\_CompleteSample.pdf](https://www.forecastinternational.com/samples/F641_CompleteSample.pdf).
- [85] U.S. Bureau of Labor Statistics , “CPI Inflation Calculator,” U.S. Bureau of Labor Statistics , [Online]. Available: [https://www.bls.gov/data/inflation\\_calculator.htm](https://www.bls.gov/data/inflation_calculator.htm). [Accessed 4 October 2021].
- [86] Conklin & de Decker Aviation Information, “Analysis of Aircraft for the Fire Fighting Mission in Colorado,” 6 December 2013. [Online]. Available: <https://wildfiretoday.com/documents/ColoradoAirTankerStudy.pdf>. [Accessed 4 October 2021].
- [87] Fire Boss, “The Most Economical Solution,” Fire Boss, [Online]. Available: <https://firebossllc.com/cost-comparison/>. [Accessed 6 October 2021].
- [88] B. Gabbert, “California Governor laments that the 747 and other air tankers are not available,” Fire Aviation, 7 August 2021. [Online]. Available: <https://fireaviation.com/2021/08/07/california-governor-laments-that-the-747-and-other-air-tankers-are-not-available/>. [Accessed 11 September 2021].